AD-A194 362 APPLICATION OF LINEARIZED KALMAN FILTER-SMOOTHER TO AIRCRAFT TRAJECTORY ESTIMATION(U) AIR FORCE INST OF TECH WRIGHT-PATTERSON AFB OH SCHOOL OF ENGI.. 1/2

UNCLASSIFIED J M RULEY JUN 88 AFIT/GAE/ENG/88J-1 F/G 1/3 NL

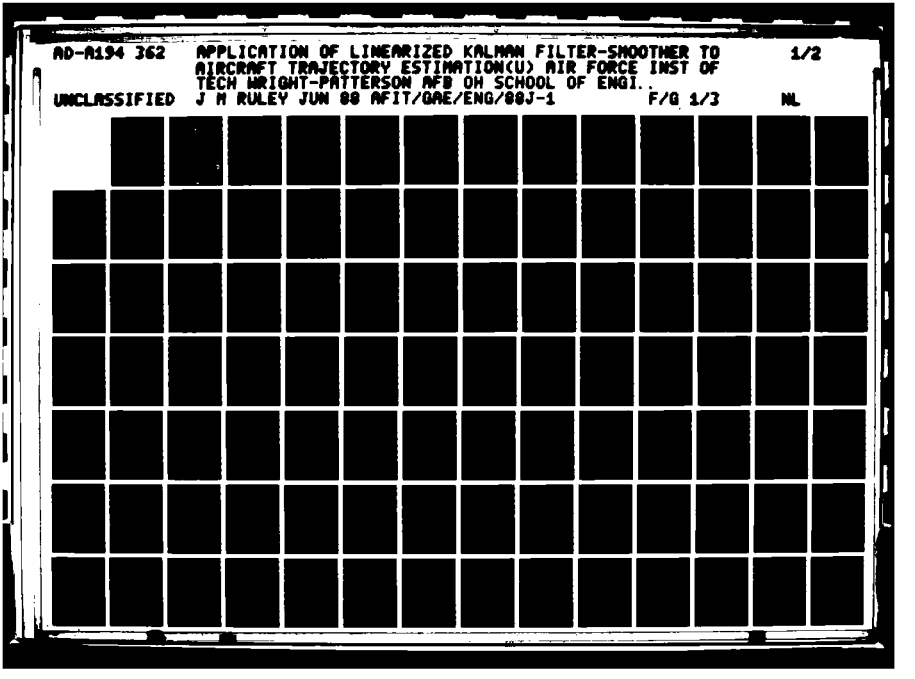

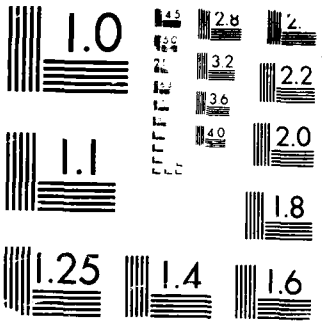

APPLICATION OF LINEARIZED KALMAN FILTER-SMOOTHER TO AIRCRAFT TRAJECTORY ESTIMATION

THESIS

James M. Ruley

AFIT/GAE/ENG-88J-1

DEPARTMENT OF THE AIR FORCE

AIR UNIVERSITY

AIR FORCE INSTITUTE OF TECHNOLOGY

Wright-Patterson Air Force Base, Ohio

AFIT/GAE/ENG-88J-1

APPLICATION OF LINEARIZED KALMAN FILTER-SMOOTHER TO AIRCRAFT TRAJECTORY ESTIMATION

THESIS

James M. Ruley

AFIT/GAE/ENG-88J-1

AFIT/GAE/ENG-88J-1

APPLICATION OF LINEARIZED KALMAN FILTER-SMOOTHER TO AIRCRAFT TRAJECTORY ESTIMATION

THESIS

Presented to the Faculty of the School of Engineering

of the Air Force Institute of Technology

Air University

In Partial Fulfillment of the

Requirements for the Degree of

Master of Science in Aeronautical Engineering

James M. Ruley, B.S.

June 1988

Approved for public release; distribution unlimited

Preface

The purpose of this study was to investigate the potential utility of the linearized Kalman filter-smoother as a tool for aircraft mishap investigations. The intention was to produce a computer analysis tool which could accurately reproduce the forcing functions required to generate a specified aircraft trajectory. This information is often of value to mishap investigation boards in determining probable pilot actions.

The resulting algorithm was subjected to a noise strength sensitivity study, a measurement device precision study, and a study to determine the effects of multiple iterations of the algorithm. The evaluation showed that the algorithm performed well and generated useful results. However, limitations in the current implementation were discovered. As a result of these, the systematic generation of nominal trajectories and elimination of unrealistic output transients were identified as topics for further study.

In developing the algorithm, evaluating its performance, and writing the report, I have had a great deal of assistance. I am deeply indebted to my faculty advisor, Dr. Peter S. Maybeck, without whose assistance and persistence this effort would have been difficult if not impossible to complete. My other thesis committee members,

Dr. Robert A. Calico and Maj. Daniel Gleason, also spent considerable effort on this project, which I gratefully acknowledge. I am indebted to Col. Daniel J. Biezad for his assistance in reviewing the document. I also wish to thank my supervisor, Mr. Thomas D. Morgan, who made it possible for me to have access to the office during the long evenings and weekends that the work often required; and a fellow AFIT student, Mr. John T. Browne, for his many helpful suggestions.

Finally, and most importantly, I wish to thank my parents, Blanche M. Ruley and the late Joseph A. Ruley, MSGT USAF (Ret). Without their encouragement and support throughout my life, this work would never have been attempted.

James M. Ruley

Table of Contents

List of Figures

List of Tables

List of Symbols

Symbol	Definition
$\underline{B}(t)$	Aircraft Control Matrix
$\underline{B}_d(t_i)$	Discretized Aircraft Control Matrix
C	Side Force
D	Drag
E{ }	Expectation Value Operator
$\underline{F}(t)$	Aircraft Plant Matrix
g	Gravitational Acceleration
$\underline{G}(t)$	Dynamic Driving Noise Input Matrix
$\underline{G}_d(t_i)$	Discretized Noise Input Matrix
h	Inertial-axis position coordinate; altitude
$\underline{h}(\underline{x}(t_i), t_i)$	Measurement Model Vector
$\underline{H}(t_i)$	Measurement Matrix, $\partial h/\partial x$
$\underline{I}$	Identity Matrix
$\underline{J}(t_i)$	Backward Filter Gain Matrix (Eq (45))
$\underline{K}(t_i)$	Forward Filter Kalman Gain Matrix
$\underline{K}_u(t_i)$	Smoother Control Input Gain Matrix
L	Lift
$\underline{L}(t_i)$	Backward Filter Gain Matrix (Eq (46))
M	Mass
m	Mean Value
n	Load Factor
$\underline{P}(t_i^-)$	Forward Filter State Covariance Matrix Before Measurement Incorporation

$\underline{P}(t_i^+)$	Forward Filter State Covariance Matrix After Measurement Incorporation
$\underline{P}_b^{-1}(t_i^-)$	Backward Filter Inverse State Covariance Matrix Before Measurement Incorporation
$\underline{P}_b^{-1}(t_i^+)$	Backward Filter Inverse State Covariance Matrix After Measurement Incorporation
$\underline{P}(t_i/t_f)$	Smoothed Estimate of State Covariance Matrix
q_w	Wind-Axis Pitch Rate
$\underline{Q}(t)$	Dynamics Driving Noise Strength Matrix
$\underline{Q}_d(t_i)$	Discretized Dynamics Driving Noise Covariance Matrix
r_w	Wind-Axis Yaw Rate
R	Radar Range
$\underline{R}(t_i)$	Measurement Corruption Noise Covariance Matrix
t_i	Time at iteration i
T	Thrust
T_{x_w}	Thrust Component in X-Wind Axis Direction
T_{y_w}	Thrust Component in Y-Wind Axis Direction
T_{z_w}	Thrust Component in Z-Wind Axis Direction
$\underline{u}(t)$	Control Input Vector; Forcing Function Vector
$\underline{U}_d(t_i/t_f)$	Smoothed Estimate of Control Input Covariance Matrix
$\underline{v}(t_i)$	Measurement Corruption Noise Vector
V	Velocity
V_{x_w}	Wind Velocity Along Inertial X-Axis

V_{y_w}	Wind Velocity Along Inertial Y-Axis
V_{z_w}	Wind Velocity Along Inertial Z-Axis
$\underline{V}(t_i)$	Smoother Gain Matrix (Eq (57))
W	Weight
$\underline{W}(t_i)$	Smoother Gain Matrix (Eq (53))
$\bar{x}_i$	Mean of Variable x_i
$\underline{x}(t)$	Aircraft State Vector
X	Inertial-Axis Position Coordinate
$\underline{X}(t_i)$	Smoother Gain Matrix (Eq (52))
$\hat{\underline{Y}}_b(t_i^-)$	Backward Filter Inverse State Vector Estimate Before Measurement Incorporation
$\hat{\underline{Y}}_b(t_i^+)$	Backward Filter Inverse State Vector Estimate After Measurement Incorporation
Y	Inertial-Axis Position Coordinate
$\underline{Y}(t_i)$	Smoother Gain Matrix (Eq (54))
$\underline{z}(t_i)$	Measurement Vector
Z	Inertial-Axis Position Coordinate
γ	Flight Path Angle; Wind-Axis Pitch Attitude
δ	Perturbation Operator
$\delta(t-t')$	Dirac Delta Function
ϵ	Numerical Tolerance
θ	Radar Azimuth Angle
μ	Wind-Axis Roll Attitude
σ	Standard Deviation
σ_{x_i}	Standard Deviation of Variable x_i
τ	Dummy Argument for Integration

ϕ	Radar Elevation Angle
$\underline{\Phi}(t_{i+1}, t_i)$	State Transition Matrix
χ	Wind-Axis Heading Angle
Δt	Time Step
$\underline{\delta u}_d(t_i)$	Discretized Control Input Perturbation Vector
$\underline{\delta \hat{u}}_d(t_i/t_f)$	Smoothed Estimate of Control Input Perturbation Vector
$\underline{\delta w}(t)$	Dynamic Driving Noise Perturbation Input Vector
$\underline{\delta w}_d(t_i)$	Discretized Dynamic Driving Noise Perturbation Input Vector
$\underline{\delta x}(t_i)$	Discretized State Perturbation Vector
$\underline{\delta \hat{x}}(t_i^-)$	Forward Filter State Estimate Before Measurement Incorporation
$\underline{\delta \hat{x}}(t_i^+)$	Forward Filter State Estimate After Measurement Incorporation
$\underline{\delta \hat{x}}_b(t_i)$	Backward Filter State Vector
$\underline{\delta \hat{x}}(t_i/t_f)$	Smoothed Estimate of State Perturbation Vector
$\underline{\delta z}(t_i)$	Measurement Perturbation
$(\dot{})$	Time Derivative
$()_0$	Nominal Trajectory Subscript
$\frac{\partial()}{\partial()}$	Partial Derivative Operator
$()^T$	Matrix Transpose
$()^{-1}$	Matrix Inverse

Abstract

The purpose of this study was to investigate the potential utility of the linearized Kalman filter-smoother algorithm as a tool for aircraft mishap investigations. The immediate objective was to develop computer software to make possible an investigation of the algorithm's capabilities for generic aircraft trajectories. Other objectives included determination of the sensitivity of the algorithm to noise strength variations, evaluation of its performance with measurement devices of differing precisions, and determination of the potential for iterative improvement of the results. All of these objectives were achieved.

The primary finding of this study was that the linearized Kalman filter-smoother technique is a viable one for mishap trajectory analysis, and that the algorithm as implemented could be useful in actual mishap investigation work.

The study also found that, although the effectiveness of the current algorithm is limited, some of the limitations could be removed through further work. In particular, systematic nominal trajectory generation and control of unrealistic transients in the filter-smoother

output warrant further attention. Suggested methods for addressing these problems are included in the report.

APPLICATION OF LINEARIZED KALMAN FILTER-SMOOTHER TO AIRCRAFT TRAJECTORY ESTIMATION

I. Background and Problem Statement

1.1 Background Information

The Flight Stability and Control Branch at Aeronautical Systems Division (ASD/ENFTC) is often called upon to assist accident boards in aircraft mishap investigations. Support provided by ENFTC has frequently included generation of probable mishap aircraft trajectories, and analysis of known or estimated trajectories to determine probable pilot actions.

This author has expended considerable effort in producing computer software to assist in these tasks. Two major computer programs especially intended for mishap investigation work have been written by the author. The first of these, called PMSIM (point-mass simulation) (Ruley, 1987b) is a three degree-of-freedom, force-equation aircraft model for trajectory generation. It generates the aircraft flight path in inertial space, using initial conditions and forcing functions supplied by the user. The second program,

OPSIM (optimal simulation) (Ruley, 1987a) is a routine to develop forcing functions which attempt to get the PMSIM model states to match a given trajectory closely. The OPSIM program works by varying the forcing functions to attempt to minimize a cost functional, defined as a user-specified combination of the states and time. This procedure is performed for each segment of the trajectory sequentially, until the entire trajectory has been matched.

Both OPSIM and PMSIM have been of assistance to ENFTC engineers in actual mishap investigation work. However, the capability of OPSIM to develop physically reasonable forcing functions is limited by the algorithm it employs. The goal of this algorithm is to produce a computed trajectory which matches each of the trajectory data points exactly, without regard to data noise corruption which is almost always present. This often results in unrealistic variations in the forcing functions. Additionally, there is no quantitative measure of the quality of the trajectory and forcing function data generated.

With these deficiencies in mind, the author considered other methods of attacking the trajectory generation problem. He concluded that stochastic estimation and control methods could be expected to be useful for the problem, since they would explicitly account for noise corruption of both the physical system and the measurement

devices. Additionally, the estimation error covariances of the trajectory states and forcing functions would be computed, and would provide a quantitative measure of the uncertainty in the results.

The author's purpose in this thesis project was to duplicate the function of the OPSIM program using the approach of a fixed-interval, linearized Kalman filter-smoother, and to validate the capabilities of the resulting program. This task is outlined more completely in the following problem statement.

1.2 Problem Statement

The linearized Kalman filter-smoother technique will be applied to the problem of aircraft trajectory estimation in three dimensions. Computer software to perform this task for generic aircraft trajectories will be developed. The potential for improving the match by successive iterations of the filter-smoother algorithm will be investigated. Measures of merit for determining the closeness with which the resulting trajectories match the actual trajectory will be investigated. These will include the filter-smoother state and control perturbations, the diagonal elements of the filter-smoother computed state covariance matrix, and the change in the filter-smoother nominal trajectory from iteration to iteration. A means of estimating the forcing

functions needed to generate the smoothed trajectory, using the filter-smoother output, will be developed.

II. Problem Formulation and Detailed Algorithm Development

2.1 Aircraft Model Formulation

In this section, the force equations for a rigid aircraft moving in three dimensions will be presented, and then linearized to obtain a form which will be shown to be usable in the Kalman filter-smoother algorithm. Additionally, simplifying assumptions and singularities will be discussed.

The coordinate system shown in Figure 1 will be used to develop the aircraft equations of motion. The coordinate axes (X, Y, Z), with origin at the fixed point O, will be referred to as the inertial axes. They form a right-handed coordinate system, with X and Y positive in the "north" and "east" directions, respectively, and Z positive downward. For convenience, the coordinate h, defined by $h = -Z$, will be used for actual computations.

The aircraft center of mass is located at the point P, which becomes the origin for the wind-axis coordinate system (X_w, Y_w, Z_w). These axes are defined so that the X_w-axis is colinear with the aircraft velocity vector, the Y_w-axis is orthogonal to the X_w-axis and lies in the aircraft plane of symmetry, and the Z_w (or h_w) axis lies perpendicular to that plane of symmetry. The orientation of

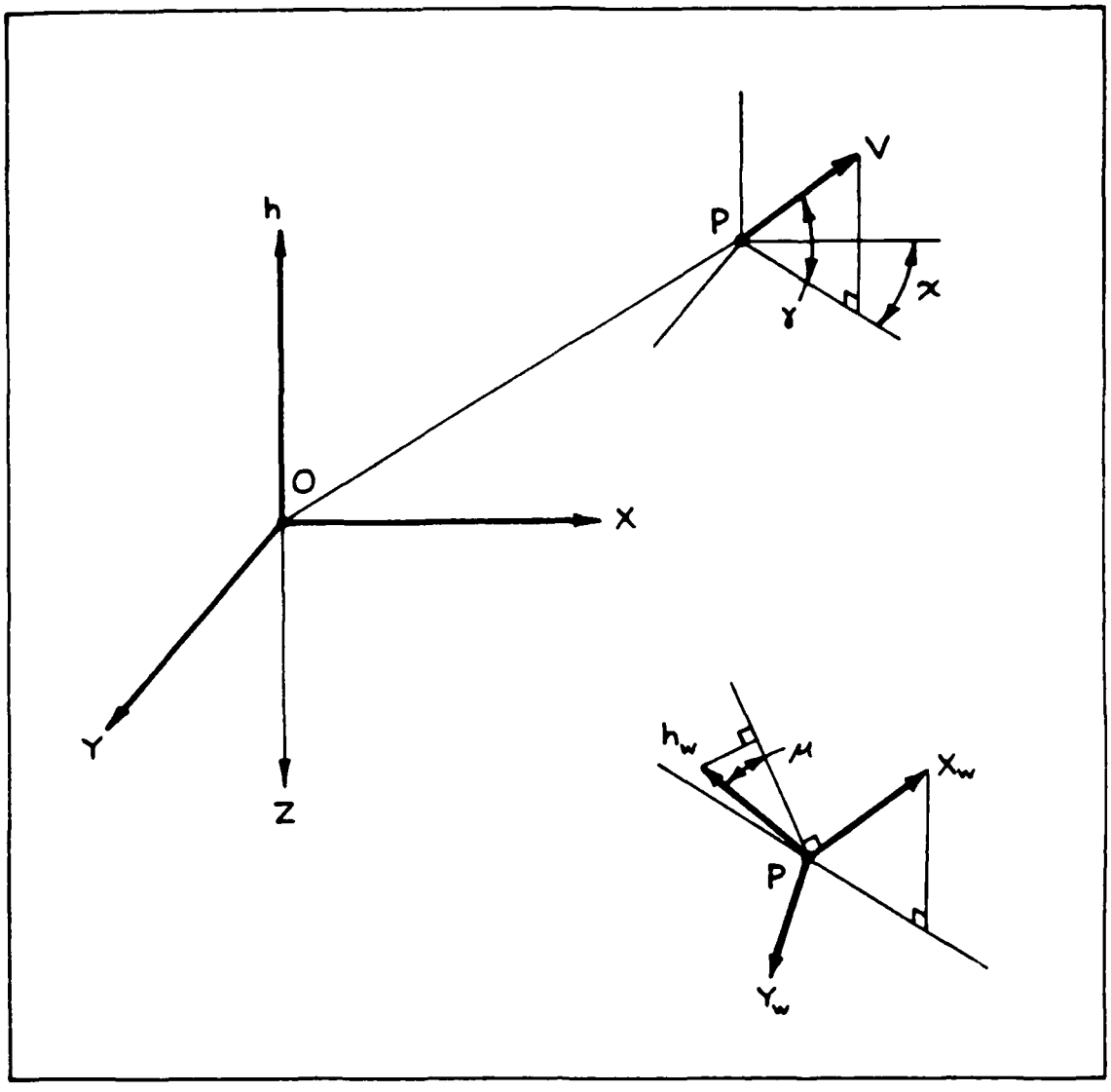

Figure 1. Wind and Inertial-Axis Coordinate Systems

the wind axes with respect to the inertial axes is defined by the Euler angles χ, γ, and μ as follows. Let us first define a set of coordinate axes parallel to the inertial axes but with the origin at point P. This axis system is rotated about the Z-axis until the X-axis lies directly

"underneath" the aircraft velocity vector, forming a "new" set of coordinate axes. This rotation defines the wind-axis heading angle, χ. Next, this "new" set of axes is rotated about its Y-axis until the X-axis becomes colinear with the velocity vector, forming another "new" set of axes. This rotation defines the wind-axis pitch attitude, γ, which is also referred to as the flight path angle. Finally, the "new" axes are rotated about the X-axis until the Z-axis is perpendicular to the aircraft plane of symmetry. This defines the wind-axis roll attitude, μ.

The force equations for a rigid aircraft moving in three dimensions, expressed in the wind-axis coordinate system are (Etkin, 1972: 149):

$$M\dot{V} = T_{x_w} - D - Mg\sin\gamma \tag{1}$$

$$MVr_w = T_{y_w} - C + Mg\cos\gamma\sin\mu \tag{2}$$

$$-MVq_w = T_{z_w} - L + Mg\cos\gamma\cos\mu \tag{3}$$

where:

T_{x_w}, T_{y_w}, T_{z_w} are components of thrust in the directions of the X_w-, Y_w-, and Z_w- axes

L is lift

C is side force

D is drag

M is mass

g is the acceleration due to gravity

V is velocity

q_w is wind-axis pitch rate

r_w is wind-axis yaw rate

($\dot{}$) denotes the time derivative (this symbol will be so used throughout the report).

The kinematic relationships between wind-axis Euler angles and angular rates are given below (Etkin, 1972: 150):

$$\dot{\gamma} = q_w \cos\mu - r_w \sin\mu \tag{4}$$

$$\dot{\chi} = (q_w \sin\mu - r_w \cos\mu)/\cos\gamma \tag{5}$$

For mathematical simplicity, let us now assume that the thrust acts along the X_w- axis, and that side force is negligible, which generally also implies negligible sideslip angle. These assumptions are adequate for a wide variety of trajectory analysis tasks, particularly those in which the aircraft operates at small to moderate angles of attack, does not posess vectored thrust capability, and is equipped with a flight control system providing automatic turn coordination, as is often the case with modern USAF aircraft. With these assumptions, we may write:

$$T_{y_w} = T_{z_w} = 0 \tag{6}$$

$$T_{x_w} = T \tag{7}$$

$$C = 0 \tag{8}$$

where T is the total thrust.

Let us also introduce the following notation:

$$W = Mg \tag{9}$$

$$n = L/W \tag{10}$$

where W is the weight, and n is defined as the load factor.

Using this notation and the assumptions of Eqs (6), (7), and (8), the force equations become:

$$\dot{V} = (g/W)(T - D - W\sin\gamma) \tag{11}$$

$$\dot{\chi} = (ng\sin\mu)/(V\cos\gamma) \tag{12}$$

$$\dot{\gamma} = (g/V)(n\cos\mu - \cos\gamma) \tag{13}$$

The relationships between velocities in the inertial and wind-axis coordinate systems are given below (Etkin, 1972: 150):

$$\dot{X} = V\cos\gamma\cos\chi \tag{14}$$

$$\dot{Y} = V\cos\gamma\sin\chi \tag{15}$$

$$\dot{h} = V\sin\gamma = -\dot{Z} \tag{16}$$

The set of equations given by (11) - (16) may be used to generate aircraft trajectories, given knowledge of the relevant variables, by simultaneous integrations. However, these equations are highly nonlinear. To employ a Kalman filter-smoother algorithm for trajectory analysis, it is advantageous to linearize the trajectory equations about a nominal trajectory. When this is done using a Taylor series expansion, keeping only the linear terms, the results are:

$$\delta\dot{V} = -g\cos\gamma_0\delta\gamma + (g/W)\delta T - (g/W)\left(\frac{\partial D}{\partial V}\delta V + \frac{\partial D}{\partial n}\delta n\right) \tag{17}$$

$$\delta\dot{\gamma} = -(g/V_0^2)(n_0\cos\mu_0 - \cos\gamma_0)\delta V + (g/V_0)\sin\gamma_0\delta\gamma - (n_0 g/V_0)\sin\mu_0\delta\mu + (g/V_0)\cos\mu_0\delta n \tag{18}$$

$$\delta\dot{\chi} = -(n_0 g\sin\mu_0/V_0^2\cos\gamma_0)\delta V + (n_0 g\sin\mu_0\sin\gamma_0/V_0\cos^2\gamma_0)\delta\gamma + (n_0 g\cos\mu_0/V_0\cos\gamma_0)\delta\mu + (g\sin\mu_0/V_0\cos\gamma_0)\delta n \tag{19}$$

$$\delta\dot{h} = \sin\gamma_0\delta V + V_0\cos\gamma_0\delta\gamma \tag{20}$$

$$\delta\dot{Y} = \cos\gamma_0\sin\chi_0\delta V - V_0\sin\gamma_0\sin\chi_0\delta\gamma + V_0\cos\gamma_0\cos\chi_0\delta\chi \tag{21}$$

$$\delta\dot{X} = \cos\gamma_0\cos\chi_0\delta V - V_0\sin\gamma_0\cos\chi_0\delta\gamma - V_0\cos\gamma_0\sin\chi_0\delta\chi \tag{22}$$

where:

the subscript $_0$ refers to the nominal trajectory

$\delta(\ ) = (\ ) - (\ )_0$ is the perturbation of each variable about the nominal trajectory

$\frac{\partial D}{\partial V}$ is the partial derivative of drag with velocity

$\frac{\partial D}{\partial n}$ is the partial derivative of drag with load factor

Eqs (17) - (22) constitute a linearized model for small perturbations about the nominal trajectory. They may be transferred to state-space notation as follows:

$$\underline{\delta\dot{x}}(t) = \underline{F}(t)\underline{\delta x}(t) + \underline{B}(t)\underline{\delta u}(t) \tag{23}$$

where:

$$\underline{\delta x}(t) = [\delta V\ \delta\gamma\ \delta X\ \delta h\ \delta Y\ \delta X]^T \tag{24}$$

$$\underline{\delta u}(t) = [\delta\mu\ \delta n\ \delta T]^T \tag{25}$$

and matrices $\underline{F}(t)$ and $\underline{B}(t)$ are composed of the coefficients of Eqs (17) - (22).

We note that this linearized model contains singularities at $V_0 = 0$ and $\cos\gamma_0 = 0$, i.e. at zero nominal velocity or vertical nominal flight path. The singularity at zero velocity is of no great concern, as this condition is not physically reasonable for heavier-than-air aircraft without vectored thrust. The singularity which

occurs when the flight path becomes vertical is of more concern, but we note that it only occurs in one equation, Eq (19). Therefore, so long as sustained vertical flight is not to be modelled, it is computationally sufficient to avoid this singularity by setting Eq (19) to zero whenever the flight path is "close" to vertical. For computational purposes, this may be done by monitoring the absolute value of $\cos\gamma_0$ and setting $\dot{\chi} = 0$ whenever the absolute value is less than some small tolerance ϵ (ϵ=0.0001 in the implementation used). Of course, this will result in a discontinuity in $\dot{\chi}$ when passing through the vertical, but χ will remain continuous and any resulting effects are not expected to be significant.

This completes the development of the linearized form of the force equations for aircraft trajectory estimation. The Kalman filter-smoother algorithm will now be presented.

2.2 Filter-Smoother Algorithm

Let a discrete-time state perturbation model of an arbitrary physical system be given by:

$$\underline{\delta x}(t_{i+1}) = \underline{\Phi}(t_{i+1}, t_i)\underline{\delta x}(t_i) + \underline{\delta u}_d(t_i) + \underline{\delta w}_d(t_i) \quad (26)$$

where:

$\underline{\delta x}(t_i)$ is the perturbation state vector

$\underline{\delta u}_d(t_i)$ is the perturbation control vector

(Note: this formulation assumes that, with proper discretization, the discretized control input matrix may be set equal to the identity matrix. This is done for reasons of computational convenience which will be discussed later).

$\underline{\delta w}_d(t_i)$ is a perturbation dynamic driving noise input vector, which is assumed to be well represented by discrete-time white Gaussian noise with statistics:

$$E\{\underline{\delta w}_d(t_i)\} = \underline{0} \tag{27}$$

$$E\{\underline{\delta w}_d(t_i)\underline{\delta w}_d{}^T(t_j)\} = \begin{cases} \underline{Q}_d(t_i), & i=j \\ \underline{0}, & i\neq j \end{cases} \tag{28}$$

$\underline{\Phi}(t_{i+1}, t_i)$ is the state transition matrix associated with matrix $\underline{F}(t)$ of Eq (23)

Now let a discrete-time measurement model be given by:

$$\underline{z}(t_i) = \underline{h}(\underline{x}(t_i), t_i) + \underline{v}(t_i) \tag{29}$$

where:

$\underline{z}(t_i)$ is the state measurement vector

$\underline{h}(\underline{x}(t_i), t_i)$ is a vector function representing the measurement device(s)

$\underline{v}(t_i)$ is the measurement corruption noise vector, which is assumed to be well represented by discrete-time white Gaussian noise with statistics:

$$E\{\underline{v}(t_i)\} = \underline{0} \tag{30}$$

$$E\{\underline{v}(t_i)\underline{v}^T(t_j)\} = \begin{cases} \underline{R}(t_i), & i=j \\ \underline{0}, & i \neq j \end{cases} \tag{31}$$

Assuming that a nominal trajectory is available, along with measurements, a measurement perturbation $\underline{\delta z}(t_i)$ may be defined in a manner analogous to the state perturbation, using a Taylor series expansion:

$$\underline{z}(t_i) = \underline{z}_0(t_i) + \left.\frac{\partial \underline{h}(\underline{x}(t_i), t_i)}{\partial \underline{x}(t_i)}\right|_{\underline{x}_0(t_i)} \underline{\delta x}(t_i) + \underline{v}(t_i) \tag{32}$$

or equivalently, in terms of $\underline{\delta z}(t_i) = \underline{z}(t_i) - \underline{z}_0(t_i)$:

$$\underline{\delta z}(t_i) = \underline{H}(t_i)\underline{\delta x}(t_i) + \underline{v}(t_i) \tag{33}$$

where $\underline{H}(t_i)$ is the measurement matrix, which is a function of the nominal trajectory states and time, as shown.

To generate a time history of the measurement perturbation $\underline{\delta z}(t_i)$ for purposes of computation, we apply Eq (29) to obtain:

$$\underline{\delta z}(t_i) = \underline{z}(t_i) - \underline{h}(\underline{x}_0(t_i), t_i) \tag{34}$$

where:

$\underline{z}(t_i)$ is the actual measurement time history

$\underline{h}(\underline{x}_0(t_i), t_i)$ is a measurement representation based on the nominal trajectory and is assumed to be error-free, since it is assumed that the nominal trajectory was generated in a deterministic, noise-free manner.

Therefore, the measurement perturbation time history may be assumed to have the same noise statistics as the measurement time history itself, provided that the first-order Taylor series expansion itself introduces no significant additional noise corruption. Accordingly, Eqs (30) and (31) describe the error statistics of the measurement perturbation, as well as the measurement itself.

Given Eqs (26) - (34), the Fraser form of the equations for a fixed-interval filter-smoother algorithm may be formulated (Maybeck, 1982: 9-11). Note that in these

equations, we have set $\underline{B}_d(t_i) = \underline{G}_d(t_i) = \underline{I}$ (the identity matrix), as shown in the state model given by Eq (26). With this assumption, the filter-smoother algorithm is given by the equations below. (Note that it is possible to use filter algorithms of a different computational form, such as U-D factorization or square root (Maybeck, 1979: 368-405), if computer numerical accuracy limitations require it. This was not required in the current implementation.)

a) Forward Filter:

i) Propagation cycle:

$$\underline{\delta\hat{x}}(t_{i+1}^-) = \underline{\Phi}(t_{i+1}, t_i)\underline{\delta\hat{x}}(t_i^+) + \underline{\delta u}_d(t_i) \quad (35)$$

$$\underline{P}(t_{i+1}^-) = \underline{\Phi}(t_{i+1}, t_i)\underline{P}(t_i^+)\underline{\Phi}^T(t_{i+1}, t_i) + \underline{Q}_d(t_i) \quad (36)$$

ii) Measurement update:

$$\underline{K}(t_i) = \underline{P}(t_i^-)\underline{H}^T(t_i)[\underline{H}(t_i)\underline{P}(t_i^-)\underline{H}^T(t_i) + \underline{R}(t_i)]^{-1} \quad (37)$$

$$\underline{\delta\hat{x}}(t_i^+) = \underline{\delta\hat{x}}(t_i^-) + \underline{K}(t_i)[\underline{\delta z}(t_i) - \underline{H}(t_i)\underline{\delta\hat{x}}(t_i^-)] \quad (38)$$

$$\underline{P}(t_i^+) = \underline{P}(t_i^-) - \underline{K}(t_i)\underline{H}(t_i)\underline{P}(t_i^-) \quad (39)$$

where $\underline{P}(t_k)$ is the state covariance matrix, and the superscripts - and + refer to before and after measurement incorporation, respectively.

The forward filter is iterated forward in time (increasing k) from the following initial conditions:

$$\underline{\delta\hat{x}}(t_0) = \underline{0} \tag{40}$$

$$\underline{P}(t_0) = \underline{P}_0 \tag{41}$$

$$\underline{\delta u}_d(t_i) = \underline{0} \quad \text{(all i)} \tag{42}$$

where $\underline{P}_0$ is a matrix of assumed initial values for the covariance, and Eq (42) will be shown to hold true later.

b) Backward Filter:

i) Measurement update:

$$\hat{\underline{Y}}_b(t_i^+) = \hat{\underline{Y}}_b(t_i^-) + \underline{H}^T(t_i)\underline{R}^{-1}(t_i)\underline{\delta z}(t_i) \tag{43}$$

$$\underline{P}_b^{-1}(t_i^+) = \underline{P}_b^{-1}(t_i^-) + \underline{H}^T(t_i)\underline{R}^{-1}(t_i)\underline{H}(t_i) \tag{44}$$

ii) Propagation cycle:

$$\underline{J}(t_i) = \underline{P}_b^{-1}(t_i^+)[\underline{P}_b^{-1}(t_i^+) + \underline{Q}_d^{-1}(t_{i-1})]^{-1} \tag{45}$$

$$\underline{L}(t_i) = \underline{I} - \underline{J}(t_i) \tag{46}$$

$$\hat{\underline{Y}}_b(t_{i-1}^-) = \underline{\Phi}^T(t_i, t_{i-1})\underline{L}(t_i)[\hat{\underline{Y}}_b(t_i^+) - \underline{P}_b^{-1}(t_i^+)\underline{\delta u}_d(t_{i-1})] \tag{47}$$

$$\underline{P}_b^{-1}(t_{i-1}^-) = \underline{\Phi}^T(t_i, t_{i-1})[\underline{L}(t_i)\underline{P}_b^{-1}(t_i^+)\underline{L}^T(t_i) + \underline{J}(t_i)\underline{Q}_d^{-1}(t_{i-1})\underline{J}^T(t_i)]\underline{\Phi}(t_i, t_{i-1}) \tag{48}$$

where, for either t_k^- or t_k^+ :

$$\hat{\underline{Y}}_b(t_i) = \underline{P}_b^{-1}(t_i)\underline{\delta\hat{x}}_b(t_i) \tag{49}$$

and $\underline{\delta\hat{x}}_b(t_i)$ is the backward filter state perturbation estimate (which is never actually computed in this formulation).

The backward filter is iterated backward in time (decreasing k) for the following final conditions:

$$\hat{\underline{Y}}_b(t_f^-) = \underline{0} \tag{50}$$

$$\underline{P}_b^{-1}(t_f^-) = \underline{0} \tag{51}$$

$$\underline{\delta u}_d(t_i) = \underline{0} \quad \text{(all i)} \tag{42}$$

where Eqs (50) and (51) express the fact that the final state is not known a priori.

c) Smoothed Estimate:

i) State Perturbation Gain Computation:

$$\underline{X}(t_i) = [\underline{I} + \underline{P}(t_i^+)\underline{P}_b^{-1}(t_i^-)]^{-1} \tag{52}$$

$$\underline{W}(t_i) = \underline{P}(t_i^+)\underline{X}^T(t_i) \tag{53}$$

$$\underline{Y}(t_i) = \underline{I} - \underline{W}(t_i)\underline{P}_b^{-1}(t_i^-) \tag{54}$$

ii) State Perturbation Estimate:

$$\underline{P}(t_i/t_f) = \underline{Y}(t_i)\underline{P}(t_i^+)\underline{Y}^T(t_i) + \underline{W}(t_i)\underline{P}_b^{-1}(t_i^-)\underline{W}^T(t_i) \tag{55}$$

$$\underline{\delta\hat{x}}(t_i/t_f) = \underline{X}(t_i)\underline{\delta\hat{x}}(t_i^+) + \underline{P}(t_i/t_f)\hat{\underline{Y}}_b(t_i^-) \tag{56}$$

iii) Control Gain Computation:

$$\underline{V}(t_i) = \underline{Q}_d(t_i)\underline{\Phi}^T(t_i, t_{i+1}) = \underline{Q}_d(t_i)[\underline{\Phi}^{-1}(t_{i+1}, t_i)]^T \quad (57)$$

$$\underline{K}_u(t_i) = \underline{V}(t_i)\underline{X}^T(t_i) \quad (58)$$

iv) Control Perturbation Estimate:

$$\underline{\delta\hat{u}}_d(t_i/t_f) = \underline{\delta u}_d(t_i) + \underline{K}_u(t_i)[\underline{\hat{y}}_b(t_i^-) - \underline{P}_b^{-1}(t_i^-)\underline{\delta\hat{x}}(t_i^+)] \quad (59)$$

$$\underline{U}_d(t_i/t_f) = \underline{Q}_d(t_i) - \underline{V}(t_i)\underline{P}_b^{-1}(t_i^-)\underline{K}_u^T(t_i) \quad (60)$$

where $\underline{U}_d(t_i/t_f)$ is the smoothed estimate of the covariance of the control perturbation $\underline{\delta\hat{u}}_d(t_i/t_f)$.

The smoothed estimate is iterated forward in time (increasing k), in parallel with the forward filter if so desired, after all elements of the backward filter results have been computed and stored in memory. The assumption of Eq (42) is also used in the smoother, and is applied in Eq (59).

This completes the presentation of the Kalman filter-smoother algorithm. We will now see how the perturbation state model developed in Eqs (17) - (23) may be adapted to this algorithm.

2.3 Filter-Smoother Applied to the Aircraft Model

In this section, the perturbation state model for the aircraft will be shown to be compatible with the filter-smoother algorithm, thus forming a complete algorithm for trajectory analysis. Let us begin by restating the state-space form of the perturbation state model, given in Eq (23):

$$\underline{\delta\dot{x}}(t) = \underline{F}(t)\underline{\delta x}(t) + \underline{B}(t)\underline{\delta u}(t) \tag{23}$$

This is the model of the aircraft when subjected to deterministic inputs only. Dynamics driving noise terms, which would be due in the physical world to such effects as wind gusts, turbulence, control system dynamics, and pilot inputs, may also be present. They may be accounted for in the following manner. Let us first deal with wind gusts directly, assuming that the wind vector has components V_{x_w}, V_{y_w}, and V_{z_w}. Eqs (14) - (16) become:

$$\dot{X}' = V\cos\gamma\cos\chi + V_{x_w} \tag{61}$$

$$\dot{Y}' = V\cos\gamma\sin\chi + V_{y_w} \tag{62}$$

$$\dot{h}' = V\sin\gamma - V_{z_w} \tag{63}$$

With the addition of these wind components, Eqs (20) - (22) become:

$$\delta\dot{h}' = \delta\dot{h} - \delta V_{z_w} \tag{64}$$

$$\delta\dot{Y}' = \delta\dot{Y} + \delta V_{y_w} \tag{65}$$

$$\delta\dot{X}' = \delta\dot{X} + \delta V_{x_w} \tag{66}$$

Let us now add noise inputs to Eqs (17) - (19), assuming for computational convenience that the noises are added at the points of entry of the deterministic controls. The equations become:

$$\delta\dot{V}' = \delta\dot{V} - (g/W)\frac{\partial D}{\partial n}\delta w_2(t) + (g/W)\delta w_3(t) \tag{67}$$

$$\delta\dot{\gamma}' = \delta\dot{\gamma} - (n_0 g/V_0)\sin\mu_0 \delta w_1(t) + (g/V_0)\cos\mu_0 \delta w_2(t) \tag{68}$$

$$\delta\dot{\chi}' = \delta\dot{\chi} + (n_0 g\cos\mu_0/V_0\cos\gamma_0)\delta w_1(t) + (g\sin\mu_0/V_0\cos\gamma_0)\delta w_2(t) \tag{69}$$

where $\delta w_1(t)$, $\delta w_2(t)$, and $\delta w_3(t)$ are the dynamics driving noise components added. These noises are not as easily related to the physical world as wind gust inputs, but

certainly it is reasonable to assume that actual noise sources such as turbulence and control system effects could be considered to manifest themselves in this manner. If the wind gust inputs are now identified as additional components of the noise perturbation input vector $\underline{\delta w}(t)$, the state-space model given in Eq (23) (dropping the primed notation) may be rewritten as:

$$\underline{\delta \dot{x}}(t) = \underline{F}(t)\underline{\delta x}(t) + \underline{B}(t)\underline{\delta u}(t) + \underline{G}(t)\underline{\delta w}(t) \qquad (70)$$

Let us assume that the noise perturbation $\underline{\delta w}(t)$ is well represented by white Gaussian noise, with statistics:

$$E\{\underline{\delta w}(t)\} = \underline{0} \qquad (71)$$

$$E\{\underline{\delta w}(t)\underline{\delta w}^T(t')\} = \underline{Q}(t)\,\delta(t-t') \qquad (72)$$

where $\delta(t-t')$ is the Dirac delta function, and $\underline{Q}(t)$ is the noise strength matrix.

The effects of non-white Gaussian noise, or non-Gaussian-distributed noise, will not be examined in this thesis. It is considered sufficient for the purposes of this study to consider only Gaussian noise, as the central limit theorem implies that noise sources in the physical world tend to be describable, or at least well approximated, as Gaussian (Maybeck, 1979: 109). Moreover, the low-pass filtering characteristics of real-world systems tend to make

possible the assumption that input noise is white (Maybeck, 1979: 7-8). Should a noise input structure which more exactly describes the noise input's time correlatedness be required, shaping filters (Maybeck, 1979: 180-190) of appropriate form could be developed and the necessary additional states added to the system model, but this will not be pursued further here.

Let us now consider how Eq (70) may be discretized in order to perform a solution on a digital computer. Suppose we assume that $\underline{\delta u}(t)$ is to be held constant over a small time interval, denoted by $\Delta t = t_{i+1} - t_i$. This assumption is not very restrictive, as Δt may be set to a small enough value to justify it for any particular problem. With this assumption, the discretized form of Eq (70) may be written as:

$$\underline{\delta x}(t_{i+1}) = \underline{\Phi}(t_{i+1}, t_i)\underline{\delta x}(t_i) + \int_{t_i}^{t_{i+1}} \underline{\Phi}(t_{i+1}, \tau)\underline{B}(\tau)\underline{\delta u}(\tau)d\tau + \int_{t_i}^{t_{i+1}} \underline{\Phi}(t_{i+1}, \tau)\underline{G}(\tau)\underline{\delta w}(\tau)d\tau \quad (73)$$

(in the non-rigorous white noise notation) or, more simply:

$$\underline{\delta x}(t_{i+1}) = \underline{\Phi}(t_{i+1}, t_i)\underline{\delta x}(t_i) + \underline{\delta u}_d(t_i) + \underline{\delta w}_d(t_i) \quad (74)$$

where:

$$\underline{\delta u}_d(t_i) = \int_{t_i}^{t_{i+1}} \underline{\Phi}(t_{i+1}, \tau)\underline{B}(\tau)\underline{\delta u}(\tau)d\tau \tag{75}$$

$$\underline{\delta w}_d(t_i) = \int_{t_i}^{t_{i+1}} \underline{\Phi}(t_{i+1}, \tau)\underline{G}(\tau)\underline{\delta w}(\tau)d\tau \tag{76}$$

and $\underline{\delta w}_d(t_i)$ has statistics given by (Maybeck, 1979: 171):

$$E\{\underline{\delta w}_d(t_i)\} = \underline{0} \tag{77}$$

$$E\{\underline{\delta w}_d(t_i)\underline{\delta w}_d{}^T(t_j)\} = \begin{cases} \underline{Q}_d(t_i), & i=j \\ \underline{0}, & i\neq j \end{cases} \tag{78}$$

where:

$$\underline{Q}_d(t_i) = \int_{t_i}^{t_{i+1}} \underline{\Phi}(t_{i+1}, \tau)\underline{G}(\tau)\underline{Q}(\tau)\underline{G}^T(\tau)\underline{\Phi}^T(t_{i+1}, \tau)d\tau \tag{79}$$

Now, in order to evaluate the state transition matrix and the various integrals on a digital computer, approximations must be made. For a time step Δt which is

sufficiently small compared to the system's natural transients, the state transition matrix may be evaluated as follows (Maybeck, 1979: 357):

$$\underline{\Phi}(t_i, t_{i-1}) \approx \sum_{k=0}^{N} \frac{1}{k!} [\underline{F}(t_{i-1})]^k (\Delta t)^k \tag{80}$$

N, the number of terms to which the series is actually taken for evaluation, must be set to yield the desired accuracy. It is uncommon to take N to be greater than two, since Δt may be chosen appropriately small for any desired problem. N = 2 was chosen for this particular implementation.

The integral in Eq (75) may be evaluated, using the trapezoidal rule, as follows:

$$\underline{\delta u}_d(t_i) \approx \frac{1}{2}[\underline{\Phi}(t_{i+1}, t_i)\underline{B}(t_i)\underline{\delta u}(t_i) + \underline{B}(t_{i+1})\underline{\delta u}(t_{i+1})]\Delta t \tag{81}$$

Note that for the chosen perturbation form of the model, however, that $\underline{\delta u}_d(t_i) = \underline{0}$ for all i. This is true because Eq (81) will always yield a zero result, since each term includes a factor of $\underline{\delta u}(t_i)$, and no deterministic control input perturbations are made. This demonstrates the validity of the assumption made in Eq (42).

Finally, the discrete noise strength matrix $\underline{Q}_d(t_i)$ (Eq (79)) may itself be evaluated using the trapezoidal rule, to yield (Maybeck, 1979: 358):

$$\underline{Q}_d(t_i) = \frac{1}{2}[\underline{\Phi}(t_{i+1}, t_i)\underline{G}(t_i)\underline{Q}(t_i)\underline{G}^T(t_i)\underline{\Phi}^T(t_{i+1}, t_i) + \underline{G}(t_{i+1})\underline{Q}(t_{i+1})\underline{G}^T(t_{i+1})]\Delta t \quad (82)$$

The model of the aircraft is now in the required form for estimation using the filter-smoother algorithm. Eq (74) is of the same form as Eq (26), and means of evaluating the state transition matrix and discrete noise strength matrix have been presented in Eqs (80) and (82).

To complete the set of equations needed to implement the filter-smoother, it is necessary to establish a measurement model of the form given in Eq (29). Such a model can be developed, on a case-by-case basis, from physical descriptions of the measurement devices available. For example, a tracking radar might be used to measure range, range rate, elevation angle, and azimuth angle data, which may be expressed as functions of the inertial coordinates X, Y, and h through the function $\underline{h}(\underline{x}(t_i), t_i)$. Alternatively, a head-up display (HUD) device in the aircraft itself might be capable of recording velocity, flight path angle, and heading angle data, which might be usable directly or might need to be corrected for angle of attack and sideslip angle. The statistics of the various

noise processes involved would have to be considered in developing the matrix $\underline{R}(t_i)$ in Eq (31). For the purposes of this section, however, it is sufficient to assume that a measurement model exists or may be developed. The white noise assumption for measurement corruption noise is good if the measurement sample period is long compared to the noise correlation time, which is a rather nonrestrictive condition.

One aspect of the trajectory analysis problem remains to be addressed, which is the estimation of control input perturbations using the filter-smoother output. This is an important part of the problem, as the magnitude of such estimates gives an indication of both the correctness of the nominal control inputs used to generate the trajectory, and the amount of input noise corruption present. Returning to Eq (75) for $\underline{\delta u}_d(t_i)$, we see that an alternative approximation for this integral, good to first order in Δt, is given by:

$$\underline{\delta u}_d(t_i) \approx \underline{B}(t_i)\underline{\delta u}(t_i)\Delta t \tag{83}$$

for a time step Δt which is sufficiently small in comparison to the system's natural transients. Expanding Eq (83), we obtain:

$$\delta u_{d_1}(t_i) = [-(g/W)\frac{\partial D}{\partial n}\delta n(t_i) + (g/W)\delta T]\Delta t \quad (84)$$

$$\delta u_{d_2}(t_i) = [-(n_0 g/V_0)\sin\mu_0\,\delta\mu(t_i) + (g/V_0)\cos\mu_0\,\delta n(t_i)]\Delta t \quad (85)$$

$$\delta u_{d_3}(t_i) = [(n_0 g\cos\mu_0/V_0\cos\gamma_0)\delta\mu(t_i) + (g\sin\mu_0/V_0\cos\gamma_0)\delta n(t_i)]\Delta t \quad (86)$$

$$\delta u_{d_4}(t_i) = \delta u_{d_5}(t_i) = \delta u_{d_6}(t_i) = 0 \quad (87)$$

Eqs (84) - (86) may be solved to obtain $\delta\mu(t_i)$, $\delta n(t_i)$, and $\delta T(t_i)$ in terms of $\delta u_{d_1}(t_i)$, $\delta u_{d_2}(t_i)$, and $\delta u_{d_3}(t_i)$, which are estimated directly by the filter-smoother. The results are:

$$\delta\mu(t_i) = (1/n_0)[-(V_0\sin\mu_0/g\Delta t)\delta u_{d_2}(t_i) + (V_0\cos\mu_0\cos\gamma_0/g\Delta t)\delta u_{d_3}(t_i)] \quad (88)$$

$$\delta n(t_i) = (V_0\cos\mu_0/g\Delta t)\delta u_{d_2}(t_i) + (V_0\cos\gamma_0\sin\mu_0/g\Delta t)\delta u_{d_3}(t_i) \quad (89)$$

$$\delta T(t_i) = (W/g\Delta t)\delta u_{d_1}(t_i) + \frac{dD}{dn}[(V_0\cos\mu_0/g\Delta t)\delta u_{d_2}(t_i) + (V_0\cos\gamma_0\sin\mu_0/g\Delta t)\delta u_{d_3}(t_i)] \quad (90)$$

Eqs (87) - (89) may be used to estimate the control perturbation inputs. The singularity at zero nominal normal acceleration in Eq (87) may be handled computationally by setting $\delta\mu(t_i)$ to zero for cases where n_0 is within a small

tolerance of zero. This assumes, of course, that sustained zero-g flight is not to be modelled.

This completes the development of the algorithm for trajectory estimation using the linearized Kalman filter-smoother. The following chapters will address details of the actual implementation used, and the results obtained.

III. Detailed Analysis Procedure

3.1 Details of Implementation

The linearized Kalman filter-smoother algorithm developed in Chapter II was implemented on the CDC Cyber computer at the Wright-Patterson Air Force Base Computer Center. Other programs were also developed or modified to support the filter-smoother. These include the author's three degree-of-freedom, force-equation aircraft trajectory program (PMSIM), previously described in Section 1.1, which was modified to generate nominal trajectory data, "true" trajectories which incorporated dynamics driving noise but no measurement corruption noise, and measurement time histories which incorporated both types of noise. Programs to plot various data as functions of time were also created. Data which could be plotted included the nominal, true, measured, and smoothed trajectories, the difference between the smoothed and true trajectories, the filter-smoother state and control perturbations, and the diagonal elements of the covariances computed by the filter-smoother and the forward filter. Certain of the plotting programs computed the temporal mean and standard deviation of each of the variables displayed, using the equations:

$$\bar{x}_i = \frac{1}{N} \sum_{k=1}^{N} x_i(t_k) \tag{91}$$

$$\sigma_{x_i} = \left(\frac{1}{N-1}\right)\left(\sum_{k=1}^{N} (x_i(t_k) - x_i)^2\right)^{1/2} \tag{92}$$

Provisions were also made for successive iterations of the filter-smoother algorithm. The approach taken was to use the results of each filter-smoother run to "correct" the computed nominal trajectory for the next run. In order to make such iterations possible, three different procedures for generating nominal trajectories were implemented. The first of these was to generate the nominal trajectory using the PMSIM program, with control input functions produced by subroutines within PMSIM. This method was always used to generate the nominal trajectory for the first run of a set of iterations. It was also used to generate true and measured trajectories, with noise corruption added at appropriate points. The second nominal trajectory generation method was to use the filter-smoother output to set the initial conditions and provide the control input functions, by summing the preceding nominal control input time history and the estimated control perturbations. The PMSIM program was then used to generate the next nominal trajectory. This technique was used for a majority of the iterations which were actually performed. An alternative

method was simply to use the smoothed trajectory, defined as the nominal trajectories of both states and controls plus the associated perturbations output by the filter-smoother, as the nominal trajectory for the next run, and provision was also made for use of this technique.

3.2 Specific Trajectories Used

Three different trajectories were used during the evaluation of filter-smoother performance. These trajectories were designed to represent plausible aircraft mishap scenarios. The various measurement models used with these trajectories are described in Section 3.3. Dynamics driving noise strength and measurement corruption noise values used in these models are noted in Sections 4.1 and 4.2.

The first trajectory, hereafter referred to as Trajectory 1, was used for the initial phase of the evaluation. It was deliberately designed to be fairly "benign", incorporating no roll attitudes or flight path angles greater than 45 deg. It basically consisted of a roll to 45 deg roll attitude, with a time-varying load factor which peaked at 5.5, followed by a relaxation of load factor to 0.1 and a descent to zero altitude. Constant thrust was maintained throughout this trajectory. Figure 2 is a plot of the true states and control input functions for this trajectory, with a representative set of measurements

also shown. (These measurements were taken using measurement model FS-1, defined in Section 4.2, which assumes all states are directly measurable. More realistic measurement models were used later in the study, and are defined in Sections 3.3 and 4.2.) Figure 2, along with all others showing trajectory time history data, may be found in the Appendix.

Trajectory 2 was a more aggressive profile, roughly simulating a tactical bomb run with a recovery attempt which failed to prevent descent below zero altitude. In this scenario, the aircraft started out in level flight at a fairly low altitude, was pulled up to a shallow flight path angle, rolled to the inverted position, allowed to decrease flight path angle until altitude was being lost, rolled back upright, and then a pullout was initiated which was unable to prevent zero altitude penetration. Thrust was adjusted to maintain a relatively constant velocity during the maneuver. Figure 3 displays the true states and control input functions for this trajectory. Representative measurements, again simulated using measurement model FS-1, are also shown in the figure.

Trajectory 3 was the most severe profile used in the evaluation, and was deliberately intended to test the behavior of the algorithm in the neighborhood of singular points in the linearized model. This flight path began in level flight. The aircraft was then pulled up through the

vertical, and the pull was continued until it was flying upside down on a heading opposite the original one. A series of rolls was then begun, and continued until the aircraft descended below zero altitude, which occurred after the third roll was complete. Thrust was held constant throughout the maneuver. Figure 4 plots the true states and control inputs for this trajectory, as well as representative measurements from measurement model FS-1. In this figure, the reader will note what appears to be a change in the noise corruption magnitude in normal acceleration during the middle portion of the trajectory. This is due to the simulated aircraft reaching its angle-of-attack limit during this portion of the trajectory, and not to any real change in the noise corruption amplitude.

The same aircraft model (the PMSIM program, ref. Ruley, 1987b) was used to generate all three trajectories. Data used for this model are representative of a modern twin-engine tactical fighter in an air-to-ground attack configuration. Due to the complexity of the model and the fact that it was not an integral part of the filter-smoother algorithm, it will not be further discussed in this report.

3.3 Measurement Models

Three mathematical models were developed to simulate different measurement devices during the study of

filter-smoother performance. The first of these was a full-state model, where measurements of all states were assumed to be directly measurable. This is probably not representative of any actual device, but was selected by the author as an easily programmed first case. This model was defined by the following equations:

$$\underline{z}(t_i) = \underline{x}(t_i) + \underline{v}(t_i) \tag{93}$$

$$\underline{H}(t_i) = \underline{I} \tag{94}$$

where the error characteristics of the measurement corruption noise vector are defined as in Eqs (30) and (31). The measurement error covariance magnitudes were set on a case-by-case basis and are tabulated in Sections 4.1 and 4.2.

The second model was created to simulate a ground-based radar measuring aircraft position only. The equations used for this model were:

$$z_1 = R = (h^2 + Y^2 + X^2)^{1/2} + v_R \tag{95}$$

$$z_2 = \phi = \sin^{-1}(h/R) + v_\phi \tag{96}$$

$$z_3 = \theta = \tan^{-1}(Y/X) + v_\theta \tag{97}$$

where:

R is radar range

ϕ is elevation angle

θ is azimuth angle

and the measurement noise statistics and covariance are defined as they were for the previous model. Again, measurement corruption noise covariance values used with this model are tabulated in Sections 4.1 and 4.2 on a case-by-case basis.

From these equations, the components of the measurement matrix (see Eqs (29) and (34)) are given by:

$$h_{14} = \frac{\partial R}{\partial h} = h/R \tag{98}$$

$$h_{15} = \frac{\partial R}{\partial Y} = Y/R \tag{99}$$

$$h_{16} = \frac{\partial R}{\partial X} = X/R \tag{100}$$

$$h_{24} = \frac{\partial \phi}{\partial h} = [R/(R-h)]^{1/2}(1/R) \tag{101}$$

$$h_{25} = \frac{\partial \phi}{\partial Y} = [R/(R-h)]^{1/2}(-hY/R^3) \tag{102}$$

$$h_{26} = \frac{\partial \phi}{\partial X} = [R/(R-h)]^{1/2}(-hX/R^3) \tag{103}$$

$$h_{34} = \frac{\partial \theta}{\partial h} = 0 \tag{104}$$

$$h_{35} = \frac{\partial \theta}{\partial Y} = [X/(X^2 + Y^2)] \tag{105}$$

$$h_{36} = \frac{\partial \theta}{\partial X} = [-Y/(X^2 + Y^2)] \qquad (106)$$

where the symbols are as defined above and in Chapter II. All other elements of the measurement matrix are zero.

The reader will note that the measurement matrix defined above has elements which are singular at zero range and where range is equal to the altitude of the aircraft. These singularities make physical sense. At zero range, elevation angle and azimuth angle are undefined, and therefore the change in these quantities with position is also undefined. Further, at zero range the Cartesian position coordinates are also zero, and the change in range with position coordinates becomes undefined, as seen from the form of Eqs (98) - (100). When range equals altitude, the aircraft must be directly over the radar, i.e. at an elevation angle of 90 deg. For this condition the azimuth angle becomes undefined, and the Cartesian coordinates X and Y become zero. Therefore, the change in azimuth angle with Cartesian position coordinates becomes undefined, and Eqs (101) - (103) show that the change in elevation with these position coordinates is also undefined. The change in range with altitude becomes unity, since range equals altitude, and the changes in range with X and Y become zero, as seen in Eqs (99) and (100).

Computationally, this problem was solved in the following manner. The magnitudes of range and the difference of range and altitude were computed along with the elements of the measurement matrix. If the range R was less than a small tolerance value (0.0001 in the implementation used), all elements of the measurement matrix were set to zero. If the range was nonzero but the magnitude of the difference of range and altitude was less than the tolerance, then the (1,4) element of the measurement matrix was set to unity and all other matrix elements were set to zero.

The third measurement model developed was a modification of the radar position model, in which range rate information was also assumed to be available (perhaps from a Doppler radar). The additional equations required to implement this feature were:

$$z_4 = \dot{R} = (1/R)(h\dot{h} + Y\dot{Y} + X\dot{X}) \tag{107}$$

$$h_{41} = \frac{\partial \dot{R}}{\partial V} = \dot{R}/V \tag{108}$$

$$h_{42} = \frac{\partial \dot{R}}{\partial \gamma} = (V/R)[h\cos\gamma - (Y\sin\chi + X\cos\chi)\sin\gamma] \tag{109}$$

$$h_{43} = \frac{\partial \dot{R}}{\partial \chi} = (V/R)[(Y\cos\chi - X\sin\chi)\cos\gamma] \tag{110}$$

$$h_{44} = \frac{\partial \dot{R}}{\partial h} = (\dot{h}/R) - (h\dot{R}/R^2) \tag{111}$$

$$h_{45} = \frac{\partial \dot{R}}{\partial Y} = (\dot{Y}/R) - (Y\dot{R}/R^2) \qquad (112)$$

$$h_{46} = \frac{\partial \dot{R}}{\partial X} = (\dot{X}/R) - (X\dot{R}/R^2) \qquad (113)$$

where all variables remain defined as above, and the measurement noise statistics and covariance are defined as they were for both previous models. Measurement corruption noise covariance values which were used are again tabulated in Sections 4.1 and 4.2 on a case-by-case basis.

These equations were used together with Eqs (95) - (106) to implement the radar model with range rate. Again, singularities existed at zero range. Physically, these corresponded to the inability of the radar to resolve position coordinates at zero range, as discussed above for the previous model. Computationally, they were handled in the same manner as for the radar without range rate.

3.4 Chapter Summary

This chapter discusses details of the implementation of the filter-smoother algorithm, describes three trajectories used for algorithm performance analysis, and discusses the three measurement models used in this analysis. Implementation details given include descriptions of the process used to generate nominal, "true", and

measured trajectories, as well as procedures used for successive iterations of the filter-smoother algorithm. Discussion of the trajectories used includes a description of the rationale behind their choice, and a description of the control inputs and resulting aircraft motions for each one. The measurement models are fully defined mathematically, and both the physical meanings of singularities and computational procedures for handling them are given.

IV. Performance Evaluation

The evaluation of filter-smoother algorithm performance included three detailed studies. The first of these, a robustness study, was intended to investigate how well the algorithm would perform when the filter-smoother's assumed dynamics driving noise strength and measurement corruption noise covariance were perturbed away from the values used to generate the true trajectory. The idea behind this study was to determine how closely the true and assumed noise magnitudes needed to be matched to obtain good performance. The second study, a measurement precision effects evaluation, was meant to determine the effect on the algorithm of changes in the actual measurement corruption noise covariances, which remained matched to the values assumed by the filter-smoother. This corresponded physically to the use of various measurement devices of differing accuracy. Both of these studies considered only one iteration of the algorithm. The third part of the evaluation was an investigation of the effects of various schemes for successive filter-smoother iterations, which were anticipated to improve the correspondence between the smoothed and true trajectories.

4.1 Robustness Study

The purpose of this study was to examine the sensitivity of the filter-smoother to perturbations of the components of the dynamics driving noise strength and measurement corruption noise covariance matrices assumed by the algorithm, while keeping the corresponding variances in the "true" trajectory generation program constant. The intention was to see how closely the true and assumed noise magnitudes needed to be matched for good performance. The approach taken was to use the filter-smoother to generate a baseline case and then make additional runs, perturbing the elements of the noise strength and covariance matrices one at a time. One iteration of the algorithm was performed for each case.

For a baseline case, Trajectory 1 was used, with the full-state measurement model and the diagonal elements of the filter-smoother assumed dynamics driving noise strength and measurement noise covariance matrices given in Tables 1 and 2. These values were not selected in order to represent any particular physical device. They were chosen to give "noticeable" noise corruption without grossly perturbing the inputs and measurements.

All off-diagonal elements of the dynamics driving noise strength and measurement corruption noise covariance matrices were assumed to be zero. Physically, this meant

Table 1

Dynamics Driving Noise Strength for Baseline Case

Element	Value	Interpretation
(1,1)	5.0 (deg^2/sec)	noise in roll attitude
(2,2)	0.2 (g^2/sec)	noise in normal acceleration
(3,3)	100. (lb^2/sec)	noise in thrust
(4,4)	1. (ft^2/sec^3)	noise in Z-wind component
(5,5)	1. (ft^2/sec^3)	noise in Y-wind component
(6,6)	1. (ft^2/sec^3)	noise in X-wind component

Table 2

Measurement Noise Covariance for Baseline Case

Element	Value	Interpretation
(1,1)	10. (ft^2/sec^2)	noise in velocity
(2,2)	5. (deg^2)	noise in flight path angle
(3,3)	5. (deg^2)	noise in heading angle
(4,4)	100. (ft^2)	noise in altitude
(5,5)	1000. (ft^2)	noise in Y-coordinate
(6,6)	1000. (ft^2)	noise in X-coordinate

that the various noise components were assumed to be uncorrelated with each other.

Nominal, true, and measured trajectories were generated for this baseline case. Control inputs which produced Trajectory 1 were first developed, and the results were used as the nominal trajectory. The measured and true trajectories were then produced by artificially noise corrupting the control inputs and (for the measured trajectory) the output. This noise corruption was accomplished in the computer software by adding computer-generated Gaussian-distributed random noise

sequences to the inputs and measurements. The variances of the noise sequences were adjusted so that the noise strength corresponded to the strength assumed by the filter-smoother, with the exception of the wind noise components. For simplicity, wind noise was not included in the trajectory generation program. Accordingly, a unit value was chosen for wind noise in the filter-smoother dynamics driving noise strength matrix because it was considered to be sufficiently small in comparison to the others to avoid an adverse impact on the results. This hypothesis was tested by including variations of the assumed wind noise strengths in the evaluation.

With the nominal, true, and measured trajectories complete, one iteration of the filter-smoother algorithm was performed for the baseline case. The results of this run formed the standard of comparison for the results of succeeding cases. Figure 5 shows a comparison of the true trajectory and the resulting smoothed trajectory, and Figure 6 shows the differences between the two. As stated in Section 3.2, figures giving time histories of trajectory data may be found in the Appendix. The temporal mean and standard deviation of the differences between the smoothed and true trajectories are given in Table 3, where m and σ represent these two quantities, respectively.

As stated above, the robustness study procedure was to use the same nominal, true, and measured trajectories for

Table 3

Means and Standard Deviations of Errors for Baseline Case

Variable		Value
V	m	2.297
	σ	9.937
γ	m	0.7045
	σ	0.5005
χ	m	0.6250
	σ	0.4510
h	m	-1.476
	σ	10.44
Y	m	10.24
	σ	34.27
X	m	-6.047
	σ	33.04
μ	m	0.05888
	σ	2.084
n	m	0.006962
	σ	0.5187
T	m	31.59
	σ	1575.

each case, but to perturb the elements of the noise strength matrices in the filter-smoother individually in order to determine the resulting effects. This perturbation was accomplished by either multiplying or dividing the affected element of the noise strength matrix by a factor of 50, which was selected arbitrarily as a significant but not unreasonably large change. The results are given in Tables 4 - 7, in terms of the temporal mean and standard deviation of the errors committed by the filter-smoother algorithm.

To generate Tables 4 and 5, the elements of the measurement corruption noise covariance matrix were individually increased and decreased, respectively.

Table 4

Errors Committed by Filter-Smoother with Increased Measurement Corruption Noise Covariance

Matrix Element Increased		(1,1)	(2,2)	(3,3)	(4,4)	(5,5)	(6,6)
Variable							
V	m	3.691	2.296	2.296	0.146	1.038	0.534
	σ	10.59	9.937	9.938	5.641	9.313	9.396
δ	m	0.705	0.705	0.705	0.702	0.704	0.704
	σ	0.500	0.500	0.500	0.508	0.500	0.500
χ	m	0.626	0.625	0.625	0.626	0.625	0.623
	σ	0.451	0.451	0.451	0.451	0.441	0.458
h	m	-1.346	-1.513	-1.515	-4.404	-1.009	-0.871
	σ	7.606	10.53	10.51	101.9	8.373	8.169
γ	m	10.25	10.25	10.23	9.346	-46.82	9.186
	σ	36.13	34.29	34.34	18.11	88.52	16.63
χ	m	-2.325	-6.069	-6.041	0.299	-1.224	-77.99
	σ	36.47	33.07	33.04	25.18	12.48	56.25
μ	m	0.065	0.059	0.060	0.080	0.028	0.058
	σ	2.030	2.084	2.081	1.991	2.152	1.996
n	m	0.016	0.007	0.007	0.006	0.020	-0.001
	σ	0.467	0.519	0.519	0.444	0.496	0.455
T	m	9.343	31.56	30.59	6.874	-0.707	4.181
	σ	1201.	1578.	1580.	756.0	1603.	589.1

Tables 6 and 7 show the results of corresponding adjustments to the values of the dynamics driving noise strength matrix. Admittedly, cases where the values were reduced were not advisable choices for noise strengths, as it is never good practice to underestimate their magnitude intentionally. However, in actual practice the noise strengths may not be precisely known, so underestimation of elements of these matrices is possible. The additional effort was also justifiable for the sake of completeness.

The results in Tables 4 - 7 show principally that the algorithm is not highly sensitive to changes in

Table 5

Errors Committed by Filter-Smoother with Decreased Measurement Corruption Noise Covariance

Matrix Element Decreased		(1,1)	(2,2)	(3,3)	(4,4)	(5,5)	(6,6)
Variable							
V	E	0.558	2.293	2.250	2.409	2.485	2.814
	σ	3.815	9.913	9.865	10.24	10.77	9.443
γ	E	0.704	0.705	0.705	0.705	0.704	0.704
	σ	0.504	0.499	0.501	0.500	0.502	0.502
χ	E	0.624	0.625	0.625	0.625	0.625	0.627
	σ	0.458	0.451	0.451	0.451	0.457	0.442
h	E	-0.966	-0.730	-0.971	-1.391	-1.579	-1.242
	σ	57.27	10.04	10.21	7.391	15.70	15.86
Y	E	9.117	9.663	10.38	10.32	10.01	9.909
	σ	90.55	33.78	34.03	35.97	26.35	69.64
X	E	3.091	-6.033	-5.733	-6.268	-9.429	2.005
	σ	59.11	33.39	33.51	34.41	53.49	22.60
μ	E	0.193	0.031	-0.017	0.062	0.190	-0.003
	σ	3.402	2.254	2.379	2.269	3.826	3.921
n	E	-0.044	-0.003	0.010	0.007	0.015	0.018
	σ	1.627	0.532	0.525	0.525	0.783	0.675
T	E	51.76	18.10	80.74	32.71	-25.51	-184.9
	σ	1143.	1488.	1439.	1631.	2724.	5671.

individual elements of the noise strength and covariance matrices. This is particularly true of the states, which tend to be less sensitive to the perturbations than do the control inputs. In fact, the results show that artificially increasing elements of the measurement corruption noise covariance matrix can help reduce the magnitude of control input "spikes" produced by the filter-smoother (see the thrust trace of Figure 5 for an example). This characteristic was exploited later, during the iteration study, which will be described in detail in Section 4.3.

Table 6

Errors Committed by Filter-Smoother with Increased Dynamics Driving Noise Strength

Matrix Element Increased		(1,1)	(2,2)	(3,3)	(4,4)	(5,5)	(6,6)
Variable							
V	m	1.969	2.297	2.259	0.417	1.649	0.571
	σ	10.11	11.82	9.719	5.784	9.676	9.386
γ	m	0.705	0.703	0.704	0.710	0.704	0.704
	σ	0.541	0.502	0.500	0.504	0.500	0.500
χ	m	0.625	0.625	0.625	0.625	0.623	0.626
	σ	0.493	0.453	0.451	0.452	0.450	0.453
h	m	-10.85	-0.900	-1.519	-1.069	-1.271	-1.045
	σ	59.12	14.44	10.35	7.573	9.780	9.035
Y	m	20.76	10.17	10.22	9.808	10.00	9.689
	σ	69.39	34.25	33.63	24.80	28.71	25.64
X	m	-1.090	2.212	-5.813	-1.043	-3.981	0.078
	σ	33.12	30.44	32.25	24.71	25.22	20.79
μ	m	0.087	0.126	0.060	0.088	0.068	0.068
	σ	7.247	2.122	2.080	2.015	2.066	2.033
n	m	0.004	-0.014	0.007	0.006	0.012	0.007
	σ	0.496	2.522	0.514	0.440	0.498	0.468
T	m	-66.62	-91.63	7.498	12.91	20.47	2.535
	σ	2612.	6288.	1544.	913.8	1390.	915.2

Despite the fact that the algorithm was shown not to be highly sensitive to perturbations in the assumed noise strength and covariance matrices, these changes did have measurable effects. Some general trends were also discernible from the results of these perturbations, and will be described below. The reader is cautioned that some of the observed trends might have been dependent upon the geometry of the trajectory used for this evaluation, the relative magnitudes of the noise strengths and covariances chosen for the baseline case, and the full-state measurement model.

Table 7

Errors Committed by Filter-Smoother with Decreased Dynamics Driving Noise

Matrix Element Decreased		(1,1)	(2,2)	(3,3)	(4,4)	(5,5)	(6,6)
Variable							
V	m	2.390	2.226	2.295	2.380	2.311	2.412
	σ	10.08	9.772	9.938	10.14	9.947	10.00
γ	m	0.705	0.705	0.705	0.704	0.705	0.705
	σ	0.499	0.501	0.500	0.500	0.500	0.500
χ	m	0.624	0.624	0.625	0.625	0.625	0.625
	σ	0.452	0.455	0.451	0.451	0.451	0.451
h	m	-1.001	-1.849	-1.476	-1.531	-1.478	-1.507
	σ	10.04	11.74	10.44	10.64	10.44	10.55
Y	m	8.800	9.746	10.23	10.25	10.26	10.29
	σ	32.03	28.40	34.28	34.69	34.52	34.73
X	m	-6.553	-10.46	-6.044	-6.209	-6.057	-6.382
	σ	33.10	38.14	33.03	33.35	33.25	33.58
μ	m	0.077	0.008	0.059	0.058	0.058	0.058
	σ	1.890	2.178	2.083	2.088	2.084	2.087
n	m	-0.004	0.024	0.007	0.007	0.007	0.007
	σ	0.521	0.432	0.579	0.523	0.519	0.522
T	m	17.25	17.62	32.09	32.51	31.94	33.23
	σ	1921.	399.5	1576.	1607.	1580.	1616.

With these qualifying statements in mind, the observed trends will now be discussed. Generally speaking, an increase in the assumed measurement noise variance value for one state resulted in a less accurate match between the filter-smoother results and the true trajectory for that state, but might improve the match for other states. Conversely, decreasing the assumed measurement corruption noise variance for a given state often resulted in a better match for that state, but this improvement was at the expense of a poorer match for some of the other states.

These effects may be seen by comparing the results in Table 3 to those in Tables 4 and 5.

Considering now the effects of perturbations in the values of the dynamics driving noise strength matrix, the results of Tables 6 and 7 show that the noise strength elements corresponding to the control inputs had different effects from those corresponding to wind noise. Increasing the assumed magnitude of control input noise could degrade the match between the filter-smoother output and the true trajectory, but only slightly in the case of the states. In particular, increasing the assumed driving noise for load factor apparently caused significant errors in the thrust match. Decreasing the assumed control input noise had a lesser effect, particularly on the states, but a decrease in the assumed value of load factor driving noise strength apparently improved the thrust match. By contrast, increasing the assumed values for wind noise strength tended to improve the match between the filter-smoother output and the true trajectory, because the algorithm put less weight on its internal model and more on the measurements in such cases. Reducing these values had little effect. Again, it should be stressed that all these effects were of small magnitude, and may well have been dependent upon trajectory geometry and the measurement models used.

In summary, the robustness study showed that the filter-smoother results were not greatly perturbed by

relatively large changes in individual elements of the dynamics driving noise strength and measurement corruption noise covariance matrices. However, artificially increasing elements of the measurement noise covariance matrix was shown to be a viable method for reducing unrealistic transients in the smoothed estimates of the control inputs.

4.2 Measurement Precision Evaluation

The next step in the performance evaluation was a study to determine how filter-smoother performance varied with measurement precision. This differed from the robustness study in that the elements of the dynamics driving noise strength and measurement corruption noise covariance matrices in the filter-smoother were always matched to the variances of the noise corruption used to generate the true and measured trajectories. While maintaining this match, the measurement corruption noise covariance was varied from run to run in order to represent more or less precise measurement devices. As in the robustness study, only one iteration was performed for each case.

The evaluation included all three trajectories and all three measurement models discussed in Chapter III. One set of dynamics driving noise strengths was used for each trajectory, and two sets of measurement corruption noise covariances were used for each measurement model. These

values are given in Tables 8 and 9, where the following symbols are used to designate the various measurement models: FS for full state, RP for radar with position measurements only, and RR for radar with position and range rate data.

The rationale behind the choices made for dynamics driving noise strength and measurement corruption noise covariance matrices was as follows. For simplicity, the

Table 8

Dynamics Driving Noise Strengths

for Measurement Precision Study

Matrix Element	(1,1)	(2,2)	(3,3)	(4,4)	(5,5)	(6,6)
Trajectory						
1	5.0	0.2	100.	1.	1.	1.
2	5.0	0.01	10000.	1.	1.	1.
3	5.0	0.01	10000.	1.	1.	1.

Table 9

Measurement Corruption Noise Covariances

for Measurement Precision Study

Matrix Element	(1,1)	(2,2)	(3,3)	(4,4)	(5,5)	(6,6)
Measurement Model						
FS-1	10.	5.	5.	100.	1000.	1000.
FS-2	10.	0.25	0.25	100.	100.	100.
RP-1	1000.	5.	5.	--	--	--
RP-2	10000.	0.25	0.25	--	--	--
RR-1	1000.	5.	5.	100.	--	--
RR-2	10000.	0.25	0.25	100.	--	--

dynamics driving noise for Trajectory 1 remained as it had been for the robustness study. For Trajectories 2 and 3, noise corruption of load factor was reduced and that of thrust was increased, as shown in Table 8. This choice was made because the original level of load factor noise corruption caused significant mismatches between the nominal and true trajectories, while the original level of thrust noise corruption was barely noticeable in comparison to the thrust magnitude. Turning to measurement corruption noise, the original full state model from the robustness study was retained as model FS-1. Values for model FS-2 were selected in order to improve the accuracy in all states except velocity and altitude, which were already being measured with little noticeable noise corruption. The values for radar model RP-1 were chosen to correspond roughly to the FS-1 values, and those for RP-2 were chosen in order to explore less accurate range measurements combined with more accurate angular measurements. This was of interest because of the uncertainty in position introduced by large angular measurement uncertainties at long ranges. Finally, radar models RR-1 and RR-2 were developed simply by adding range rate measurement capability to models RP-1 and RP-2, with the same amount of corrupting noise in each case. No attempt was made to choose any of these sets of measurement noise covariance values based upon actual measurement device capabilities, as the intention of the study was to explore

the theoretical performance of the algorithm, and not of the measurement system.

Results obtained included plots of the smoothed and true trajectories, the errors committed by the filter-smoother algorithm, and the diagonal elements of the filter-smoother computed covariance, all as functions of time. Numerical values for the temporal means and standard deviations of the errors and diagonal covariance elements were also obtained. These values are recorded in Tables 10 - 15, where the square roots of the covariance statistics have been taken to provide numbers which correspond more directly with the error magnitudes than the variances themselves would.

Figures 7 - 12 are samples of the graphical output obtained. Figures 7 - 9 are plots of the errors committed by the filter-smoother algorithm for Trajectory 2 and a selection of measuring devices (FS-1, RP-2, and RR-2). Figures 10 - 12 are plots of the diagonal terms of the corresponding computed filter-smoother covariances. These cases were chosen from the full set to present typical results to the reader, without overloading him with graphical data. As stated in Section 3.2, these figures and other time history data may be found in the Appendix.

Trends which were observed in the results of this study will now be discussed. Comparing Figures 7 - 9, we see that for the chosen magnitudes of measurement corruption

Table 10

Errors Committed by Filter-Smoother with Various Measurement Devices -- Trajectory 1

Measurement Device		FS-1	FS-2	RP-1	RP-2	RR-1	RR-2
Variable							
V	m	2.297	2.248	2.499	5.525	-0.508	4.607
	σ	9.937	9.958	9.222	10.57	5.983	10.28
γ	m	0.704	0.704	0.706	0.707	0.710	0.704
	σ	0.500	0.502	0.511	0.509	0.508	0.512
χ	m	0.625	0.625	0.622	0.620	0.624	0.623
	σ	0.451	0.453	0.462	0.462	0.463	0.459
h	m	-1.476	-1.834	91.16	77.06	142.3	82.31
	σ	10.44	21.14	75.47	48.59	111.2	58.17
Y	m	10.24	3.941	56.47	20.32	51.33	14.97
	σ	34.27	20.23	43.42	29.66	42.00	23.56
X	m	-6.047	0.687	-46.56	2.906	-58.34	-6.592
	σ	33.04	22.80	49.77	68.97	50.47	49.39
μ	m	0.059	0.088	0.004	0.009	0.087	0.158
	σ	2.084	2.109	1.866	1.942	1.975	2.104
n	m	0.007	-0.009	-0.015	-0.010	-0.007	-0.014
	σ	0.519	0.569	0.426	0.426	0.428	0.424
T	m	31.59	-6.594	-5.270	-12.15	-2.577	-14.15
	σ	1575.	2302.	194.7	307.3	224.7	325.9

noise, the full-state measurement device caused the filter-smoother to commit smaller errors than did either radar. This makes physical sense, as more measurements were available when the full-state device was used.

It is also noted that the magnitude of the errors committed when radar was used tended to increase with time, reaching a maximum at or near the end of the trajectory. This also makes physical sense, as the magnitude of the noise corruption in radar azimuth and elevation angles was considered to be time-invariant. Thus increasing radar ranges would tend to increase errors committed in the

Table 11

Errors Committed by Filter-Smoother with Various Measurement Devices -- Trajectory 2

Measurement Device		FS-1	FS-2	RP-1	RP-2	RR-1	RR-2
Variable							
V	m	-0.209	-0.116	-2.165	-1.427	-2.001	-1.753
	σ	0.486	0.515	6.082	2.335	5.750	2.158
γ	m	0.001	0.002	0.025	0.013	0.025	0.012
	σ	0.124	0.123	0.102	0.107	0.102	0.109
χ	m	-0.004	-0.008	-0.015	-0.016	-0.016	-0.016
	σ	0.076	0.086	0.080	0.081	0.077	0.087
h	m	-6.139	-6.272	22.88	1.265	20.82	2.223
	σ	5.397	4.497	127.5	49.81	120.7	46.29
Y	m	0.949	-0.138	-31.89	-1.528	-30.95	2.615
	σ	4.653	2.647	32.65	11.91	29.99	9.142
X	m	-4.938	-0.223	-33.75	-17.83	-32.44	-16.91
	σ	37.44	18.09	67.12	38.50	59.22	27.43
μ	m	0.064	-0.009	-0.116	-0.244	-0.089	-0.130
	σ	2.237	2.218	2.377	2.268	2.406	2.329
n	m	0.012	0.007	-0.004	-0.004	-0.003	-0.004
	σ	0.117	0.114	0.127	0.118	0.125	0.119
T	m	11.37	-1.185	-32.18	-34.40	-31.47	-36.25
	σ	180.6	175.1	300.2	210.3	283.6	246.6

Cartesian coordinates of aircraft position, and therefore also in velocity. We note that the radar range was increasing at the end of the time interval for Trajectory 2, reaching its maximum at the final time, and therefore the observed behavior is to be expected. Turning to Figures 10 - 12, we see that the computed covariance also tended to predict this behavior correctly for radar measurements.

We also note that the full-state measurement device covariance displayed a final, and sometimes an initial, transient. These are characteristic of the filter-smoother algorithm, and come about because the algorithm includes

Table 12

Errors Committed by Filter-Smoother with Various Measurement Devices -- Trajectory 3

Measurement Device		FS-1	FS-2	RP-1	RP-2	RR-1	RR-2
Variable							
V	m	-1.285	-1.958	5.407	0.454	5.292	0.029
	σ	1.639	3.052	6.251	1.692	6.412	2.176
γ	m	-0.155	-0.157	-0.171	-0.158	-0.170	-0.157
	σ	0.175	0.212	0.183	0.176	0.187	0.176
χ	m	-5.866	-5.071	-5.484	-4.399	-5.489	-4.400
	σ	14.31	17.00	10.55	11.16	10.54	11.14
h	m	-1.866	-1.255	-1.619	-24.46	2.930	-23.01
	σ	6.269	17.80	84.60	19.77	87.19	20.09
Y	m	11.27	18.77	30.89	11.82	25.23	7.605
	σ	150.9	204.6	50.62	46.72	39.67	37.04
X	m	-12.03	-12.82	-27.62	0.429	-28.18	-2.648
	σ	88.44	123.0	80.63	36.99	80.40	33.59
μ	m	-0.786	-1.186	0.649	0.577	0.655	0.557
	σ	15.97	19.19	10.54	10.54	10.54	10.55
n	m	0.003	-0.000	0.007	0.006	0.008	0.008
	σ	0.101	0.260	0.095	0.093	0.096	0.097
T	m	111.5	-72.05	68.27	59.00	119.7	135.9
	σ	2158.	9710.	727.3	709.1	884.2	988.9

Table 13

Square Roots of Filter-Smoother Computed Covariances with Various Measurement Devices -- Trajectory 1

Measurement Device		FS-1	FS-2	RP-1	RP-2	RR-1	RR-2
Variable							
V	m	1.720	1.519	9.826	3.728	9.432	3.517
	σ	3.737	3.288	14.31	4.966	13.74	4.858
γ	m	0.031	0.031	0.038	0.036	0.034	0.030
	σ	0.059	0.058	0.060	0.058	0.056	0.055
χ	m	0.035	0.032	0.048	0.040	0.045	0.035
	σ	0.059	0.058	0.060	0.058	0.056	0.055
h	m	10.55	10.09	176.1	61.20	168.7	52.70
	σ	13.14	12.85	236.0	72.82	227.2	67.42
Y	m	18.34	9.400	202.5	62.07	202.3	61.02
	σ	13.74	12.62	222.8	67.91	222.9	67.64
X	m	13.42	6.771	119.7	50.07	119.0	42.42
	σ	12.71	8.103	137.4	58.71	136.8	46.76

Table 14

Square Roots of Filter-Smoother Computed Covariance with Various Measurement Devices -- Trajectory 2

Measurement Device		FS-1	FS-2	RP-1	RP-2	RR-1	RR-2
Variable							
V	m	0.960	0.827	5.017	2.183	4.922	2.107
	σ	1.063	1.045	5.729	2.325	5.557	2.273
γ	m	0.027	0.025	0.046	0.034	0.040	0.027
	σ	0.047	0.041	0.058	0.054	0.042	0.038
χ	m	0.089	0.079	0.102	0.106	0.080	0.080
	σ	0.130	0.113	0.153	0.147	0.108	0.106
h	m	8.548	7.759	94.54	28.34	92.69	26.78
	σ	10.73	9.462	104.0	29.61	101.1	27.83
Y	m	8.324	4.490	41.47	19.00	40.97	18.06
	σ	7.332	5.260	42.00	18.31	41.24	17.15
X	m	29.69	18.77	63.23	57.69	58.04	42.68
	σ	29.17	25.50	74.48	39.77	69.96	32.05

Table 15

Square Roots of Filter-Smoother Computed Covariance with Various Measurement Devices -- Trajectory 3

Measurement Device		FS-1	FS-2	RP-1	RP-2	RR-1	RR-2
Variable							
V	m	2.048	1.862	8.980	4.200	8.696	4.007
	σ	1.888	1.762	8.265	2.968	8.006	2.870
γ	m	0.059	0.055	0.089	0.074	0.078	0.063
	σ	0.081	0.077	0.108	0.095	0.094	0.082
χ	m	11.85	11.84	11.86	11.85	11.85	11.85
	σ	49.26	49.26	49.27	49.26	49.26	49.26
h	m	8.990	7.831	69.39	26.78	66.60	24.66
	σ	9.667	8.709	67.58	20.32	67.81	17.88
Y	m	37.19	28.55	117.5	60.83	104.0	50.26
	σ	42.26	37.35	103.1	49.58	88.75	41.26
X	m	23.95	17.75	98.08	40.85	91.93	36.46
	σ	23.81	21.26	74.02	28.43	74.25	24.16

both forward and backward filters. Each of these devices commonly produces an initial covariance transient which reduces to a nearly steady-state value after a number of measurements have been processed. Therefore the smoother covariance, which combined the covariances of both filters, commonly displayed both transients. The backward filter transient occurred at the end of the time interval, since that was initial point for this filter.

Study of the graphical and tabular results also shows that radar measurements tended to reduce thrust "spikes", compared to full state measurements, particularly for trajectories where the thrust was held constant. This can be seen by comparing the temporal standard deviations of the thrust errors in Tables 10, 11, and 12 for the various measurement devices. Physically, this is attributed to a tendency by the filter-smoother to use thrust aggressively to match velocity, while using load factor to match flight path angle and heading angle, when full state measurements were available. With radar measurements, velocity, flight path angle, and heading angle information had to be derived from time histories of position data and were assumed to be less accurate by the algorithm. Therefore, the controls were varied less aggressively.

Another general observation which may be drawn from a study of Figures 8 and 9 is that addition of range rate information to the radar reduces the magnitude of the

filter-smoother errors. This is again physically reasonable, as adding another measurement to a radar may be expected to increase the accuracy of the device if the range and angle measurement errors remain constant. Range rate is a particularly good choice for this additional measurement, as it depends upon all six components of the state vector (see Eq (107)).

It is instructive to compare the magnitudes of the errors committed by the filter-smoother algorithm with the magnitudes of the square roots of the corresponding elements of the filter-smoother computed covariance, in terms of their temporal means and standard deviations. Looking at Tables 10 and 13, we see that for Trajectory 1, based on these data, the filter-smoother tended to underestimate the magnitude of the errors committed. This was consistently true for all six measurement devices. We also note that when the covariance data predicted a reduction in error, it was not necessarily borne out by the actual error data. For Trajectory 2, by contrast, the filter-smoother overestimated its errors, and reductions in the error predicted by the standard deviation of the covariance tended to predict trends correctly for the standard deviation of the actual errors. Finally, for Trajectory 3, we find that the filter-smoother sometimes overpredicted and sometimes underpredicted its errors, for all six measurement models. Additionally, in this case the error trends predicted by the

standard deviation of the covariance did not correspond to trends in the standard deviation of the actual errors for the full state measurement models, but did for the radar models.

These observations demonstrate the difficulty in using temporal averages and standard deviations to judge filter-smoother algorithm performance, and attempting to compare actual errors and algorithm-assumed errors on the basis of such statistics. Recalling the development in Section 2.2, we note that close correspondence between single-run errors and the square roots of algorithm-computed covariances is not necessarily to be expected. Error time histories such as those discussed above show errors committed by one particular filter-smoother run, and depend upon the one particular noise sequence encountered for that run in the dynamics driving noise and the measurements. By contrast, covariance time histories show how well the filter-smoother would theoretically estimate the states as a function of time, with this estimate averaged over an ensemble of infinitely many filter-smoother runs, each with a different noise sequence in both the dynamics driving noise and the measurements.

The results noted above point out the danger of confusing ensemble statistics and temporal statistics of given parameters. If time had permitted the generation of ensemble averages of the errors committed by the filter-

smoother algorithm (as in a Monte Carlo evaluation), then a close correspondence to the covariance statistics could have been expected. With the procedures actually used, the covariance data only provide an indication of the filter-smoother's internal estimate of its precision, and should not be used to judge actual error characteristics for any given case. However, these data may still prove useful for algorithm tuning purposes, and for studies of trends.

Evaluation of the graphical output for the remainder of the cases in this study showed that some of the conclusions drawn earlier may be generalized. The larger the number of available measurements, the less the errors committed by the filter-smoother. Radar measurements with time-invariant noise corruption yield less accurate Cartesian position coordinate estimates as range increases. These results are physically reasonable, for the reasons cited above, and may prove valuable to users of the algorithm.

4.3 Iteration Effects and Procedures

One of the objectives of this thesis project was to determine whether the match between the filter-smoother output and the true trajectory could be improved by successive iterations of the algorithm. Accordingly, multiple iterations were performed for selected combinations of trajectories and measurement devices.

Iterations were first performed on the "benign" Trajectory 1, using the FS-1 measurement device. The method adopted was to use the filter-smoother computed control inputs and initial states from each run as inputs to the nominal trajectory program (PMSIM, ref. Ruley, 1987b) to generate the nominal trajectory for the next run. A total of five iterations were carried out.

The temporal means and standard deviations of several parameters were recorded in an effort to quantify any resulting improvement in the trajectory match and to see if this was signalled by any easily recognizable effect. These parameters included the filter-smoother state and control input perturbations, the diagonal elements of the filter-smoother computed state covariance, and the change in the filter-smoother nominal trajectory from iteration to iteration. It was hoped that convergence of the filter-smoother state and control estimates to the true trajectory would be reflected through recognizable trends in these parameters. Results obtained are discussed below.

Before examining the parameters discussed above, it was necessary to see if convergence of the algorithm was in fact occurring. Table 16 presents the means and standard deviations of the errors committed by the filter-smoother for the five iterations. Considering this table, we see that the iterations reduced the errors in velocity and Cartesian position coordinates. Errors in flight path and

Table 16

Errors Committed by Filter-Smoother over Five Iterations for Trajectory 1

Iteration		1	2	3	4	5
Variable						
V	m	2.297	-0.485	0.643	-0.084	0.528
	σ	9.937	7.542	3.305	5.955	3.423
γ	m	0.705	-0.621	0.520	-0.652	0.308
	σ	0.500	0.502	1.335	0.436	1.392
χ	m	0.625	-1.222	0.215	-0.660	0.579
	σ	0.451	0.470	1.463	0.413	1.420
h	m	-1.476	-0.143	-1.667	-1.705	-1.098
	σ	10.44	8.267	6.231	5.606	5.629
Y	m	10.24	9.249	9.726	8.850	9.416
	σ	34.27	33.76	19.26	21.27	18.28
X	m	-6.047	13.41	1.060	7.213	-0.886
	σ	33.04	32.55	11.84	26.34	13.60
μ	m	0.059	0.309	0.257	0.405	0.436
	σ	2.084	2.200	2.361	2.456	2.685
n	m	0.007	-0.001	-0.003	-0.010	-0.003
	σ	0.519	0.742	0.481	0.730	0.472
T	m	31.59	-8.537	53.58	91.29	176.4
	σ	1575.	1661.	1985.	2509.	3184.

heading angle were not reduced. However, these errors were already of very small magnitude. Errors in control inputs remained relatively constant, or even increased in the case of thrust. Figure 13 shows the errors committed by the filter-smoother after the fifth iteration. As stated in Section 3.2, this figure and other time history plots may be found in the Appendix. Comparison of Figure 13 with Figure 6, which shows the same parameters for the first iteration, reinforces the conclusions drawn above. Therefore, at least some iterative improvement was experienced in this case.

The state and control input perturbations produced by the filter-smoother algorithm were tracked as one possible means of determining convergence of the iteration sequence. These quantities are defined by Eqns (56) and (88) - (90), and should not be confused with the filter-smoother errors. Table 17 shows the means and standard deviations of these parameters for the five iterations. Study of the data revealed no discernible trend that would permit the user to determine whether the errors committed by the filter-smoother were being minimized.

Table 17

Filter-Smoother State and Control Perturbations over Five Iterations -- Trajectory 1

Iteration		1	2	3	4	5
Variable						
V	m	7.448	-10.73	-6.760	-8.875	-6.670
	σ	7.020	4.305	8.230	2.264	7.433
γ	m	-0.010	0.010	-0.009	0.011	-0.005
	σ	0.015	0.020	0.024	0.012	0.026
χ	m	-0.010	0.023	-0.003	0.012	-0.009
	σ	0.022	0.032	0.022	0.016	0.023
h	m	-256.1	247.8	24.83	245.7	105.1
	σ	155.0	147.1	133.9	152.9	134.6
Y	m	-130.0	239.1	-1.868	109.8	-80.91
	σ	112.6	179.1	130.1	84.46	185.0
X	m	177.7	-344.5	-226.3	-220.0	-155.1
	σ	124.3	207.3	124.2	135.6	91.50
μ	m	-0.021	0.251	-0.052	0.148	0.031
	σ	0.661	0.918	0.567	0.497	0.528
n	m	0.011	0.002	-0.066	-0.004	-0.060
	σ	0.289	0.802	0.336	0.818	0.325
T	m	31.09	-40.15	62.14	37.78	117.2
	σ	1575.	1924.	851.8	1091.	1475.

The next parameters examined as possible indicators of convergence or minimization of the filter-smoother errors were the diagonal elements of the state covariance. Table 18 presents these data, where the square roots of the actual covariance means and standard deviations have been taken to provide numbers which should be more directly comparable in magnitude to the actual filter-smoother errors. As in the case of the state and control perturbations, no trend was observed which might be correlated with the reduction observed in actual filter-smoother error.

Finally, the change in the nominal trajectory, defined as the difference between the trajectory used for each run of the filter-smoother algorithm and that used for the next run, was monitored as a possible indicator of

Table 18

Square Roots of Filter-Smoother Computed Covariance over Five Iterations -- Trajectory 1

Iteration		1	2	3	4	5
Variable						
V	m	1.720	1.654	1.705	1.699	1.762
	σ	3.737	3.541	3.545	3.599	3.685
γ	m	0.031	0.029	0.030	0.029	0.030
	σ	0.059	0.055	0.053	0.054	0.053
χ	m	0.035	0.033	0.033	0.032	0.032
	σ	0.059	0.056	0.053	0.053	0.053
h	m	10.55	10.32	10.54	10.17	10.59
	σ	13.14	11.95	11.61	11.31	11.36
Y	m	18.34	18.47	17.99	18.11	18.03
	σ	13.74	13.75	11.66	11.61	11.37
X	m	13.42	13.19	13.71	13.30	13.93
	σ	12.71	12.61	13.48	12.83	13.56

convergence. Table 19 contains the relevant means and standard deviations. In this case we note that there is a definite trend which correlates with the observed reduction in actual error magnitude. The changes in the nominal trajectory tended to become smaller as the errors grew smaller. This trend is not monotonic, as there are cases where these numbers were reduced when the filter-smoother errors increased, and vice versa. However, it may be used as a general indicator of algorithm convergence. A sequence of time history plots for the nominal trajectory change

Table 19

Change in Filter-Smoother Nominal Trajectory over Five Iterations -- Trajectory 1

Iteration		1	2	3	4	5
Variable						
V	m	15.37	-2.822	1.429	-1.614	1.410
	σ	9.380	4.657	3.906	3.362	4.358
γ	m	-1.346	1.160	-1.191	0.976	-1.343
	σ	0.909	1.182	1.070	1.249	1.079
χ	m	-1.880	1.463	-0.891	1.260	-1.111
	σ	0.777	1.496	1.319	1.425	1.243
h	m	-502.6	221.4	-220.9	141.2	-259.2
	σ	311.9	239.7	248.1	227.8	287.8
Y	m	-370.0	241.5	-112.6	191.3	-181.0
	σ	263.1	269.5	195.4	256.7	239.6
X	m	541.8	-130.6	-0.280	-72.98	18.82
	σ	337.1	120.1	64.24	100.2	74.88
μ	m	-0.021	0.250	-0.052	0.148	0.031
	σ	0.661	0.918	0.567	0.497	0.528
n	m	0.002	0.066	-0.069	0.063	-0.062
	σ	0.256	0.701	0.334	0.679	0.324
T	m	31.25	-40.12	62.12	5.212	45.24
	σ	1575.	1924.	851.8	708.9	299.2

would probably assist in providing insight as to the exact manner in which changes are occurring.

This trend in the nominal trajectory change is observed for the states but less so for the controls, particularly the thrust, which was undergoing less change from iteration to iteration as the error in thrust increased. However, looking at Figures 6 and 13, we see that the changes in thrust were occurring in the form of temporally narrow "spikes". It is anticipated that these affected the trajectory very little, since they were "integrated out" by the filter-smoother, and were therefore less significant than more slowly-varying control input changes of the same order of magnitude would have been. Thus, this lack of correspondence is not of great concern, and the tentative conclusion is that the sequence of nominal trajectory changes may be used to help indicate convergence of the filter-smoother states to the true states. Figures 14 and 15 show time histories of the nominal trajectory changes for the first and fifth iterations, respectively, and show the reduction in nominal trajectory change between these two cases.

Iterations were then performed on the more "severe" Trajectory 3, using the same techniques discussed above for nominal trajectory generation, and the radar with range rate measurement device RR-2. Table 20 shows the results in terms of the means and standard deviations of the errors

Table 20

Errors Committed by Filter-Smoother over Five Iterations for Trajectory 3

Iteration		1	2	3	4	5
Variable						
V	m	0.029	-2.363	-8.033	-20.96	-10.65
	σ	2.176	3.191	6.441	11.21	8.947
γ	m	-0.157	-0.189	-0.754	-0.429	0.822
	σ	0.176	0.387	1.190	1.202	0.760
χ	m	-4.400	-4.469	-5.606	-14.33	-9.218
	σ	11.14	11.02	15.22	17.04	15.45
h	m	-23.01	-31.38	-54.61	-44.91	-35.26
	σ	20.09	19.40	30.12	41.83	34.06
Y	m	7.605	2.924	10.22	10.76	8.784
	σ	37.04	31.74	36.43	44.78	33.03
X	m	-2.648	-7.618	-0.728	75.26	37.32
	σ	33.59	37.26	47.29	96.26	67.84
μ	m	0.557	0.434	0.849	-0.548	-0.741
	σ	10.55	10.63	14.98	15.10	15.21
n	m	0.008	0.039	0.045	0.034	0.073
	σ	0.097	0.341	0.562	0.920	1.051
T	m	135.9	1102.	1646.	1901.	4431.
	σ	988.9	10771.	23142.	34827.	35099.

committed by the filter-smoother algorithm. A study of the data reveals that convergence was not being achieved as it was for the "benign" trajectory. The state errors were slowly growing, as was the roll attitude error, and the normal acceleration and thrust errors were increasing rapidly. Figures 16 and 17 show the errors for the first and fifth iteration.

Considering these figures, we see that the difficulties the filter-smoother was experiencing appear to be due to "spikes" in the control inputs. A large thrust spike appeared after the first iteration (see Figure 16).

This apparently introduced normal acceleration spikes, as both normal acceleration and thrust spikes are very much in evidence after the fifth iteration (as seen in Figure 17). (The "flat spot" in normal acceleration seen in Figure 16 is due to the angle-of-attack limiting discussed in Section 3.2. Similar effects may be seen in later figures, due to the same cause.) The situation was made more serious by spikes and large changes that occurred in roll attitude and heading angle at approximately $t = 9.0$ sec , at which point the aircraft flew through the vertical. Since flight path angle is limited to ±90 deg, flight through the vertical resulted in an instantaneous change of 180 deg in both heading angle and roll attitude, while flight path angle peaked at 90 deg and began to decrease. The filter-smoother was unable to follow these sudden changes closely, due to the singularity which occurs in its internal model at vertical flight path angle, resulting in the generation of the observed spikes. It should be noted here that calculations are performed within the filter-smoother algorithm to ensure that angular perturbations are taken to be the smallest in magnitude within the ±180 deg angular range. This feature was implemented against the possibility of the algorithm differencing large positive and large negative angles, resulting in perturbations which appear numerically to be large until appropriately resolved.

All these effects combined to cause the filter-smoother results to diverge to some degree from the true trajectory. Even though the spikes were narrow in time, there were enough of them and they were of sufficient magnitude to cause unrealistic changes in the filter-smoother results. The resulting sequence of iterations could not improve the match between the filter-smoother output and the true trajectory.

In order to rectify this deficiency, it was recalled from the sensitivity study that an artificial increase in measurement corruption noise strength could assist in spike suppression. After experimentation, it was determined that increasing all measurement noise covariance matrix elements by a factor of 125 produced a trajectory for which the match with the true states was not degraded, and which was largely devoid of control input spikes. Accordingly, iterations were performed using the same nominal trajectory generation technique discussed above, but with the increased measurement corruption noise. The temporal mean and standard deviation of the filter-smoother errors for these iterations appears in Table 21. Figures 18 and 19 show the time history data corresponding to this table for the first and fifth iteration.

Considering these data, we see that while the agreement between the filter-smoother results and the true trajectory was not being degraded by the iterations, it was

Table 21

Errors Committed by Filter-Smoother over Five Iterations with Increased Measurement Noise -- Trajectory 3

Iteration		1	2	3	4	5
Variable						
V	m	-0.337	-0.334	-0.371	-0.405	-0.457
	σ	0.948	1.006	1.036	1.069	1.098
γ	m	-0.161	-0.155	-0.150	-0.147	-0.145
	σ	0.178	0.179	0.181	0.184	0.189
χ	m	-5.576	-5.527	-5.505	-5.510	-5.505
	σ	10.62	10.61	10.60	10.59	10.59
h	m	-15.54	-15.69	-15.72	-15.94	-15.93
	σ	20.78	20.91	20.89	21.06	21.15
Y	m	-0.269	-0.635	-0.598	-1.047	-1.316
	σ	20.24	20.37	20.46	20.47	20.67
X	m	-7.296	-7.824	-8.196	-8.621	-9.007
	σ	25.33	25.20	25.38	25.57	25.79
μ	m	0.669	0.657	0.646	0.636	0.626
	σ	10.53	10.53	10.53	10.53	10.53
n	m	-0.001	-0.001	-0.001	-0.001	-0.001
	σ	0.087	0.087	0.087	0.087	0.088
T	m	11.26	18.94	28.01	38.34	49.93
	σ	126.7	186.8	260.6	343.6	435.3

also not being improved. Moreover, the error in thrust was increasing with each iteration, and Figure 19 shows that spikes were beginning to appear in the filter-smoother output, although they were much smaller than those seen in the previous case. Therefore, although this change in iteration procedure improved matters, by reducing the tendency for filter-smoother divergence, it did not yield the objective of algorithm convergence.

The behavior of the filter-smoother algorithm in this case is easily explained. Table 22 shows the mean and standard deviation of the nominal trajectory changes for

Table 22

Change in Filter-Smoother Nominal Trajectory over Five Iterations with Increased Measurement Noise -- Trajectory 3

Iteration		1	2	3	4	5
Variable						
V	m	0.031	0.046	0.050	0.057	0.081
	σ	0.113	0.113	0.117	0.120	0.129
γ	m	0.006	0.004	0.003	0.002	0.005
	σ	0.011	0.010	0.010	0.010	0.010
χ	m	0.048	0.022	-0.005	0.005	-0.003
	σ	0.059	0.051	0.033	0.036	0.032
h	m	-0.249	-0.361	-0.404	-0.478	-0.411
	σ	0.443	0.565	0.609	0.657	0.639
Y	m	-3.219	-1.402	-0.239	-0.944	-0.230
	σ	2.847	1.342	0.699	0.963	0.700
X	m	-0.309	-0.651	-0.814	-0.791	-1.153
	σ	1.043	0.754	0.588	0.692	0.870
μ	m	-0.011	-0.011	-0.011	-0.011	-0.010
	σ	0.045	0.044	0.044	0.043	0.042
n	m	0.000	0.000	0.000	0.000	0.000
	σ	0.002	0.002	0.002	0.002	0.002
T	m	6.279	7.674	9.070	10.33	11.59
	σ	74.92	78.13	83.42	90.22	98.24

these five iterations. Examination of the data shows that the nominal trajectory change was nearly constant from iteration to iteration. What was happening was that the filter-smoother control input perturbations were so small that the nominal trajectory was changing by only a very small amount from iteration to iteration. Accordingly, the filter-smoother was "solving the same problem" for every iteration, and the error in the states remained the same. The error in the control inputs was increased from iteration to iteration, since the control perturbation was added to

the nominal control inputs at every iteration. Under these circumstances, iteration produces no benefit.

Another iteration technique was tried with this trajectory in a further attempt to produce iterative improvement. For this method the artificially large measurement corruption noise was retained, but nominal trajectories were generated simply by using the resulting smoothed trajectory from each filter-smoother run as the nominal trajectory for the next. It was hoped that this might induce more rapid convergence than the method previously used.

Tables 23 and 24 show the temporal means and standard deviations of the filter-smoother errors and nominal trajectory changes, respectively, for the five iterations. Figure 20 shows the error data for the fifth iteration, and may be compared with Figure 15, which also applies to this case for the first iteration. The nominal trajectory change data indicate that the iteration sequence was converging. However, the error data indicate that it was converging to the wrong result. This conclusion is based on the fact that the error magnitudes were growing as the iterations proceeded.

This behavior is also easily explainable. The validity of the filter-smoother control input perturbation estimate is based upon having a consistent set of nominal states and nominal controls. That is, the nominal control

Table 23

Errors Committed by Filter-Smoother over Five Iterations with Smoothed Trajectory used as Nominal

Iteration		1	2	3	4	5
Variable						
V	m	-0.337	-0.391	-0.483	-0.623	-0.774
	σ	0.948	1.072	1.280	1.426	1.544
γ	m	-0.161	-0.161	-0.162	-0.162	-0.162
	σ	0.178	0.178	0.179	0.180	0.180
χ	m	-5.576	-5.550	-5.536	-5.528	-5.524
	σ	10.62	10.62	10.61	10.61	10.61
h	m	-15.54	-11.40	-7.315	-3.207	0.539
	σ	20.78	22.84	26.07	27.80	28.70
Y	m	-0.269	-18.72	-29.95	-35.52	-38.51
	σ	20.24	63.37	87.54	103.4	116.0
X	m	-7.296	-32.57	-39.11	-40.97	-41.10
	σ	25.33	10.89	19.78	27.76	34.40
μ	m	0.669	0.668	0.668	0.667	0.665
	σ	10.53	10.53	10.53	10.53	10.54
n	m	-0.001	-0.002	-0.002	-0.002	-0.002
	σ	0.087	0.087	0.088	0.090	0.093
T	m	11.26	10.86	10.40	9.967	9.502
	σ	126.7	129.9	134.9	141.1	148.4

inputs must be those which will produce the nominal states when applied to the system. Generating the nominal trajectory by applying control inputs to an aircraft model which solves the trajectory equations given by Eqs (11) - (16) guarantees that the required consistency will be maintained, because the filter-smoother's linearized model is generated from the time histories of the resulting nominal states and controls. However, if the nominal states are produced without reference to the nominal controls, as in the case where smoother results are used as nominal trajectory states, then these states and controls cease to

Table 24

Change in Filter-Smoother Nominal Trajectory over Five Iterations with Smoothed Trajectory used as Nominal

Iteration		1	2	3	4	5
Variable						
V	m	-0.489	-0.054	-0.092	-0.141	-0.151
	σ	0.665	0.225	0.246	0.206	0.189
γ	m	-0.004	-0.000	-0.001	-0.000	-0.000
	σ	0.008	0.002	0.003	0.003	0.003
χ	m	0.074	0.025	0.014	0.008	0.005
	σ	0.067	0.042	0.037	0.030	0.025
h	m	-0.667	4.141	4.089	4.108	3.745
	σ	8.545	3.112	3.923	2.971	2.710
Y	m	-259.6	-18.46	-11.22	-5.575	-2.990
	σ	260.2	58.14	28.48	20.00	16.05
X	m	60.11	-25.28	-6.538	-1.857	-0.133
	σ	61.34	27.27	13.31	9.046	7.272
μ	m	-0.009	-0.000	-0.001	-0.001	-0.001
	σ	0.048	0.071	0.083	0.088	0.086
n	m	0.000	-0.000	-0.000	0.000	0.000
	σ	0.002	0.007	0.008	0.009	0.009
T	m	6.279	-0.399	-0.465	-0.432	-0.465
	σ	74.92	9.047	10.85	11.81	12.24

correspond. The filter-smoother's internal model will not be correctly relinearized, and the results will become unreliable.

Having examined three different techniques for iterative improvement and noting the good points and shortcomings of each, a few words of summation are now appropriate. From the results above, it appears that the best way to proceed is to run the filter-smoother once with measurement corruption noise matched as closely as possible to the "real-world" value. Should this result in spikes in the control input estimates, one may artificially increase

the measurement corruption noise to a level which suppresses these, if this may be done without spoiling the agreement between the filter-smoother states and the nominal states. Iterations may then be performed, and the nominal trajectory sequence may be monitored for indications of convergence. This will generally be indicated by a reduction in the nominal trajectory change from iteration to iteration, for both the nominal states and the nominal controls. The nominal trajectories used for iterations must be generated by applying the filter-smoother estimates of control inputs to an aircraft model implementing the trajectory equations given by Eqs (11) - (16).

While it is possible that iterations will improve the agreement of the filter-smoother results and the true trajectory, this is not guaranteed. If the nominal trajectory changes do not tend to converge, then iterations cannot be expected to improve the agreement between the true trajectory and the filter-smoother output.

4.4 Chapter Summary

Chapter IV discusses the evaluation of the filter-smoother algorithm's performance. This was composed of a robustness study, a measurement precision evaluation, and an assessment of the effects of iterations on the accuracy of the filter-smoother results. The robustness study showed that filter-smoother performance was not greatly affected by

relatively large mismatches between the noise statistics used by the algorithm and those used to generate the true trajectory. Moreover, this study showed that artificially increasing elements of the measurement noise covariance matrix could help reduce unrealistic transients in the smoothed estimates of the control inputs. The measurement precision evaluation demonstrated that the algorithm responded to changes in measurement device characteristics in a physically reasonable manner. Finally, the iteration study showed that iterations could improve the match between the filter-smoother state and control estimates and the true trajectory. However, this improvement was not guaranteed to occur for all trajectories. Methods were evaluated for assisting this iterative improvement by artificially raising the magnitude of the filter-smoother measurement corruption noise covariance matrix, to reduce the magnitude of the "spikes" in the smoother-estimated time histories. Several parameters were evaluated as possible indicators of convergence for a sequence of filter-smoother iterations, and the change in the nominal trajectory from iteration to iteration was found to be fairly reliable as such an indicator.

V. Conclusions and Recommendations

5.1 Conclusions

The preceding chapters have shown how the filter-smoother algorithm was developed, implemented, and evaluated. Conclusions will now be drawn from previous work, and ways in which the current implementation might be improved will be considered.

The most important conclusion to be drawn is that the objectives outlined in Chapter 1 have been achieved. Given a nominal trajectory which reasonably well matches the measured data, a set of nominal control inputs which will generate that trajectory when applied to the aircraft model, and measured data which is corrupted by a zero-mean, Gaussian-distributed white noise sequence, the filter-smoother will produce an output trajectory which matches the true trajectory well. This holds even when the noise statistics assumed by the algorithm do not correspond to the true values, and for several different measurement devices.

However, as currently implemented, the filter-smoother algorithm is not an infallible predictor of true trajectories, and has some limitations. Some of these shortcomings are serious, and users must bear them in mind.

A very serious limitation is the dependence of the algorithm on the provision of a nominal trajectory which

AD-A194 382 APPLICATION OF LINEARIZED KALMAN FILTER-SMOOTHER TO AIRCRAFT TRAJECTORY ESTIMATION(U) AIR FORCE INST OF TECH WRIGHT-PATTERSON AFB OH SCHOOL OF ENGI.. 2/2

UNCLASSIFIED J M RULEY JUN 88 AFIT/GAE/ENG/88J-1 F/G 1/3 NL

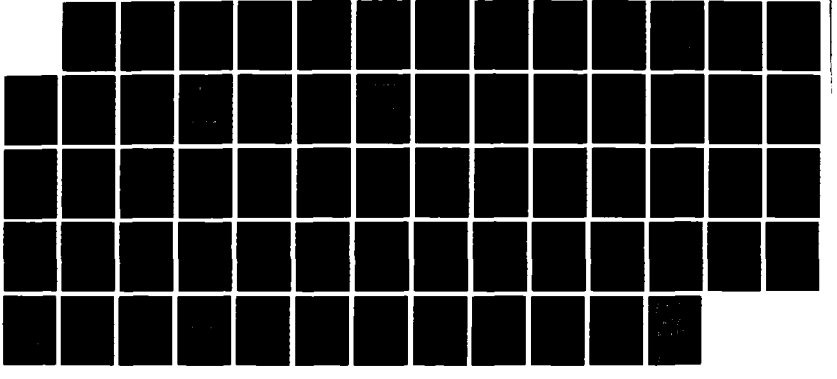

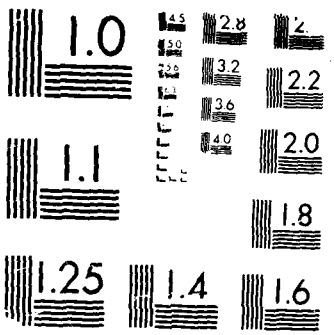

MICROCOPY RESOLUTION TEST CHART

closely matches the measurements, and on a set of nominal control inputs which correspond to the nominal states. The situation where the original nominal states are ill-matched to the measurements was not addressed in this thesis. Therefore, it may not be assumed that the algorithm gives satisfactory performance under such circumstances. Additionally, it has been shown that if the nominal control inputs and states do not correspond, the filter-smoother output may diverge from the true trajectory. Accordingly, if good results from the current algorithm are to be expected, the user must provide a consistent set of nominal states and nominal control inputs, and they must match the measurements closely. This limitation will be given further attention in Section 5.2 below.

Another limitation of the current filter-smoother implementation is that iterations may not improve the match between the smoothed and true trajectories. In fact, when the trajectory includes singularities of the filter-smoother's linearized aircraft model, iterations of the algorithm may actually cause poorer agreement. However, monitoring the degree of change in the nominal trajectory from iteration to iteration will indicate whether or not iterations are helpful.

The tendency of the filter-smoother to corrupt the control input estimates with artificially generated "spikes" is also a limitation to be considered. A method for

eliminating this tendency by increasing the measurement corruption noise covariance has been shown to be effective. However, this method may have the undesirable consequence of making iterations of the algorithm slow to converge. Additional proposed solutions for this problem will be discussed in Section 5.2.

Despite these limitations, the filter-smoother algorithm is a useful tool, which could be of assistance in actual aircraft mishap investigations. Ways in which it could be improved will now be discussed.

5.2 Recommendations

The generation of nominal trajectories which meet the requirements discussed above warrants further attention. A possible method for doing this in a systematic manner is to use a curve-fitting algorithm to "smooth" the actual measurement time histories (in the sense of introducing continuous second derivatives) and then to differentiate them numerically to obtain the control input time histories. These control inputs could then be applied to a nonlinear model of the aircraft, such as the PMSIM program (Ruley, 1987b), and used to generate a candidate nominal trajectory which may be compared with the measurements. Further adjustments of the control inputs could then be made in a trial-and-error fashion to improve the agreement between the nominal trajectory and the measurements. A program to

explore this technique has been written, using the raw measurement data for selected cases, and has shown that valuable "trend" information could be deduced from raw measurements. Additional study of this technique is recommended.

A possible method for elimination of spikes in the control input estimates would be to change the implementation of the filter-smoother so that the current state vector is augmented with the current control inputs, and the time derivatives of the current control inputs are used as new "controls". While spikes might still occur in these "controls", it is probable that they would be less likely to occur in the roll attitude, normal acceleration, and thrust output, since these would now be treated as filter-smoother states. This technique would also permit the modelling of additional measurement devices, such as a head-up display (HUD), which record variables which are used as controls in the current implementation. Inclusion of these additional measurements would be very likely to make the filter-smoother algorithm more capable.

Other methods for elimination or reduction of control input "spikes" associated with model singularities are possible. One of these would be to increase the values in the measurement corruption noise covariance matrix as the trajectory nears a singular point. This would cause the algorithm to give less weight to measurements at that point,

and to follow the nominal trajectory until the singularity had been passed. Another way to accomplish the same objective would be to re-formulate the aircraft model with Euler parameters or quaternions (McKern, 1968; Whittaker, 1944:8) used in place of Euler angles. These parameters do not exhibit the singular behavior associated with Euler angles, and the adverse effects of the singularities could thus be eliminated. Finally, some evaluation of the effects of artificially increased dynamics driving noise on the "spikes" might prove profitable. The actual driving noise strength will probably not be as well established as measurement noise covariance for practical problems, and thus the matrix $\underline{Q}(t_i)$ could be manipulated as well as the matrix $\underline{R}(t_i)$ in order to obtain good results.

At present, the filter-smoother algorithm requires a nominal trajectory which is well matched to the measurements. Suggestions for generating such trajectories have already been made. An alternate approach, which might relax this requirement to some degree, would be to increase the magnitude of the dynamics driving noise strength matrix. This is expected to permit convergence of the iterations despite a poorer match between the initial nominal trajectory and the measurements. Some increase in the noise statistics is to be recommended anyway, since one ought to account for the model inadequacy introduced by the

first-order Taylor series expansions used to generate the state and measurement models.

Finally, the model is limited at present by the assumptions that thrust acts along the velocity vector and that side force is negligible. These assuptions reduce the utility of the algorithm, as some mishap scenarios involve high angles of attack and sideslip. Attention should be given to removing these limitations by modifying the equations of motion appropriately. Some additional complexity would be introduced, but this would probably be justified by the resulting increase in algorithm utility.

Appendix: Trajectory Time History Plots

This Appendix includes Figures 2 - 20, which are plots of the time histories of variables processed by the filter-smoother algorithm. Features of plot symbology and characteristics which have not been mentioned in the text are discussed below.

Figures 2 - 4 are plots of the true trajectories and measurement data for Trajectories 1 - 3, described in Section 3.2. In these plots the solid lines represent the true trajectory, and the plus signs represent measured data points.

Figure 5 is a plot of the smoother output trajectory and the true trajectory for the baseline case described in Section 4.1. In this figure the solid line represents the filter-smoother output, while the plus signs represent the true trajectory. In all succeeding figures only one solid line appears, which is defined as indicated in the text and by the figure title.

In the roll attitude trace of Figure 3, the reader will observe what appears to be a "jump" discontinuity in the data. This effect is caused by the plotting software, which restricts all angles to the ±180 deg range. A related effect occurs in Figure 4. In this figure, at a time shortly before 9 sec, the aircraft flies through the

vertical, defined by a flight path angle of 90 deg. In accordance with conventional practice, the plotting software limits flight path angle to ±90 deg, and changes roll attitude and heading angle by 180 deg when the aircraft flies through the vertical. These effects are seen in Figure 4 as an abrupt change in slope in the flight path angle plot, and 180 deg "jumps" in the heading angle and roll attitude plots.

Additional jumps seen later in the heading angle and roll attitude plots in Figure 4 are due to the angular range limit discussed above. The first several of these, occurring between $t = 9$ sec and $t = 12$ sec, are caused by the aircraft flying at a roll attitude of approximately 180 deg. As noise is introduced, the roll attitude goes back and forth between +180 deg and -180 deg. The second group of jumps occur at the end of the trajectory and are caused by the aircraft being put through several 360 deg rolls. All of these discontinuities occur in the plotting software, and do not mean that discontinuities are occurring in the data being processed by the filter-smoother algorithm.

The reader is cautioned that the scales appearing on the plots were set automatically within the plotting software. Therefore, care is required when comparing corresponding plots, as the scales are usually different.

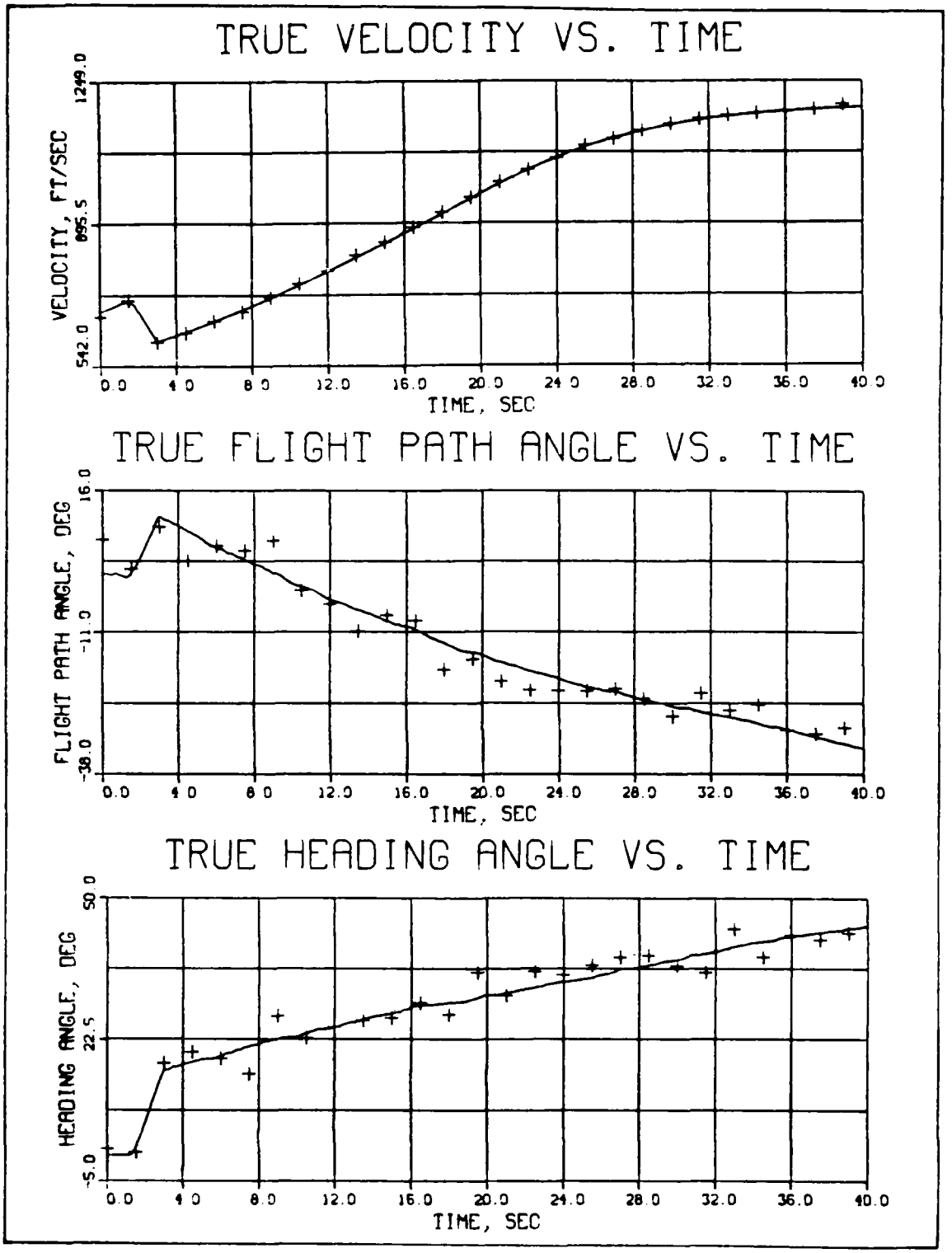

Figure 2. Time Histories of True States and Control Inputs for Trajectory 1

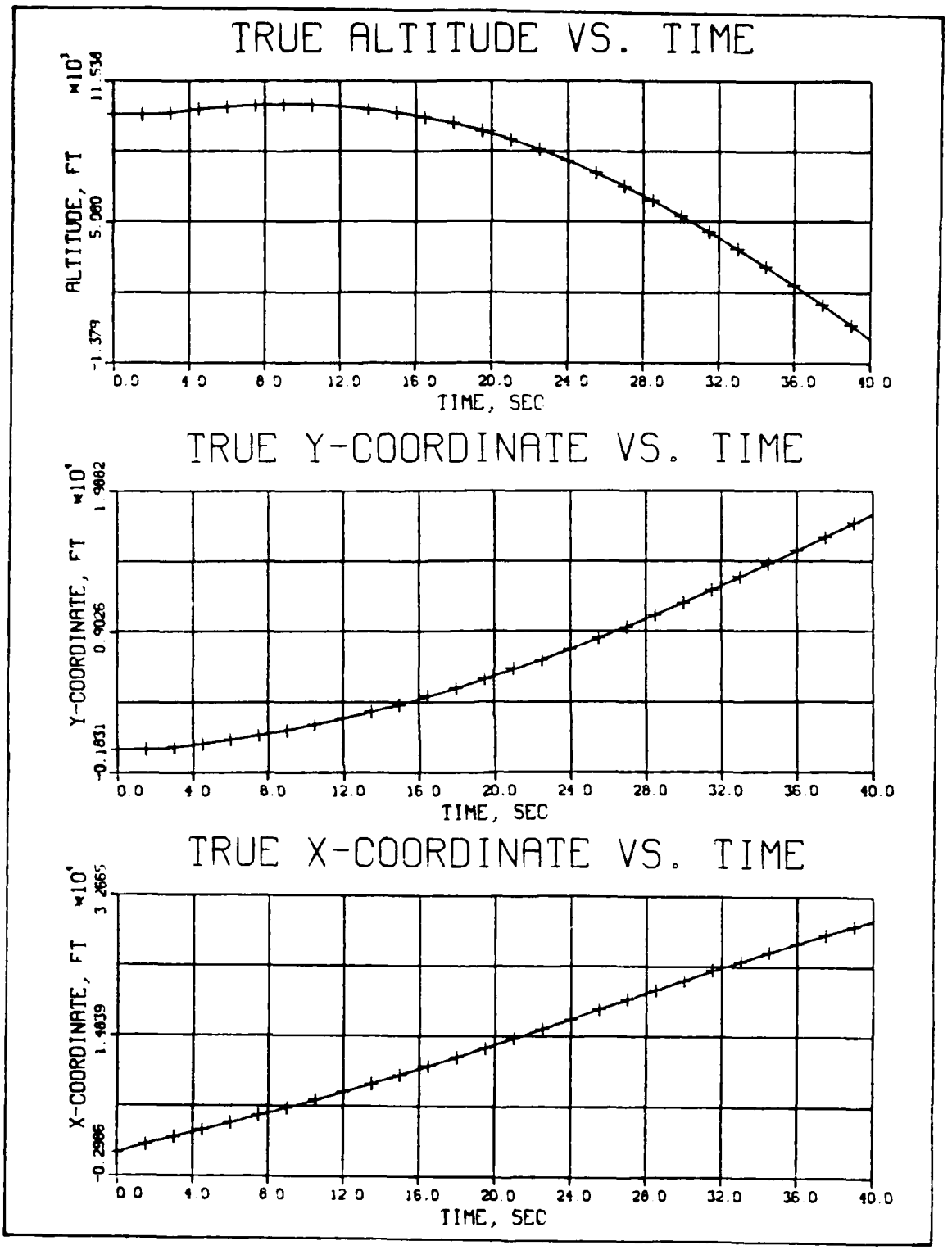

Figure 2 (continued)

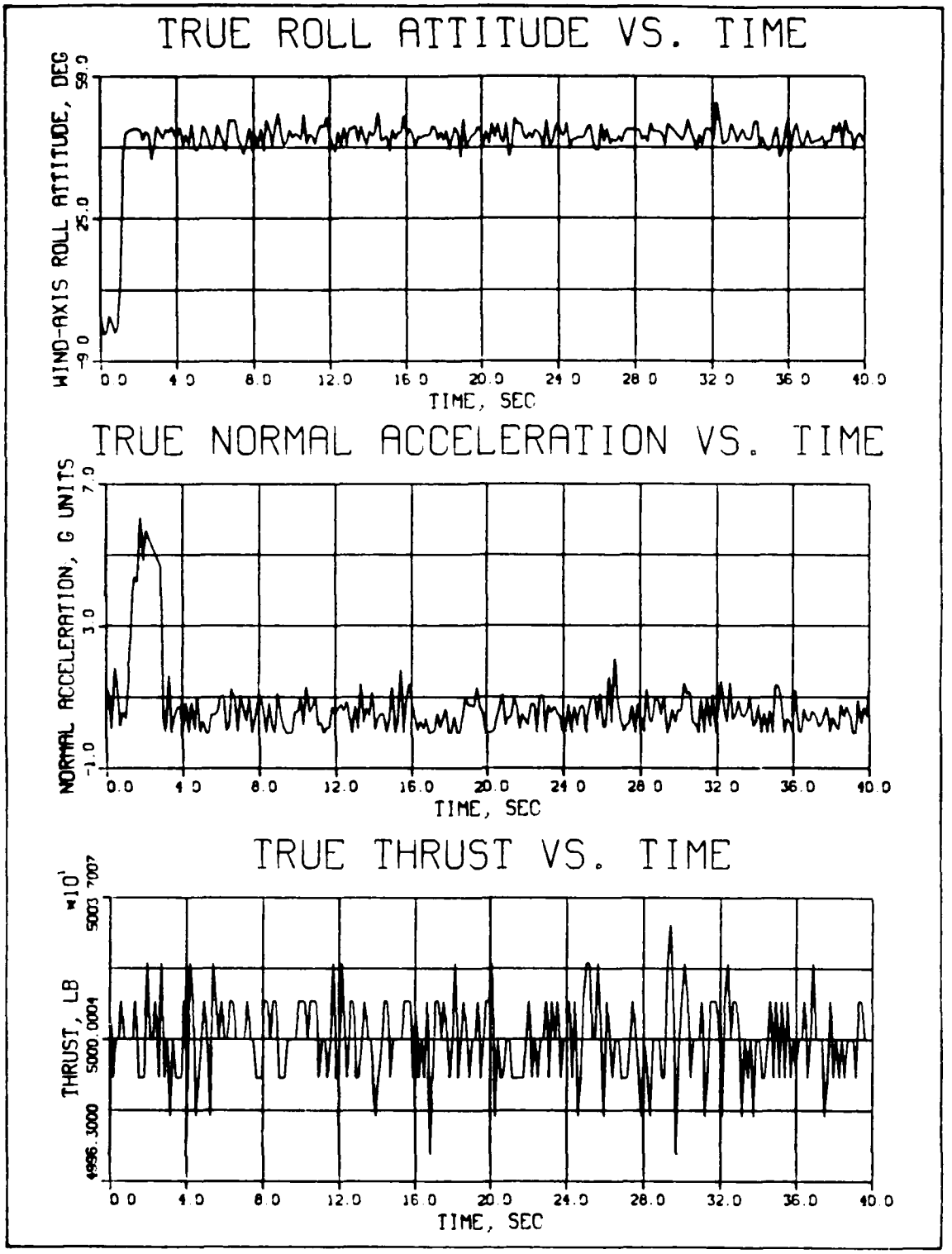

Figure 2 (continued)

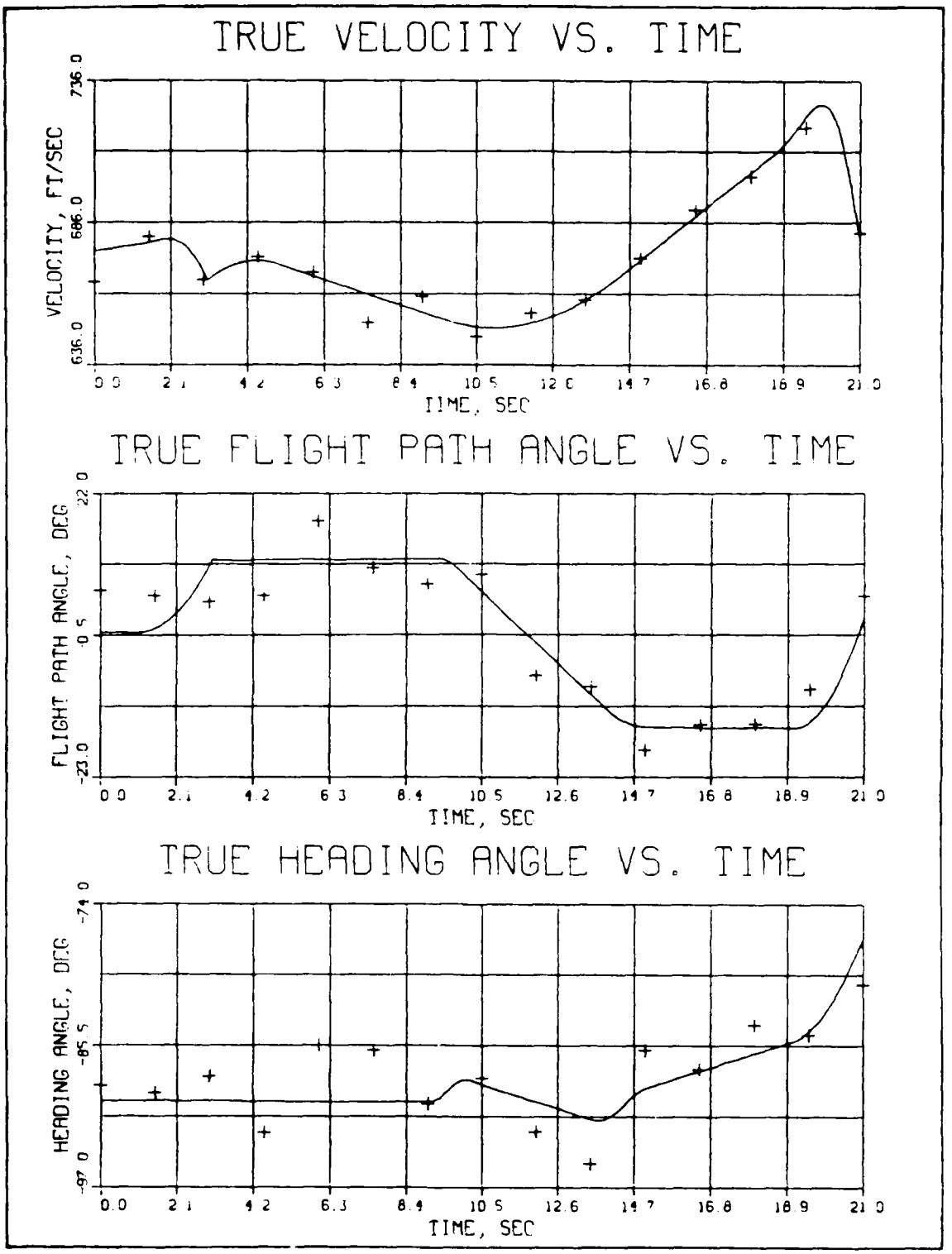

Figure 3. Time Histories of True States and Control Inputs for Trajectory 2

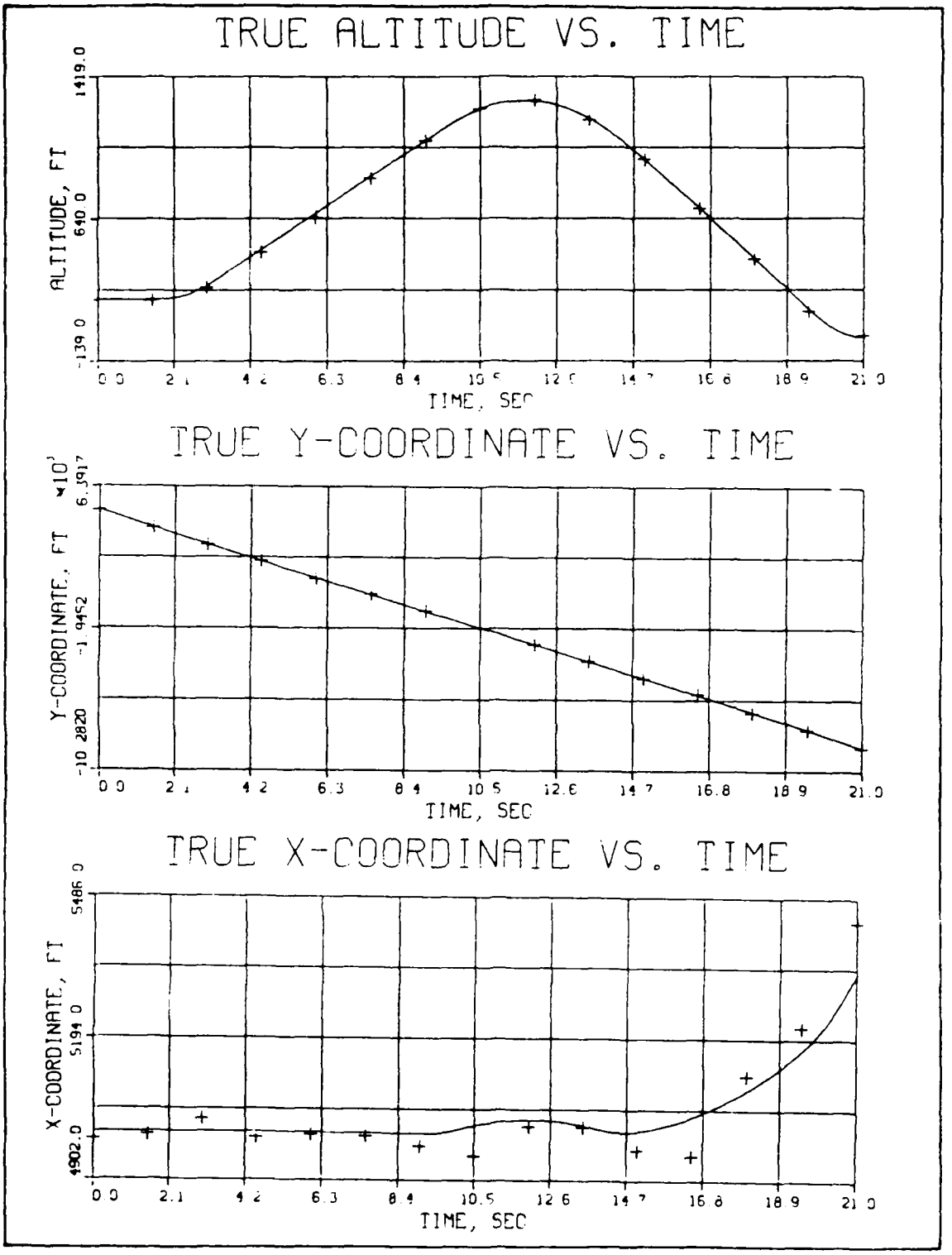

Figure 3 (continued)

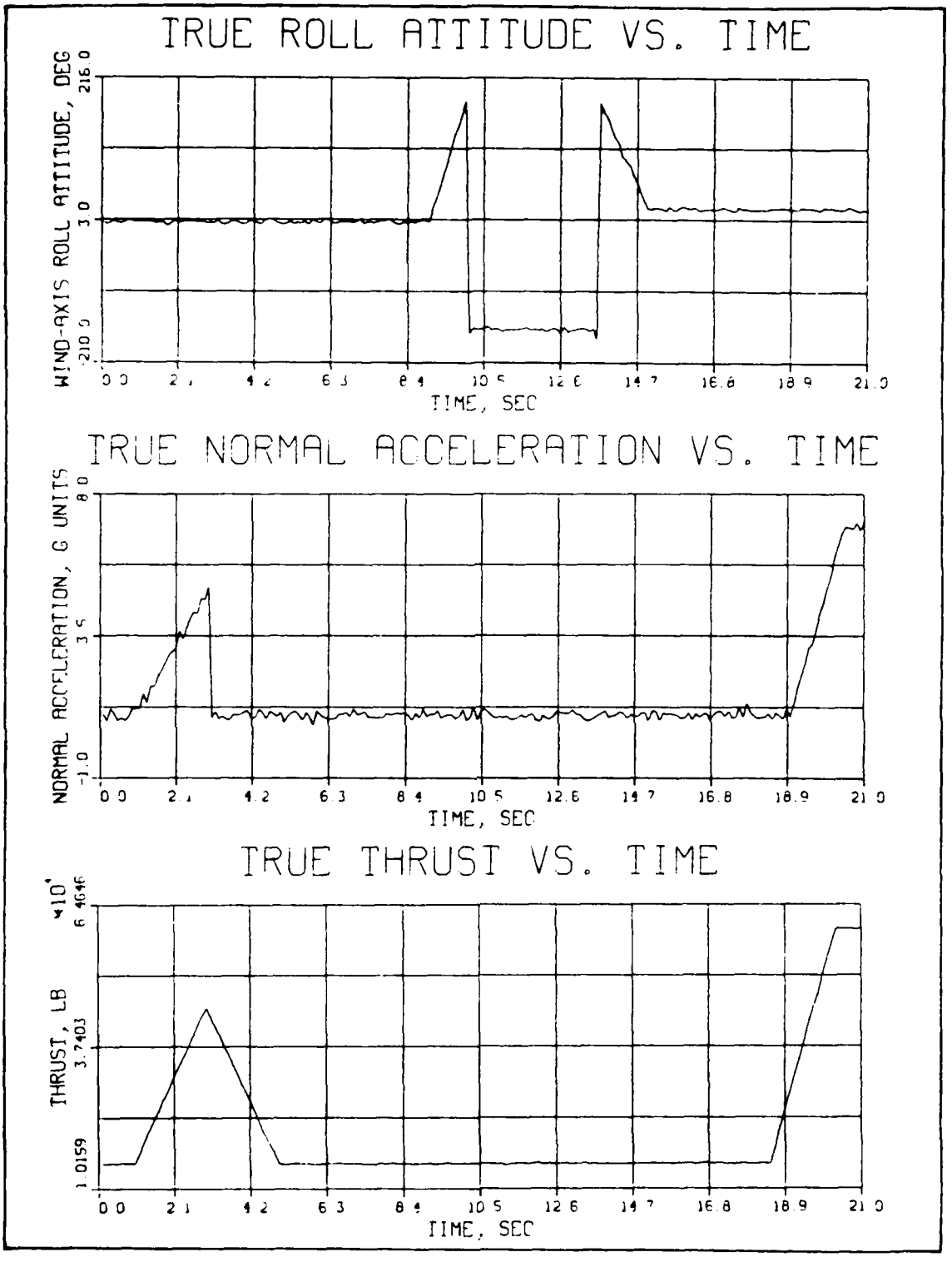

Figure 3 (continued)

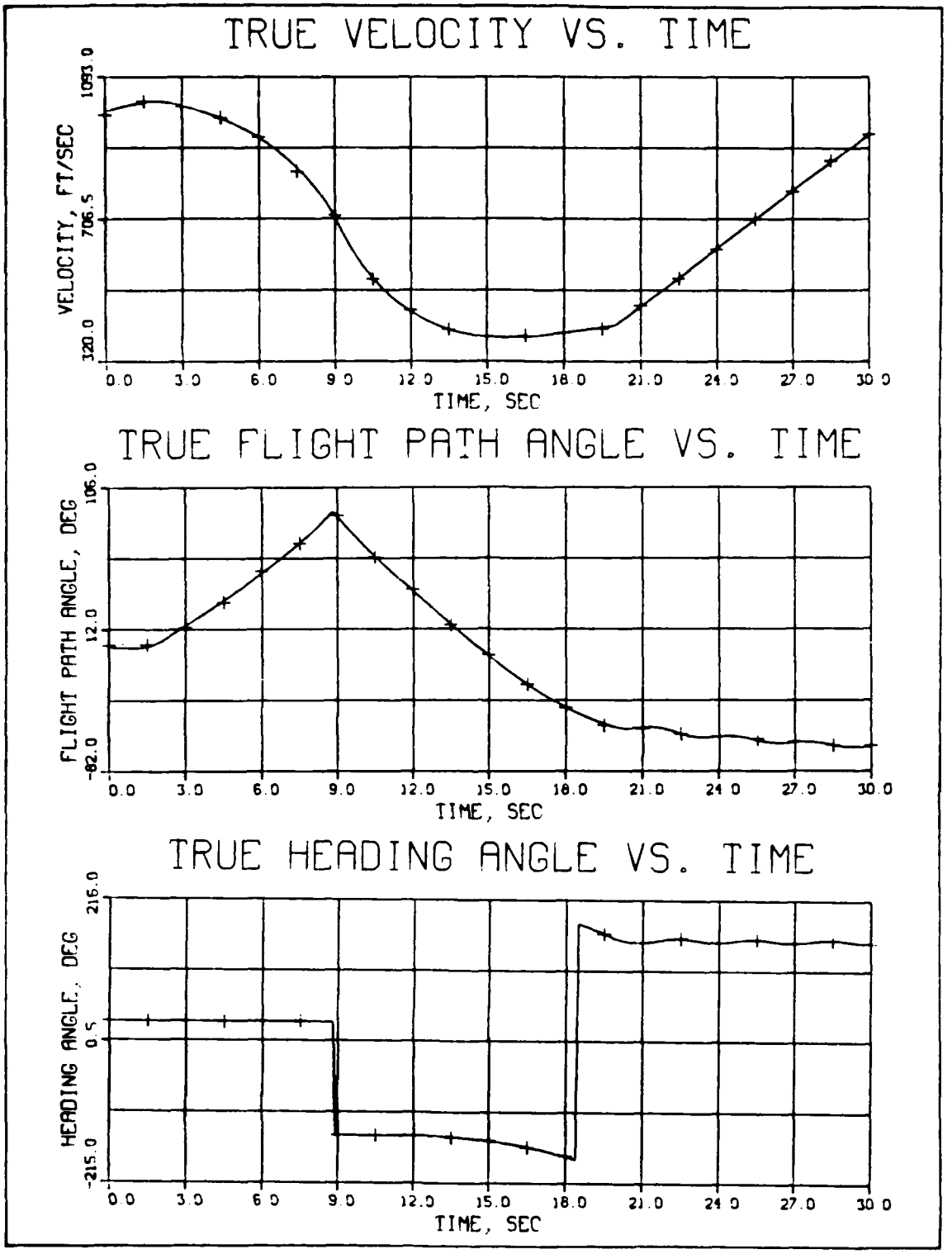

Figure 4. Time Histories of True States and Control Inputs for Trajectory 3

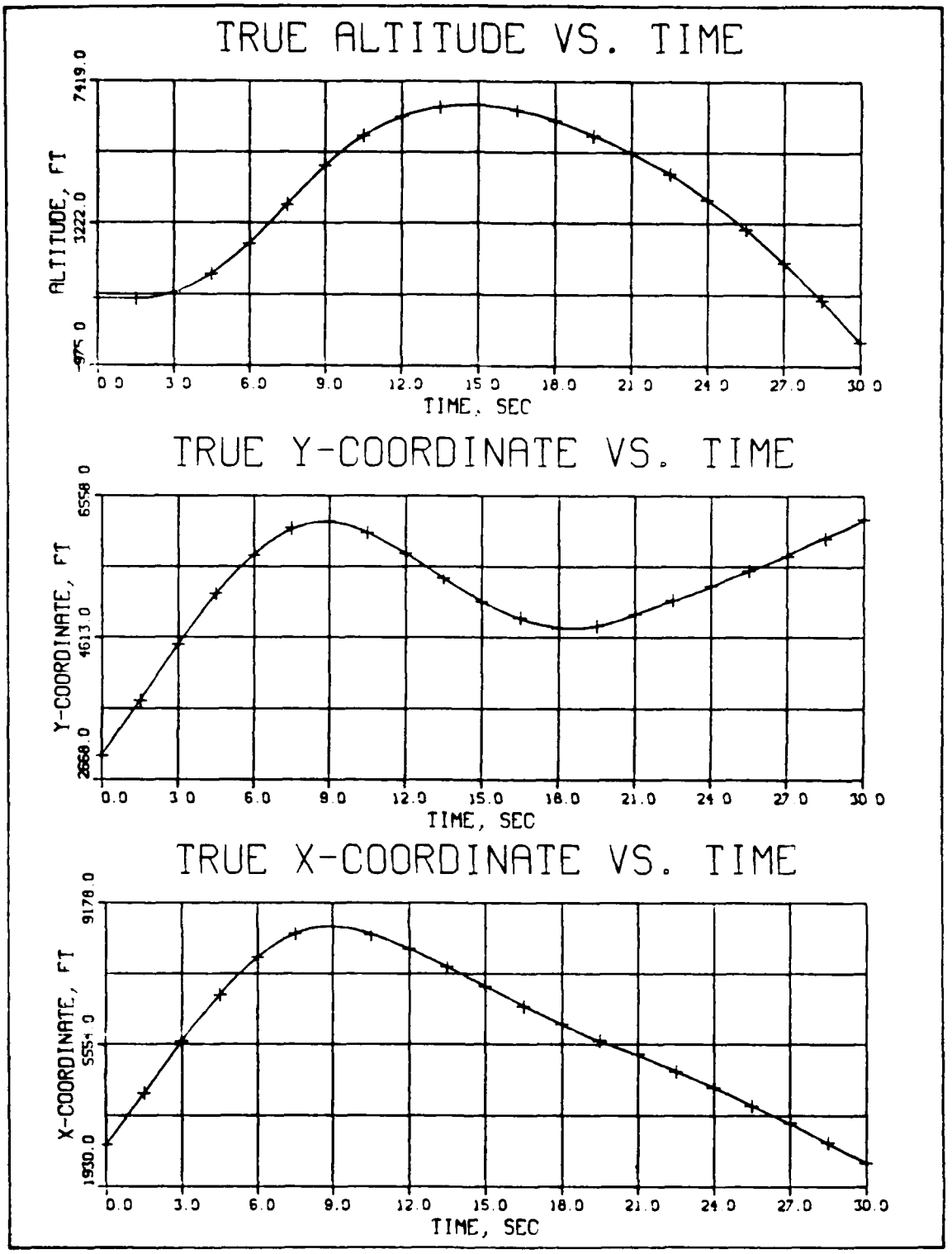

Figure 4 (continued)

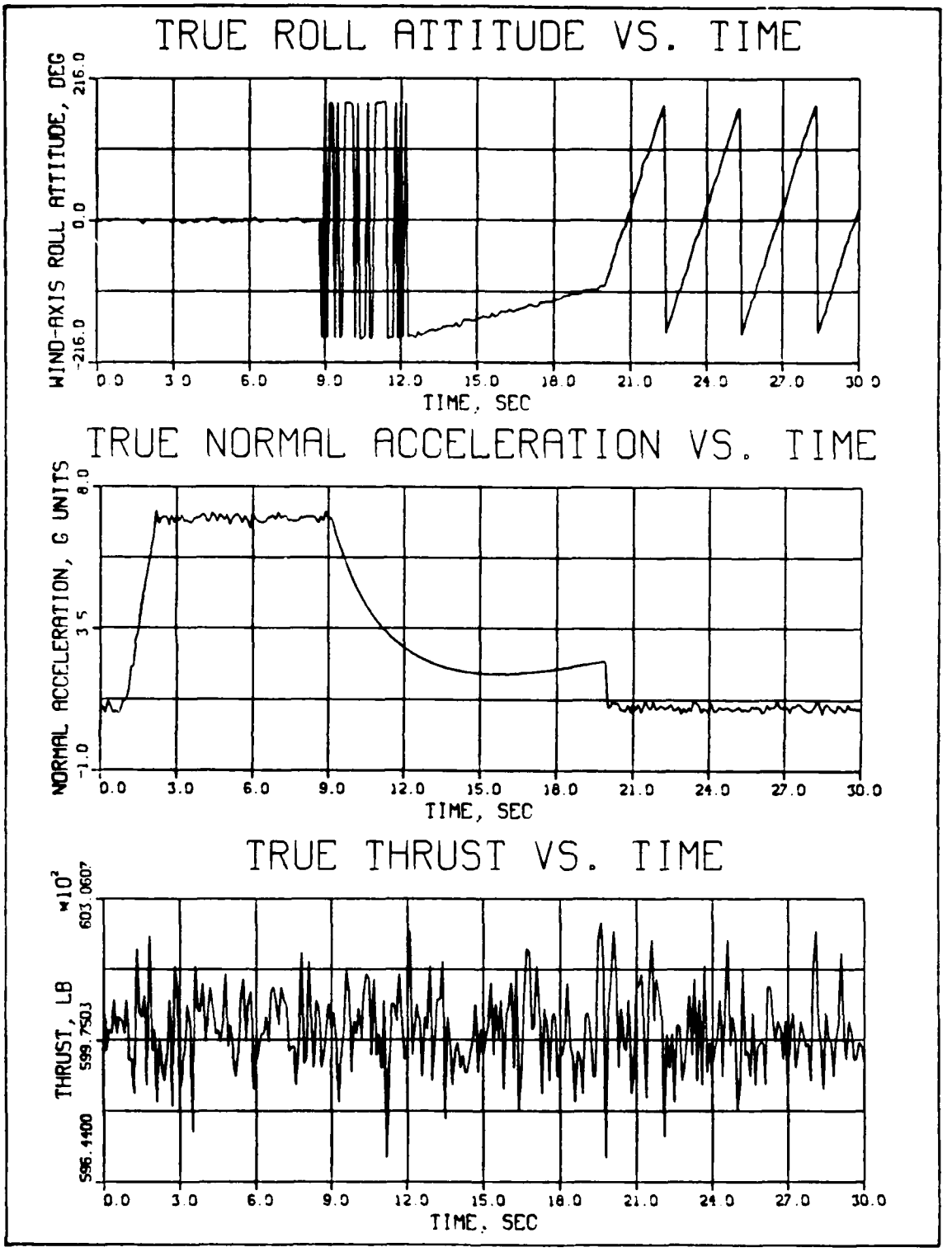

Figure 4 (continued)

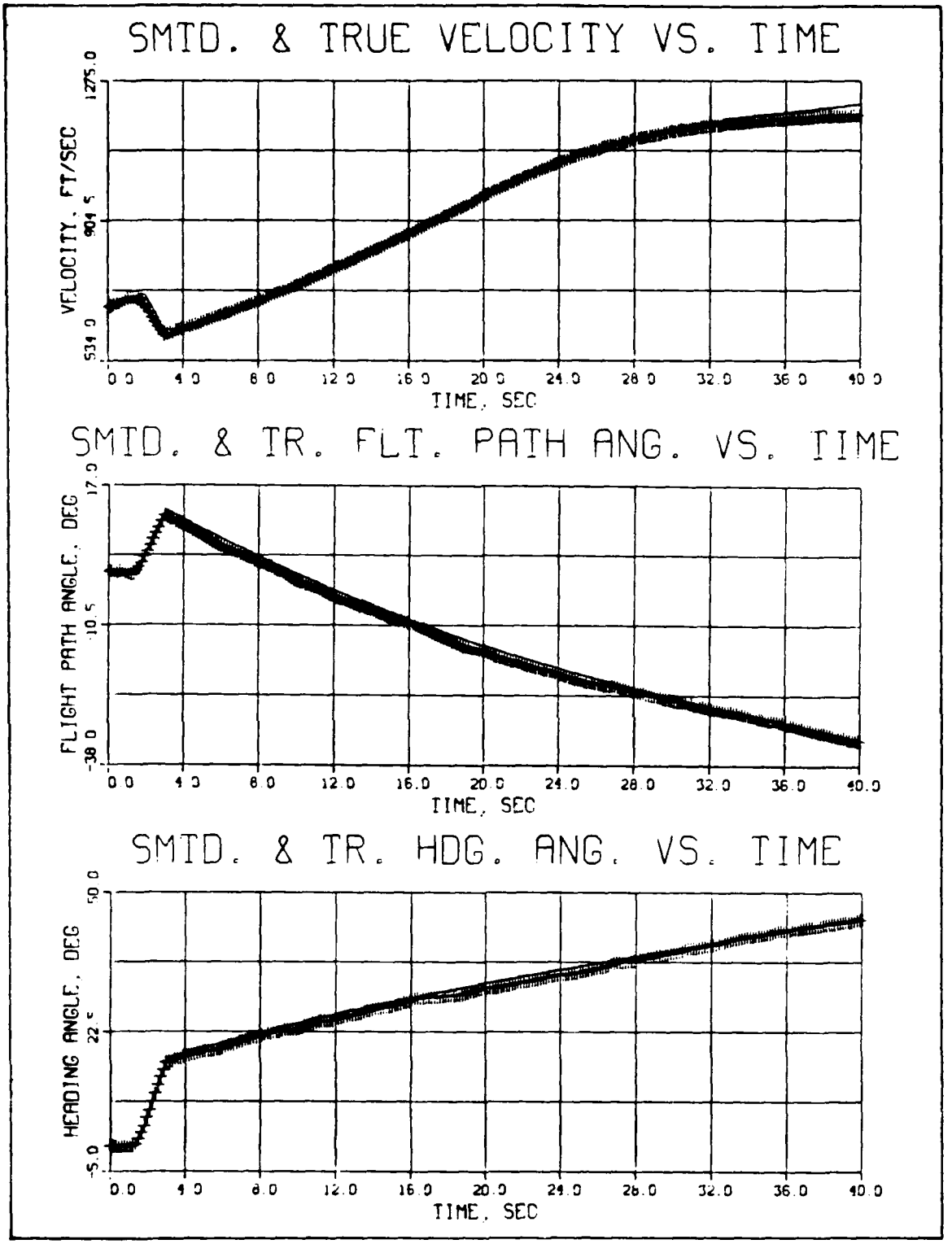

Figure 5. Time Histories of Smoothed and True Trajectories for Baseline Case

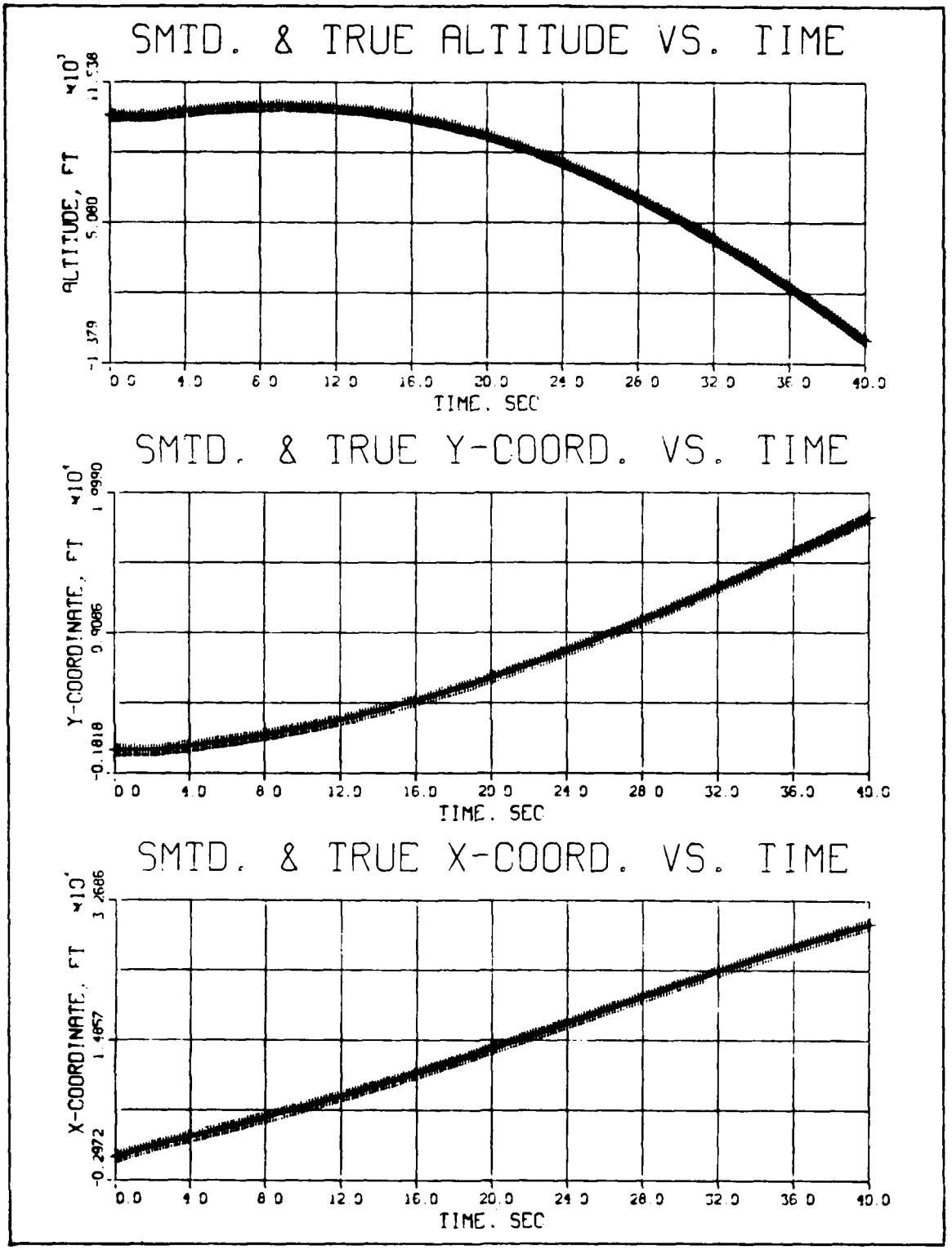

Figure 5 (continued)

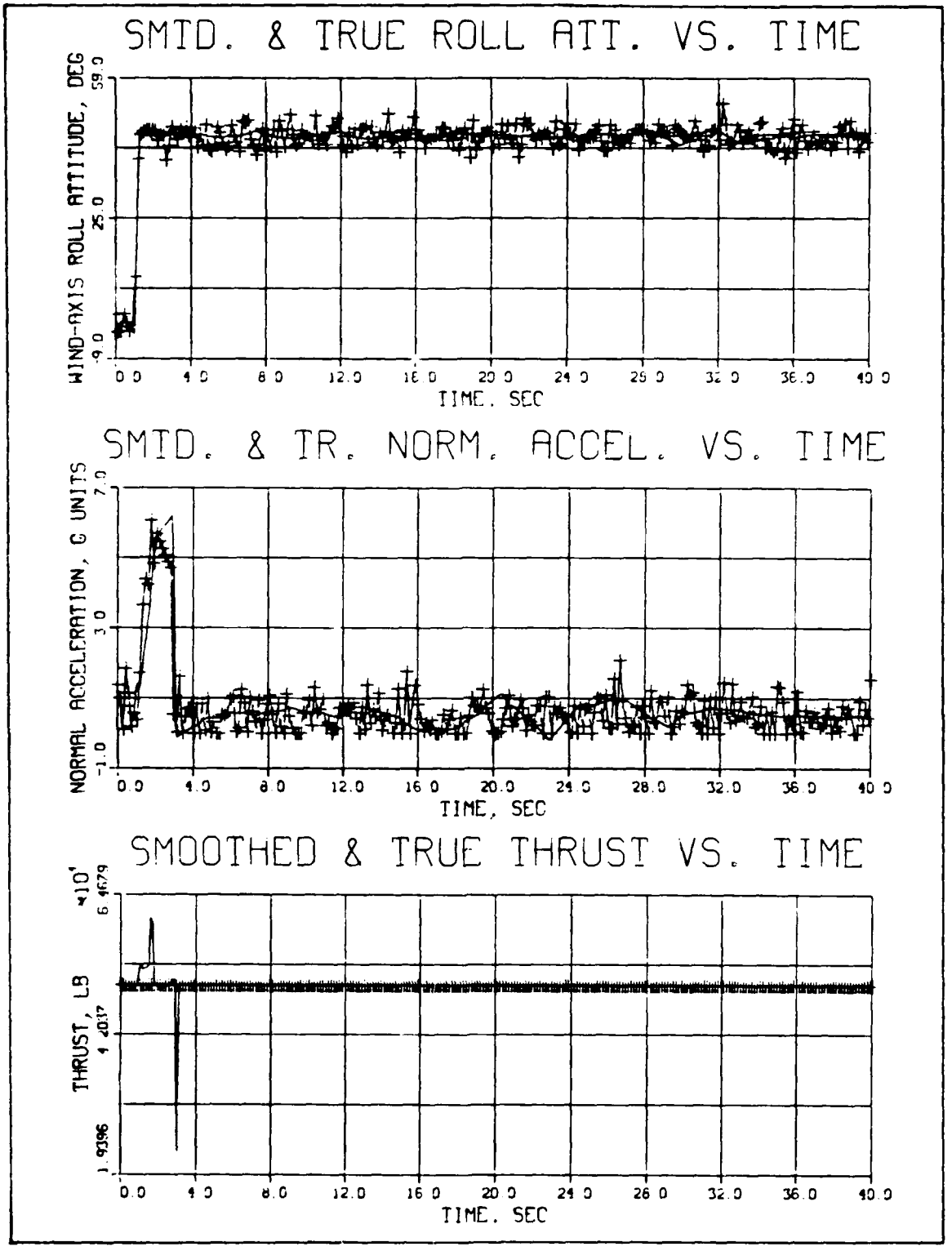

Figure 5 (continued)

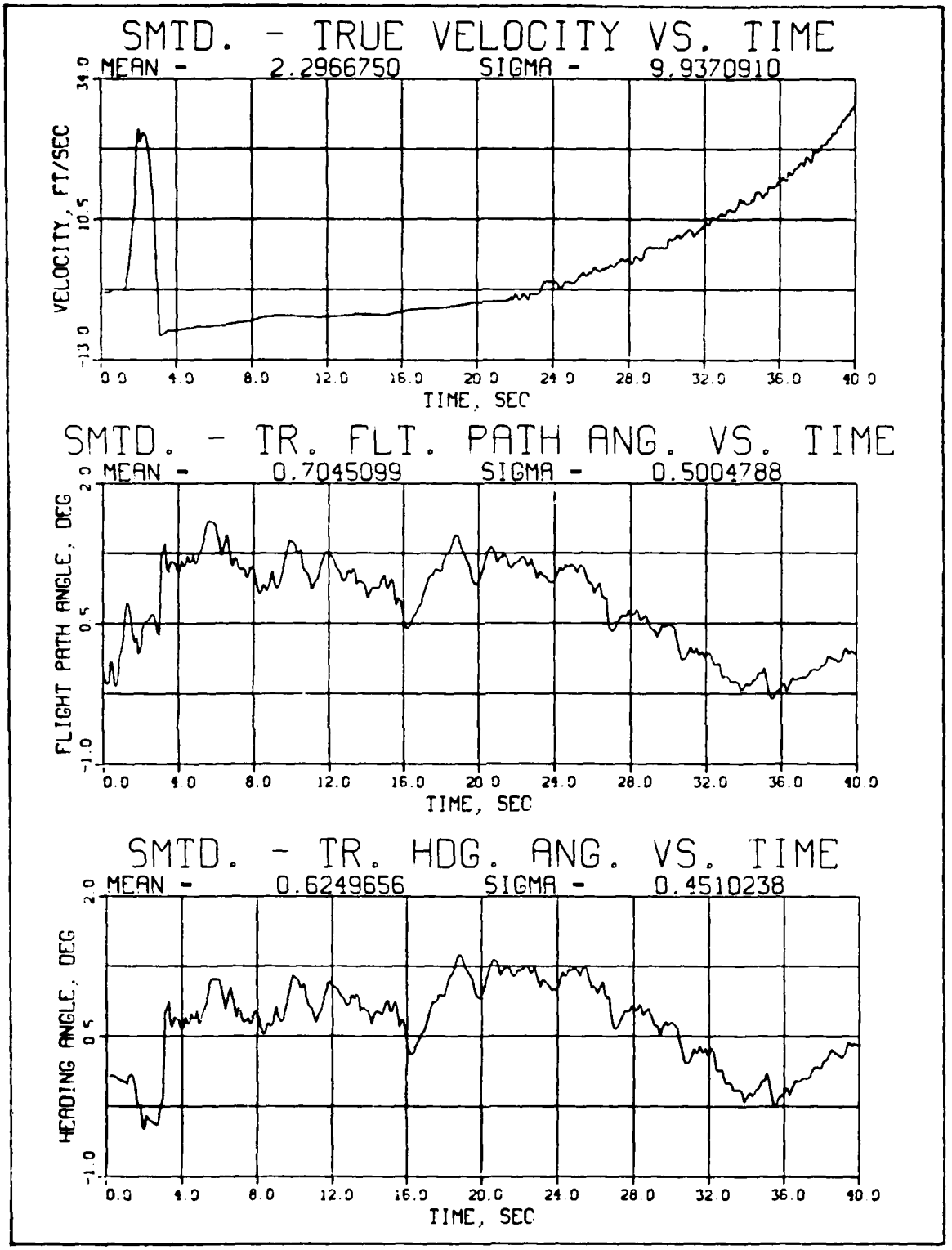

Figure 6. Time Histories of Errors Committed by Filter-Smoother Algorithm for Baseline Case

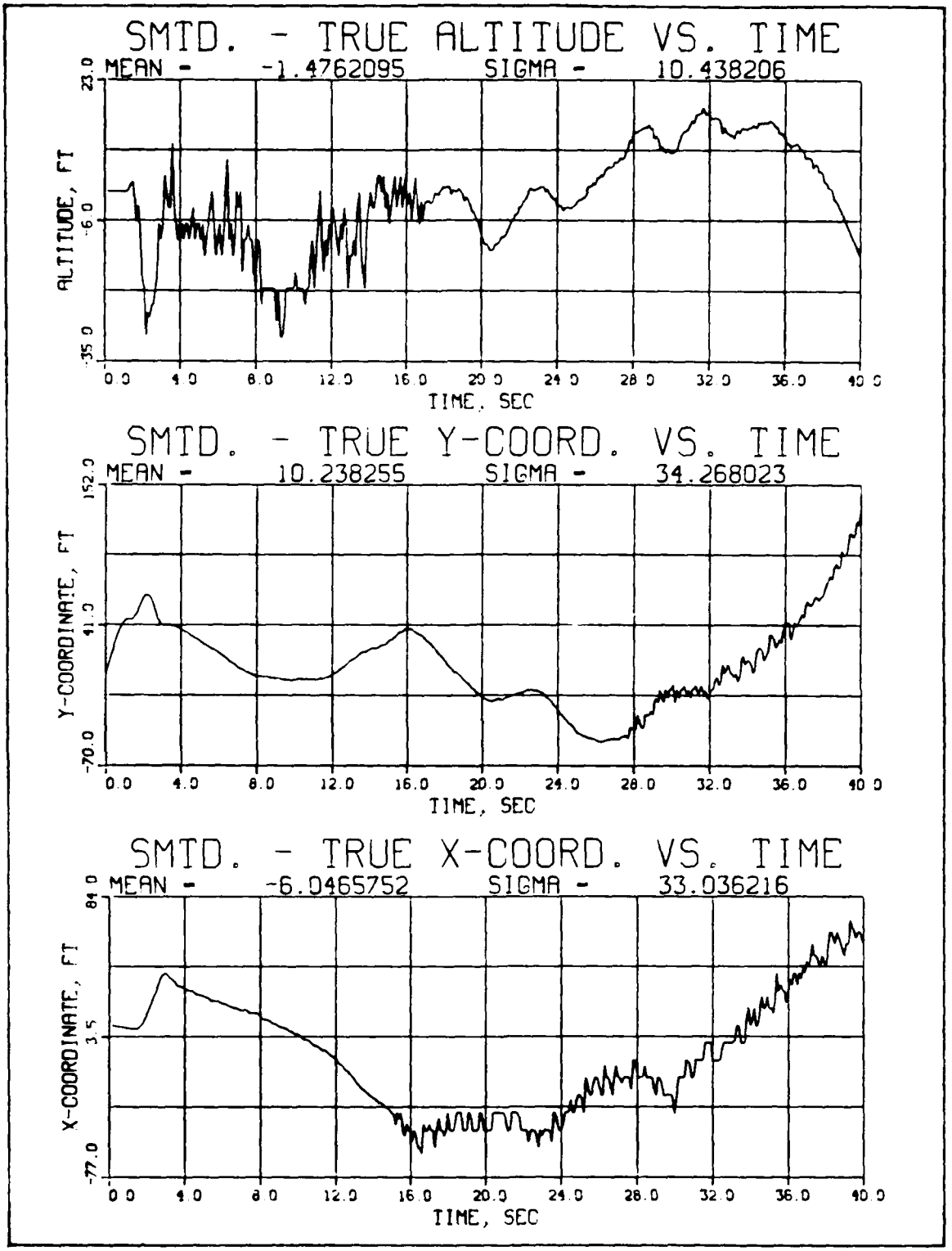

Figure 6 (continued)

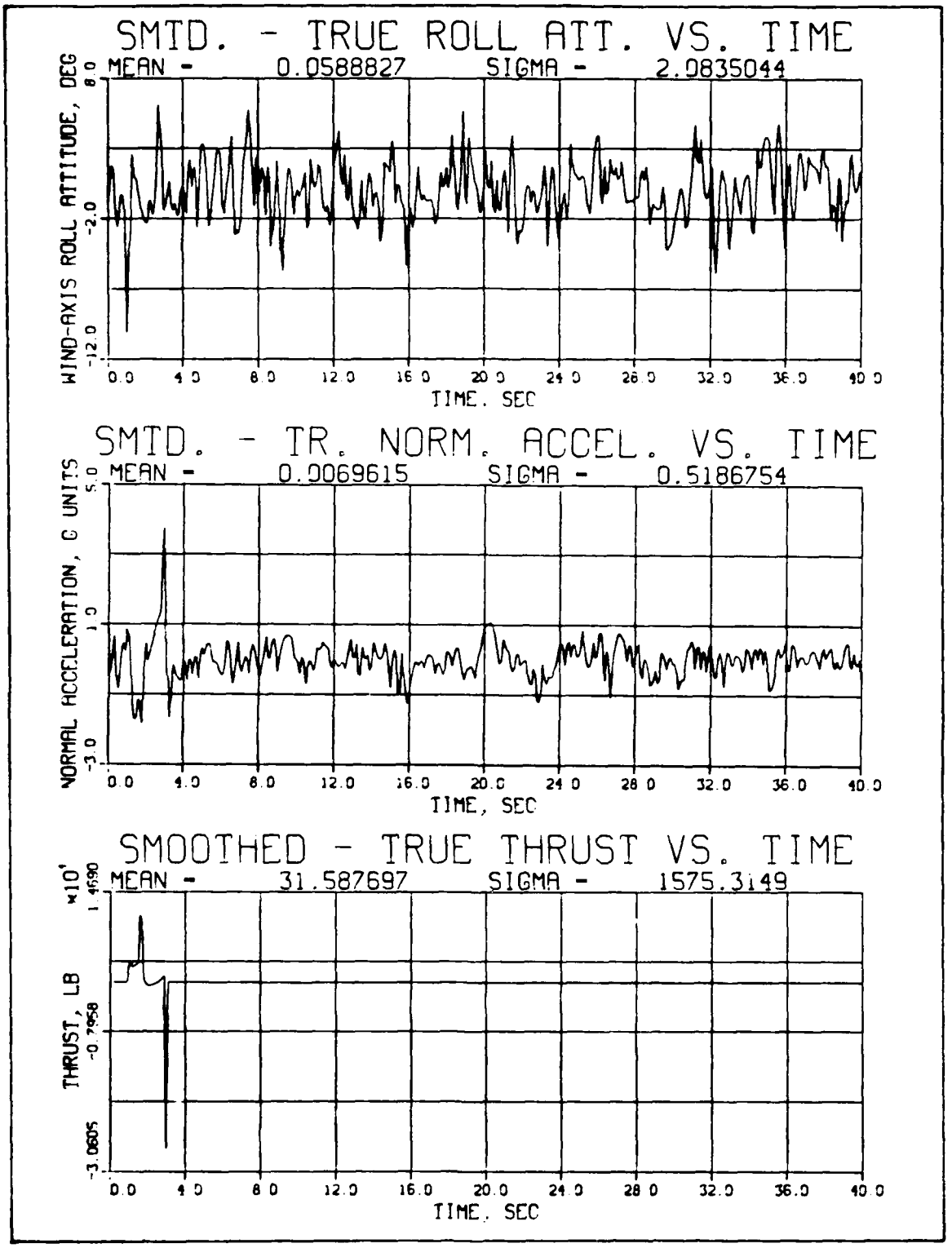

Figure 6 (continued)

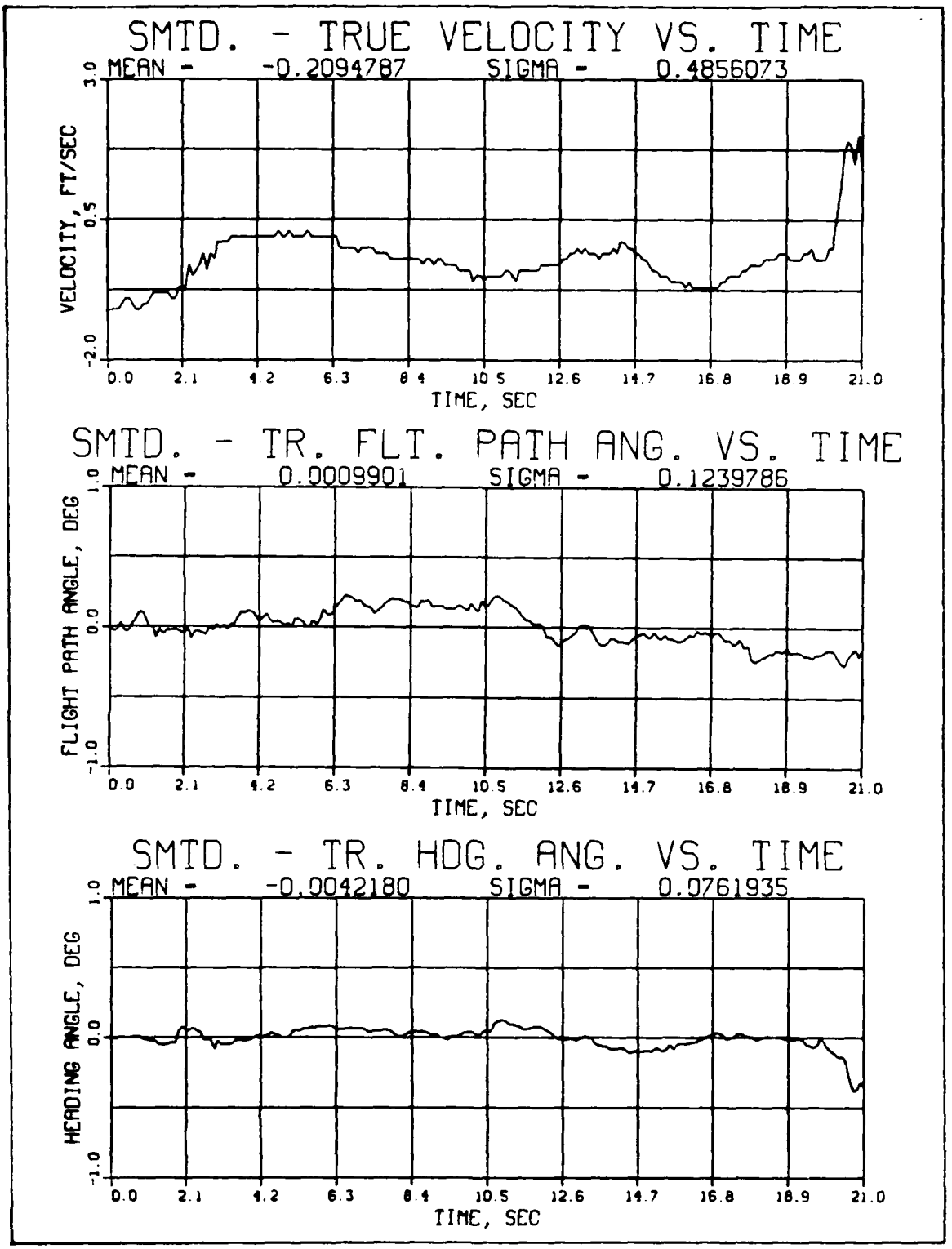

Figure 7. Errors Committed by Filter-Smoother Algorithm for Trajectory 2, Measurement Model FS-1

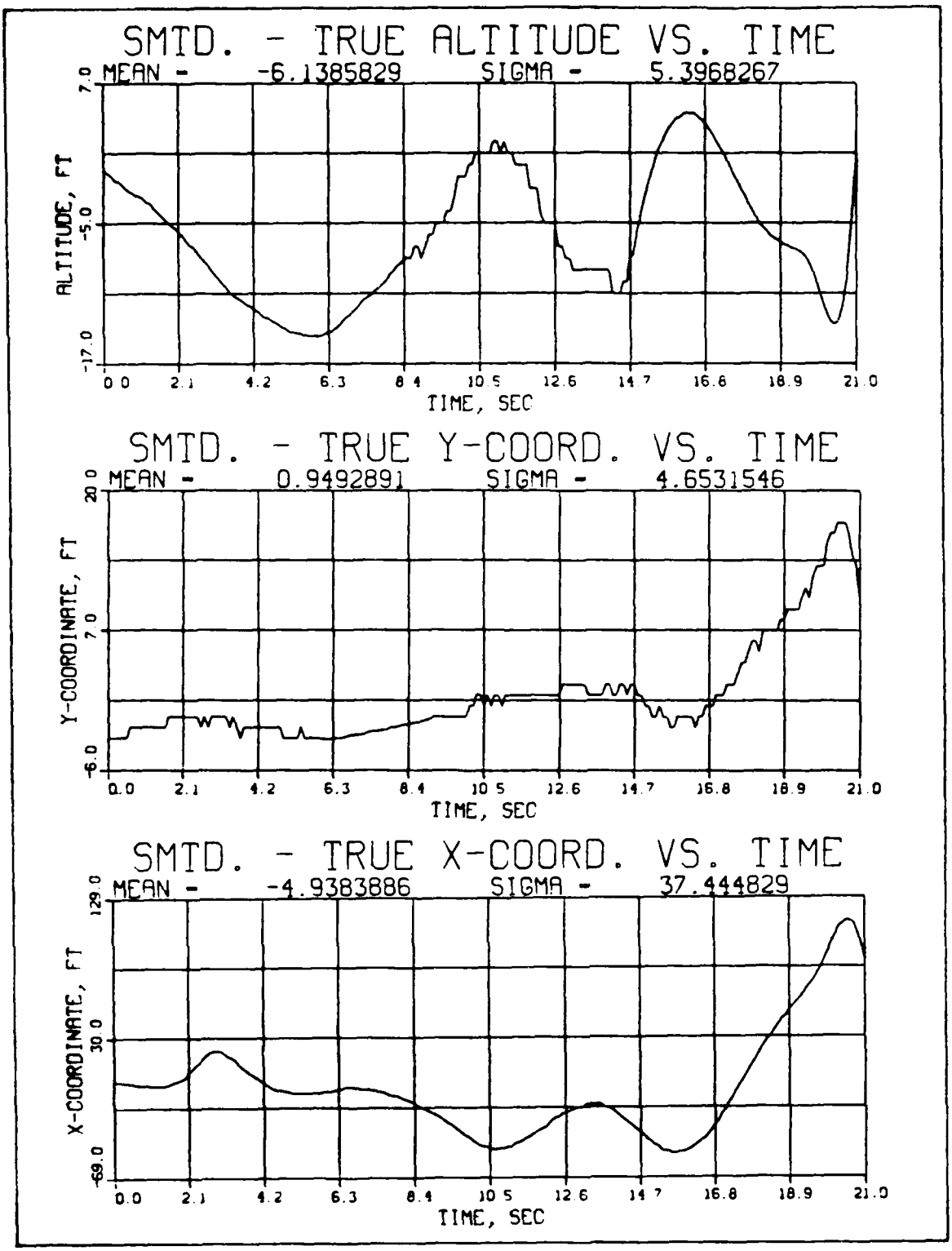

Figure 7 (continued)

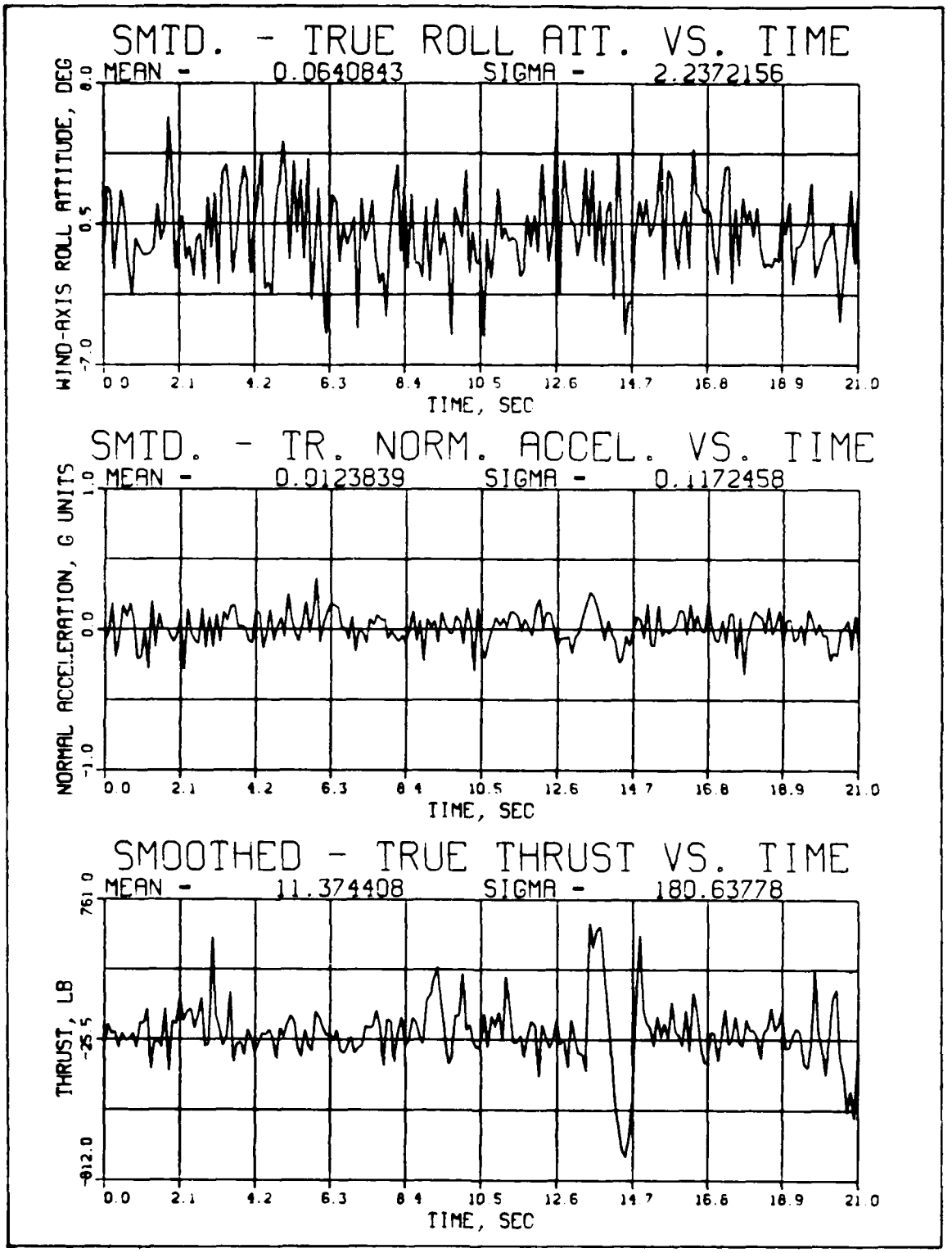

Figure 7 (continued)

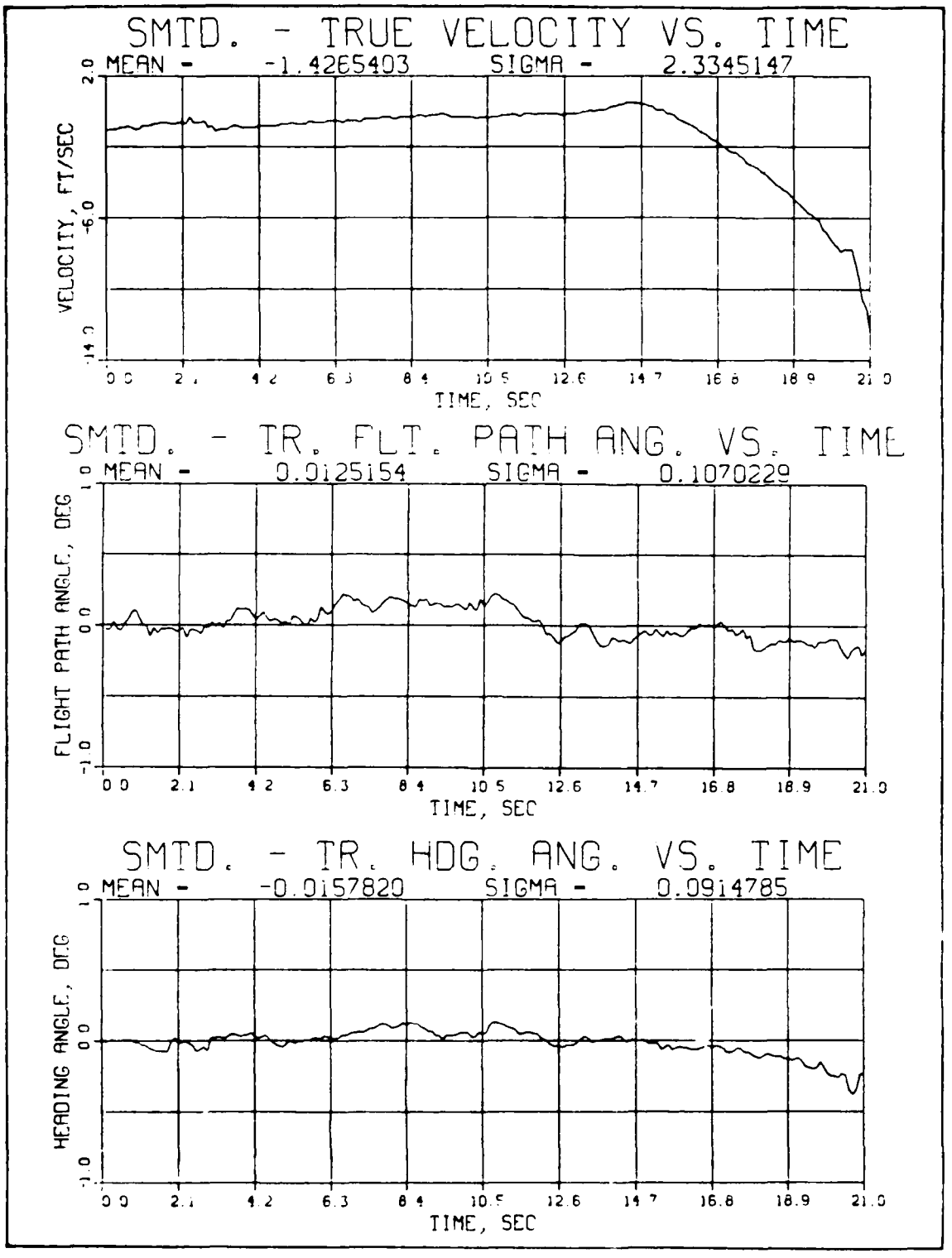

Figure 8. Errors Committed by Filter-Smoother Algorithm for Trajectory 2, Measurement Model RP-2

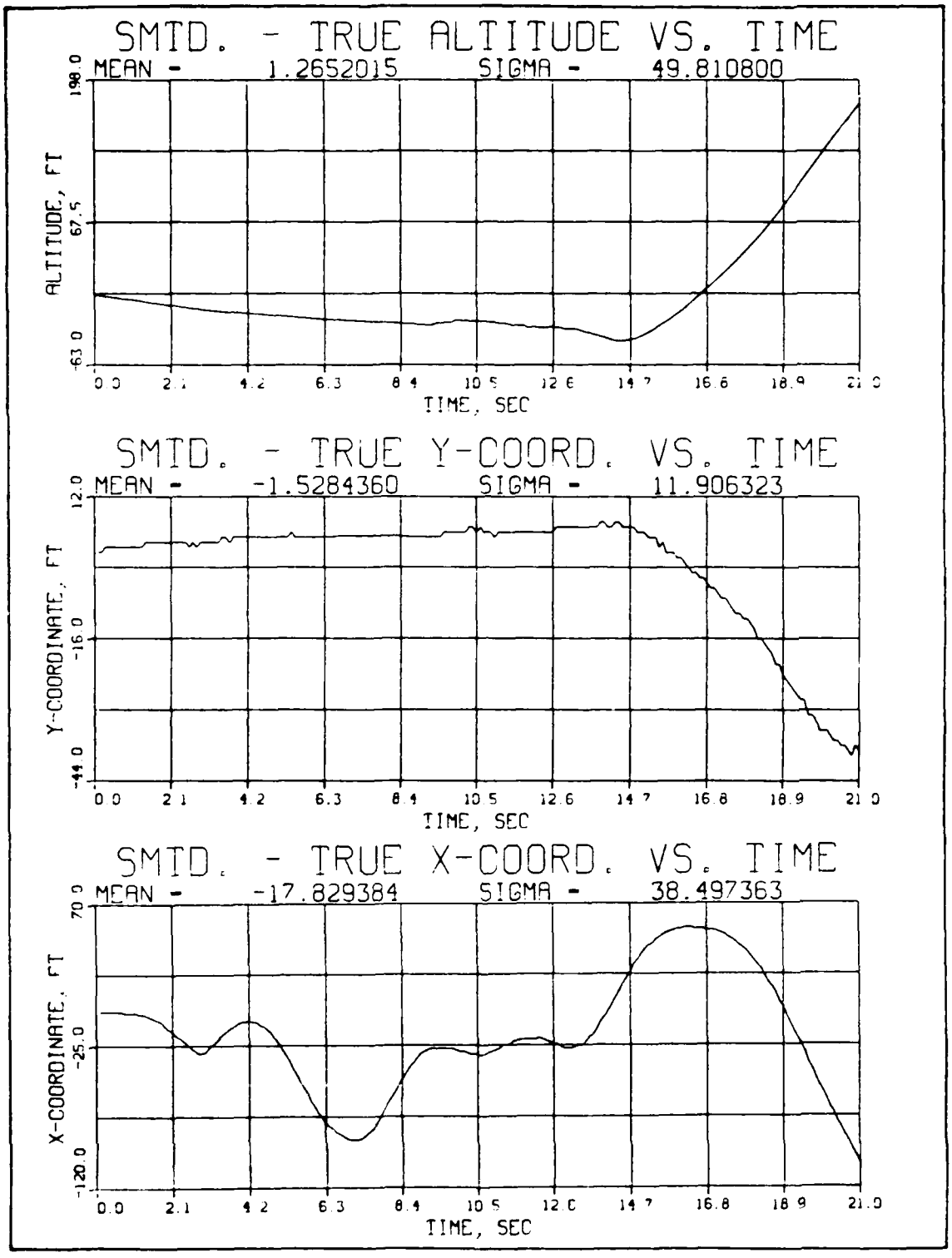

Figure 8 (continued)

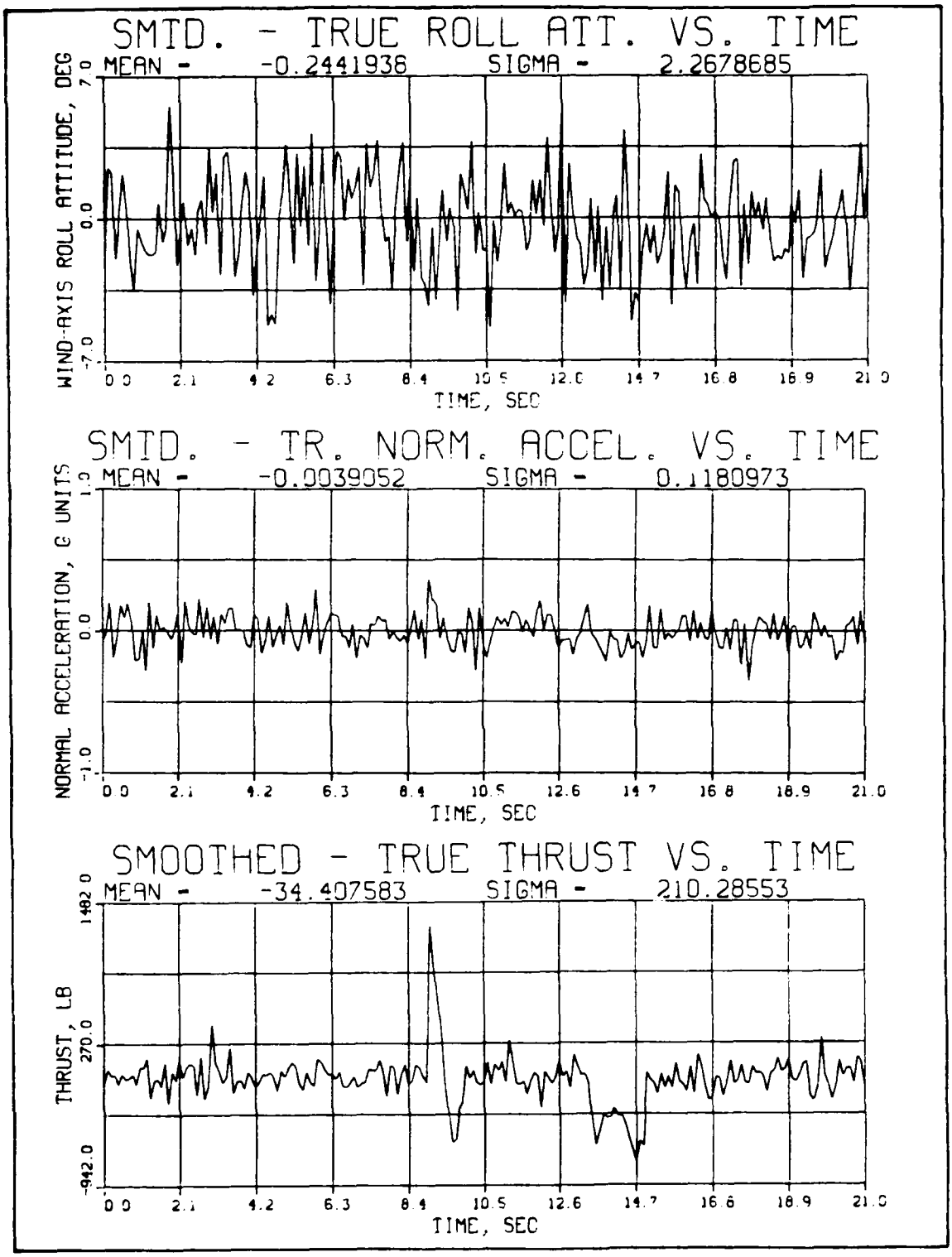

Figure 8 (continued)

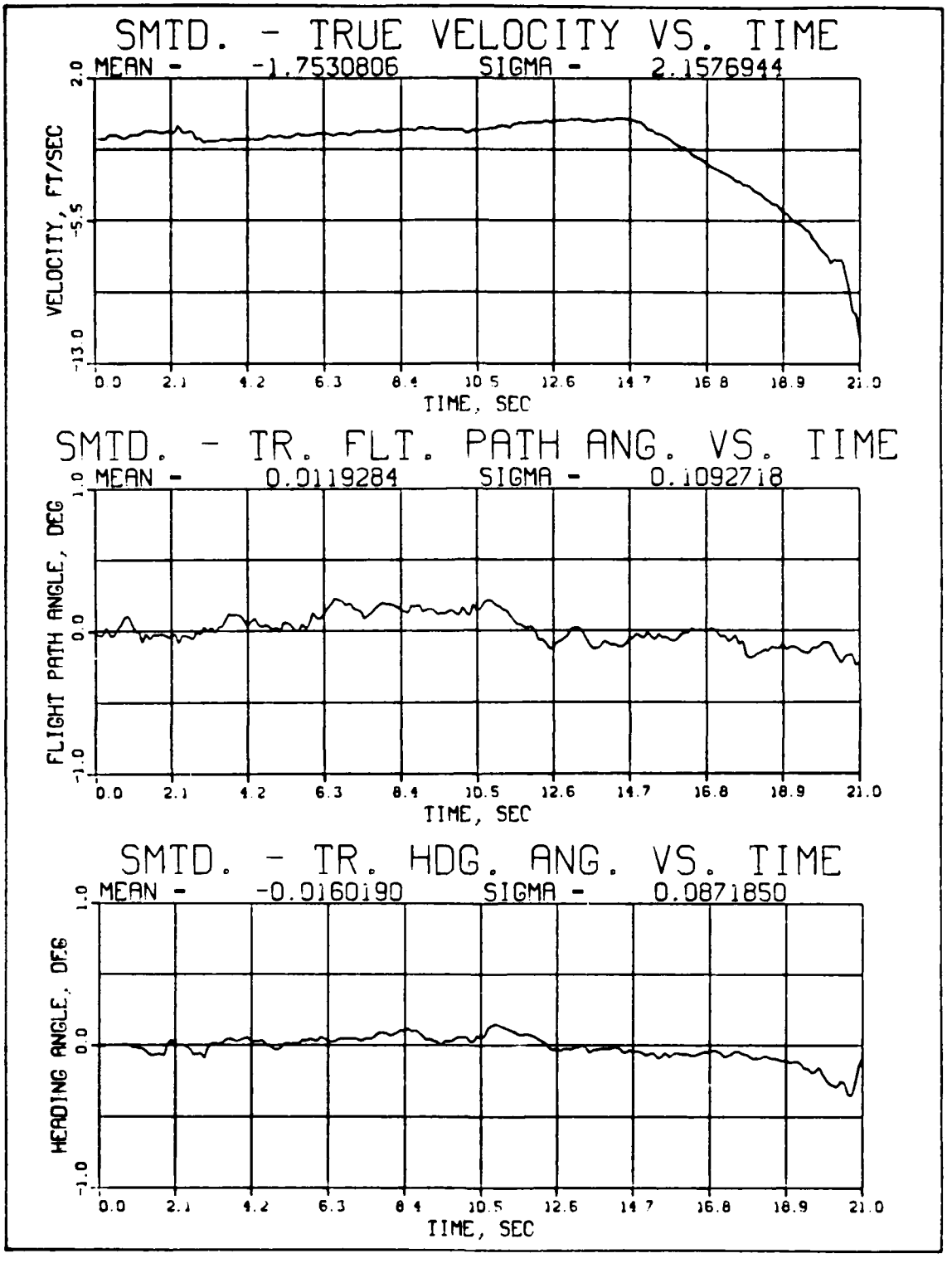

Figure 9. Errors Committed by Filter-Smoother Algorithm for Trajectory 2, Measurement Model RR-2

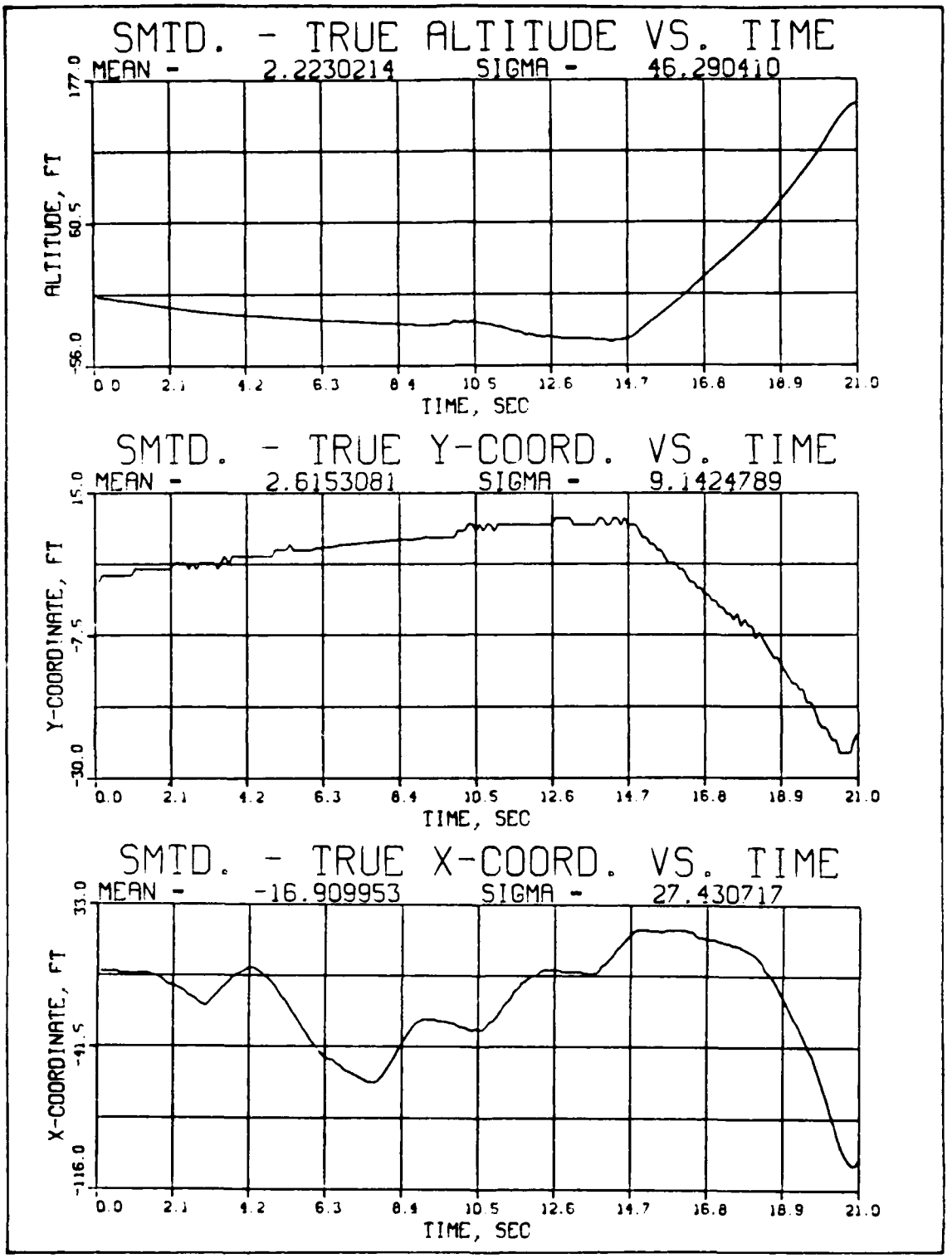

Figure 9 (continued)

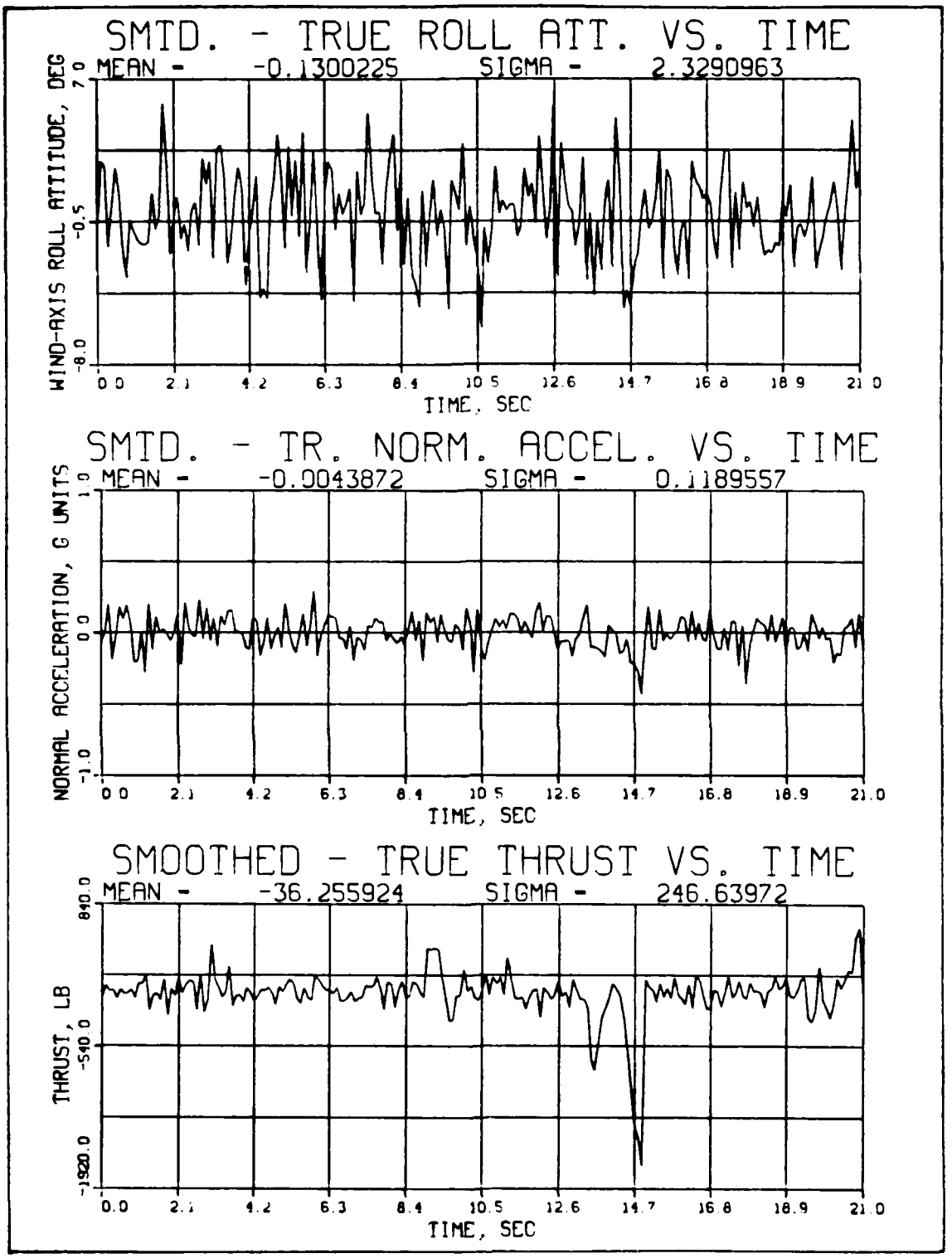

Figure 9 (continued)

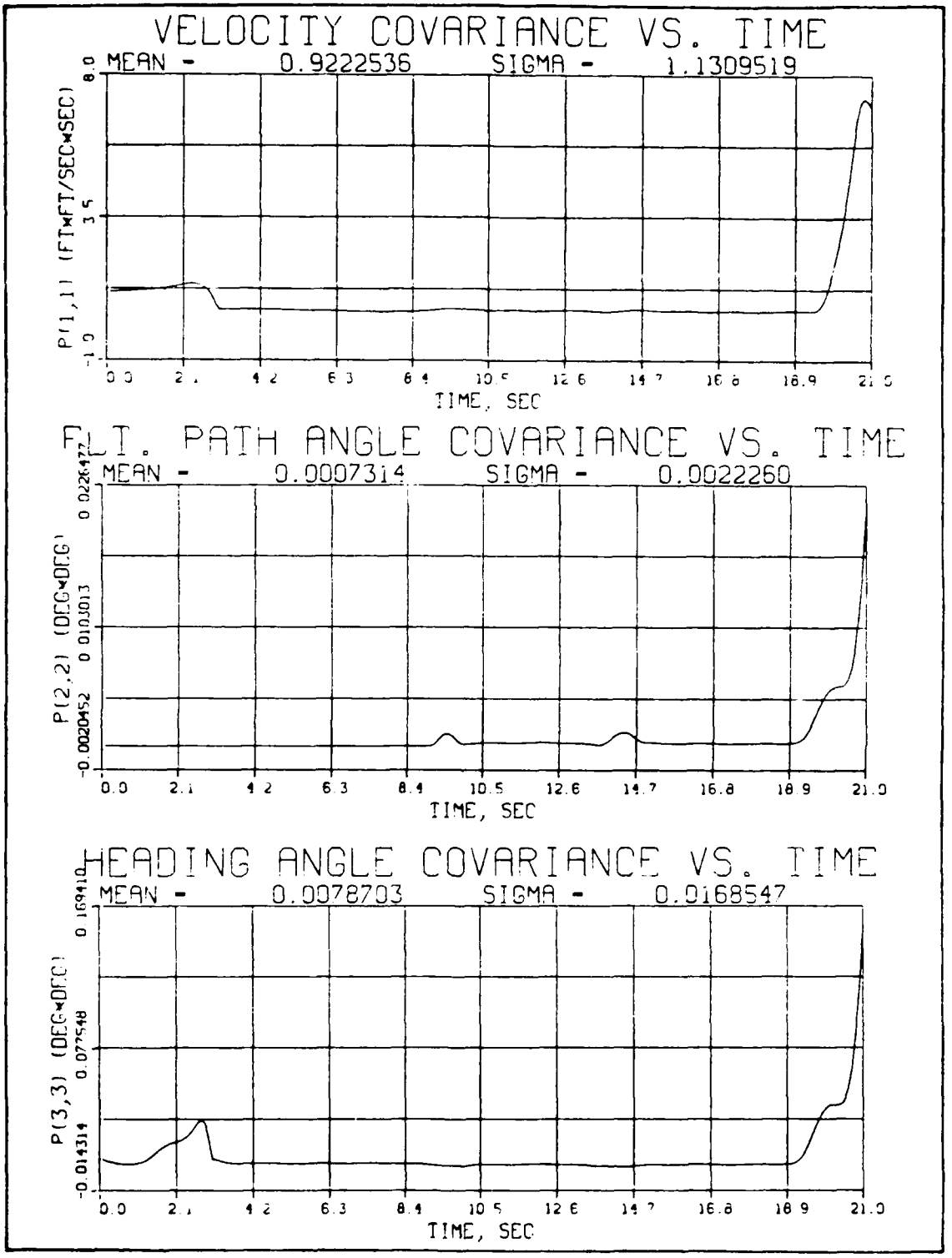

Figure 10. Diagonal Elements of Filter-Smoother Computed Covariance for Trajectory 2, Measurement Model FS-1

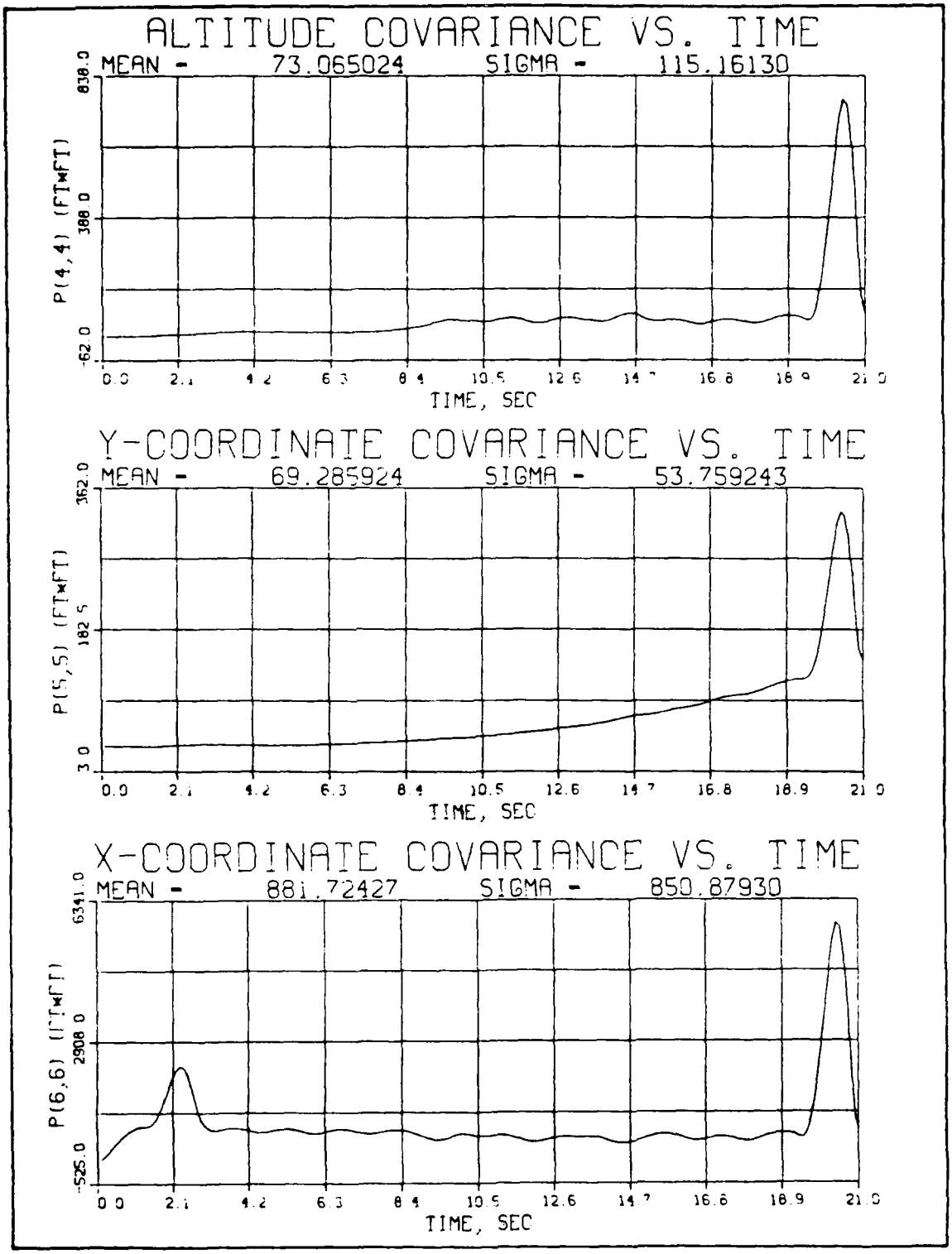

Figure 10 (continued)

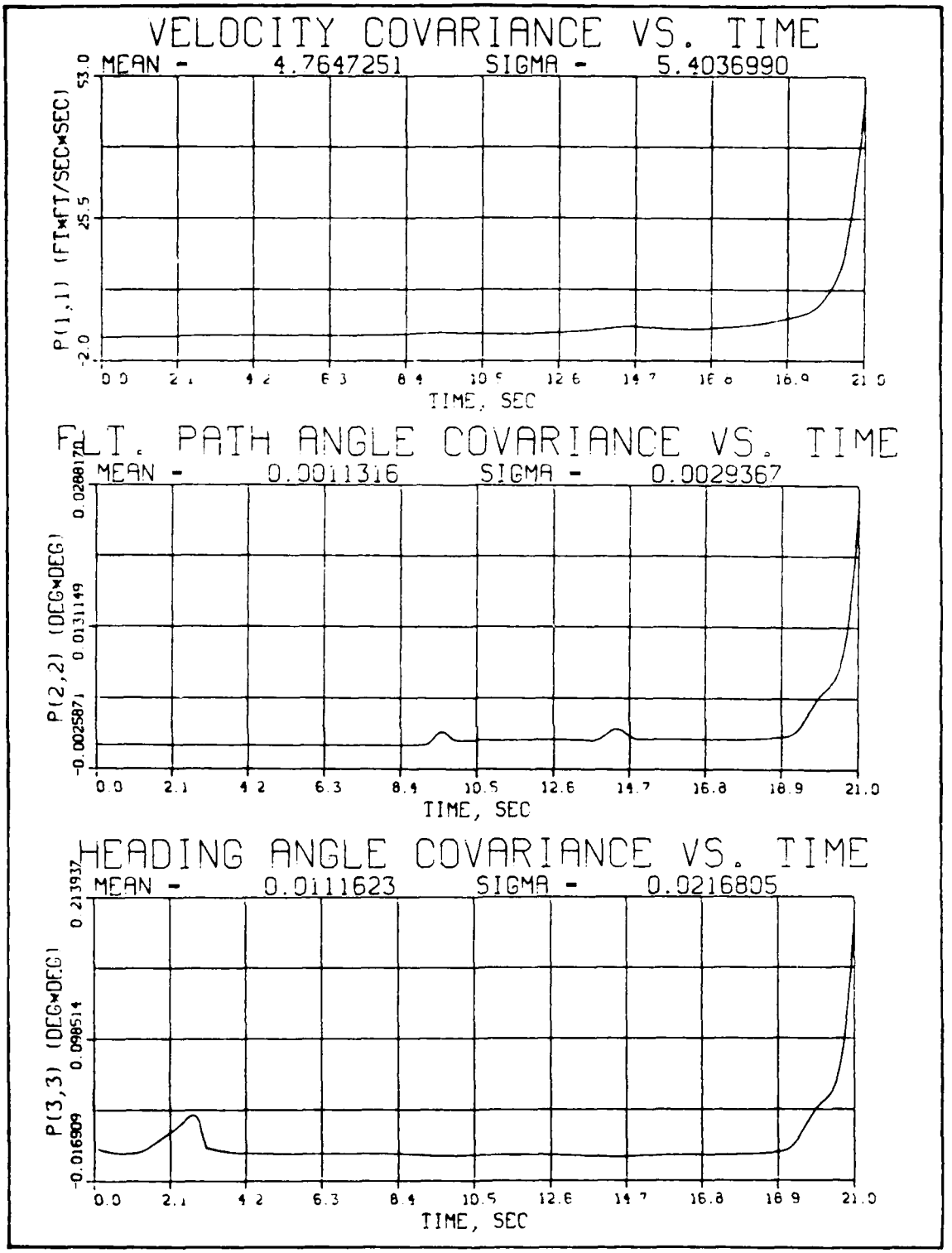

Figure 11. Diagonal Elements of Filter-Smoother Computed Covariance for Trajectory 2, Measurement Model RP-2

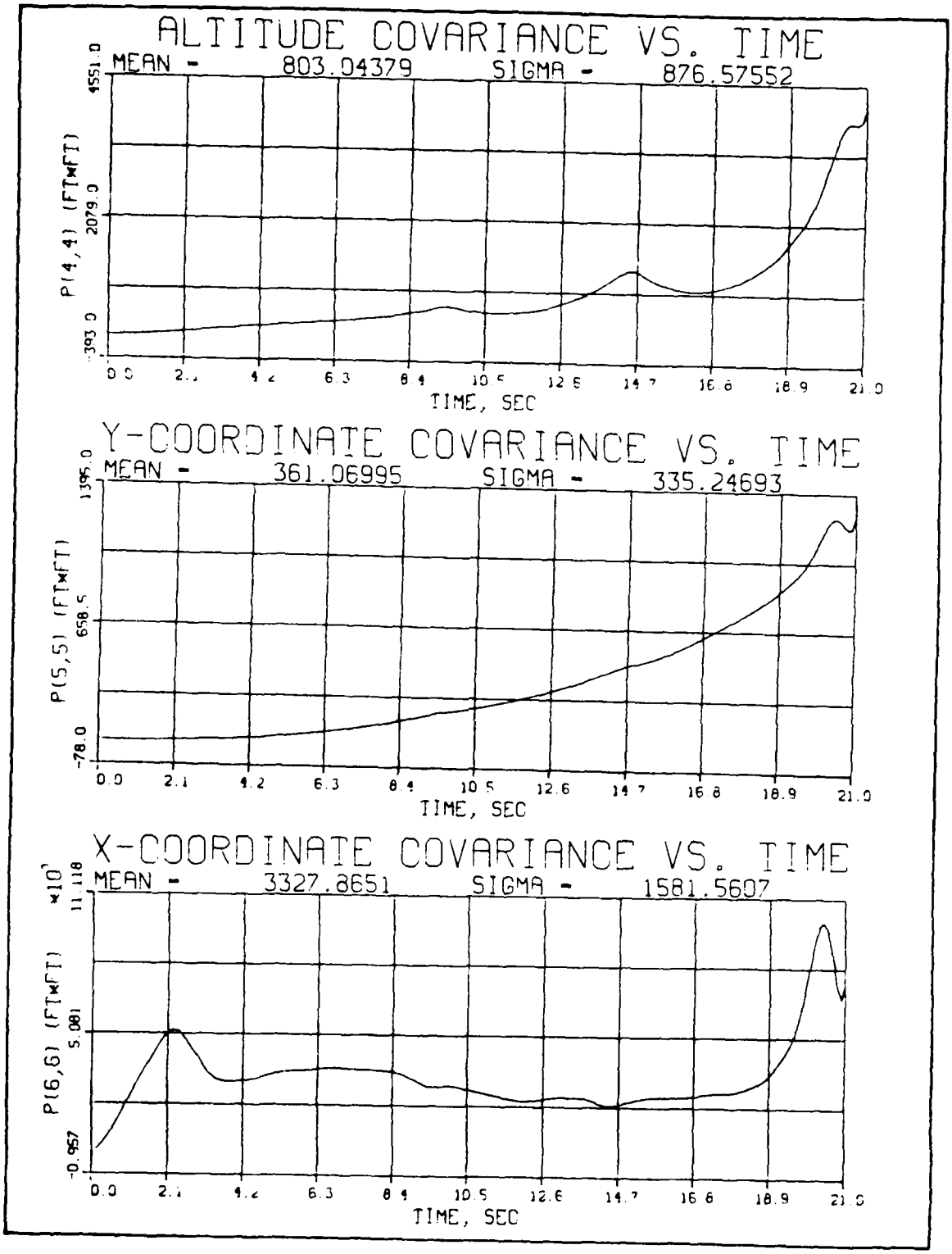

Figure 11 (continued)

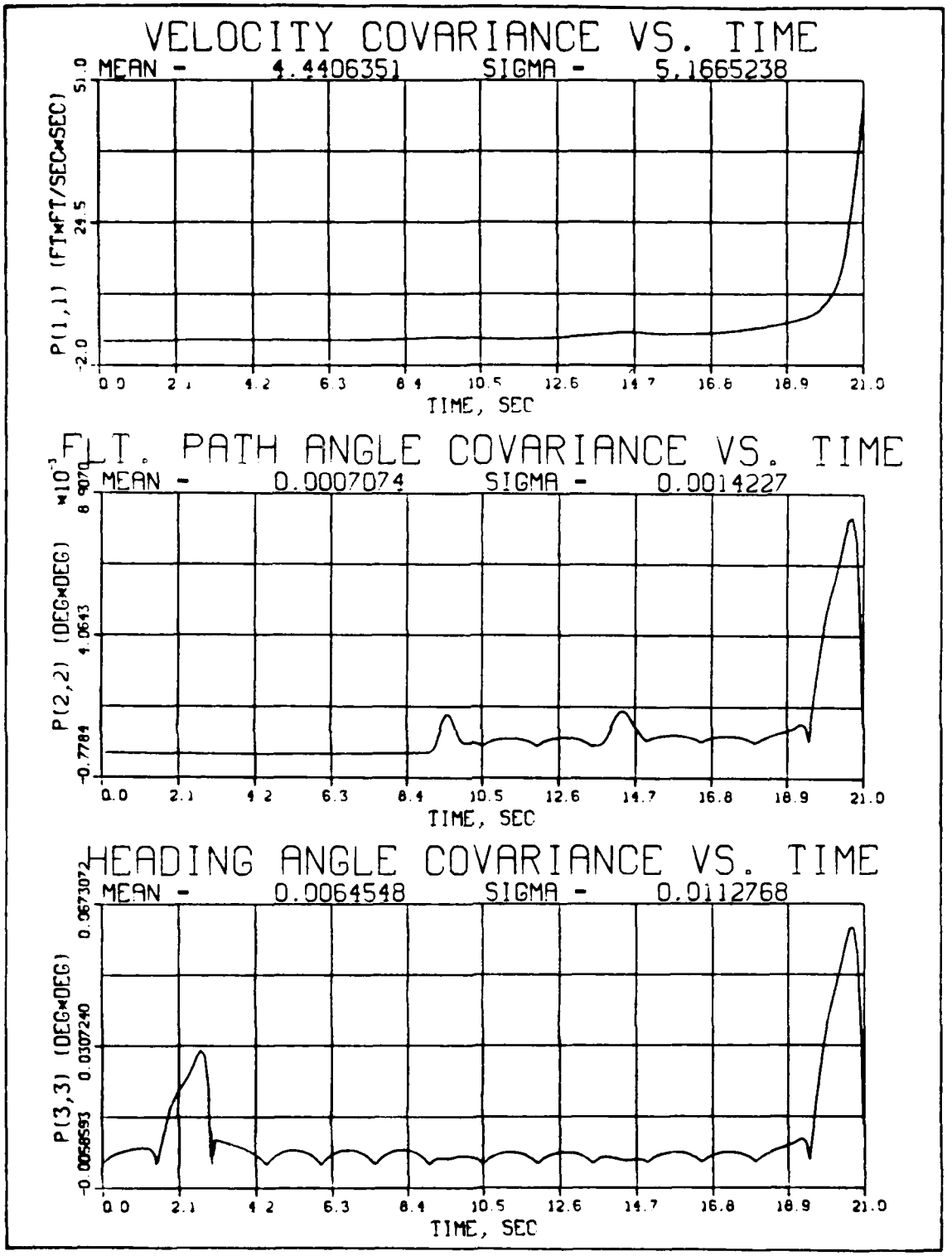

Figure 12. Diagonal Elements of Filter-Smoother Computed Covariance for Trajectory 2, Measurement Model RR-2

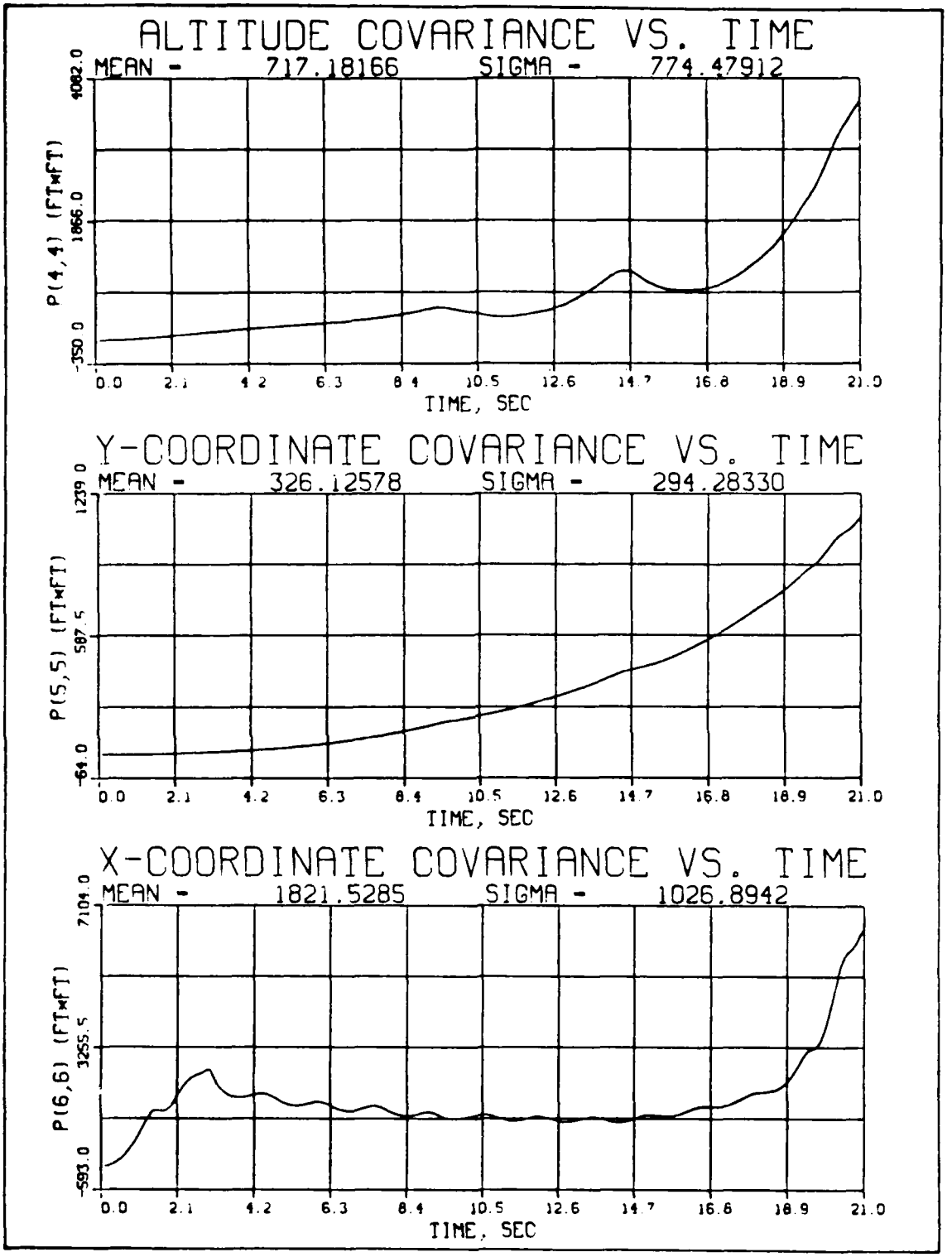

Figure 12 (continued)

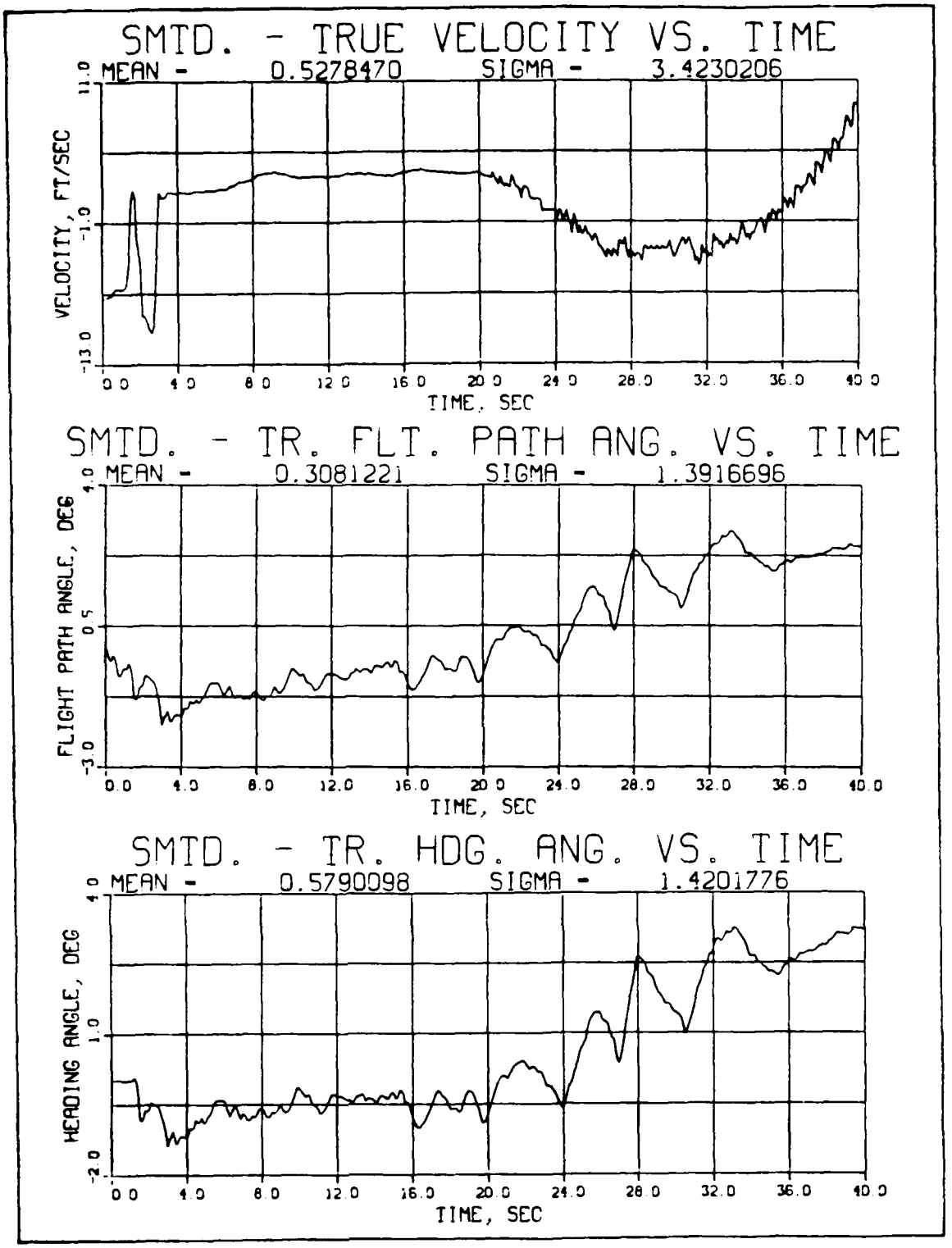

Figure 13. Errors Committed by Filter-Smoother after 5 Iterations -- Trajectory 1, Measurement Model FS-1

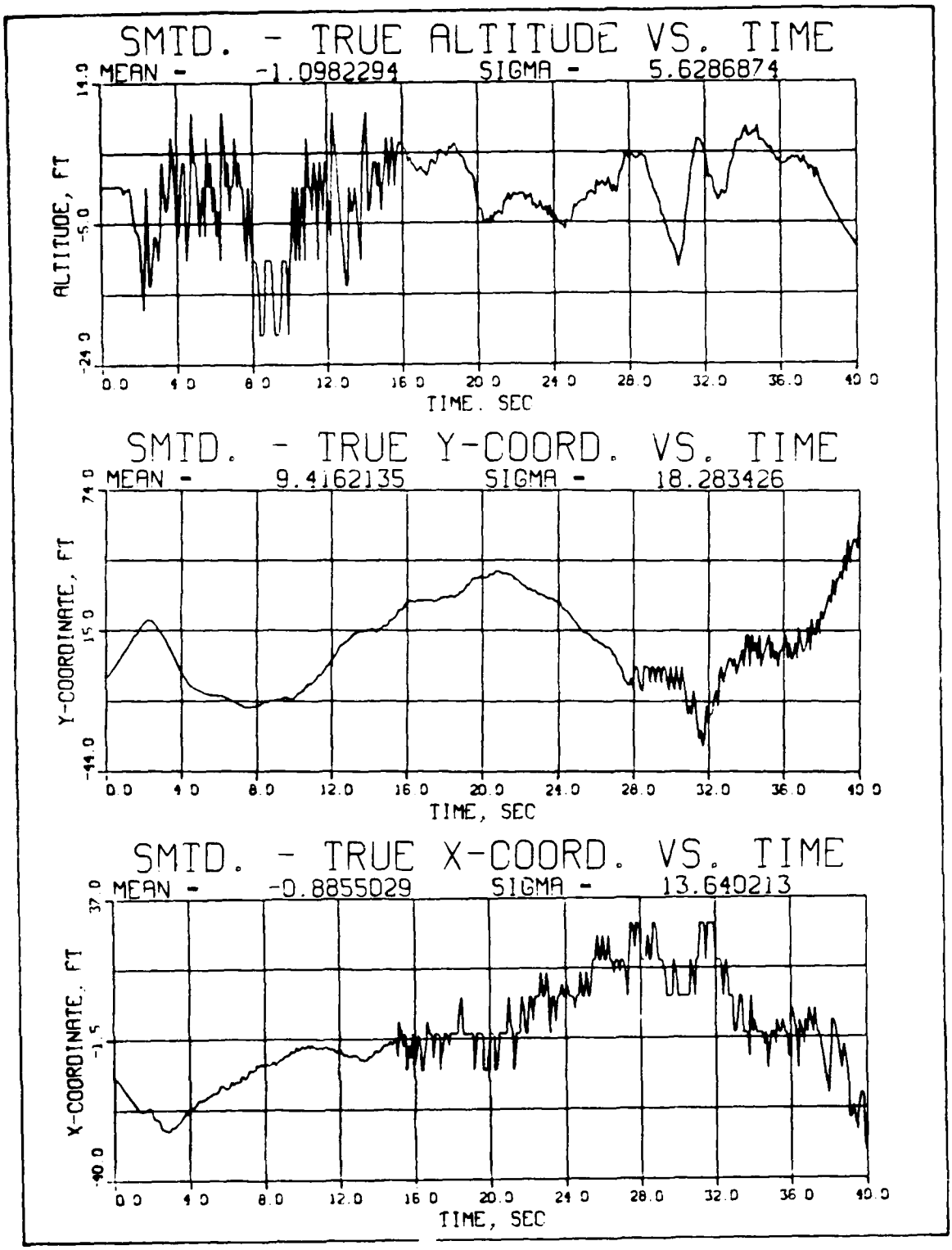

Figure 13 (continued)

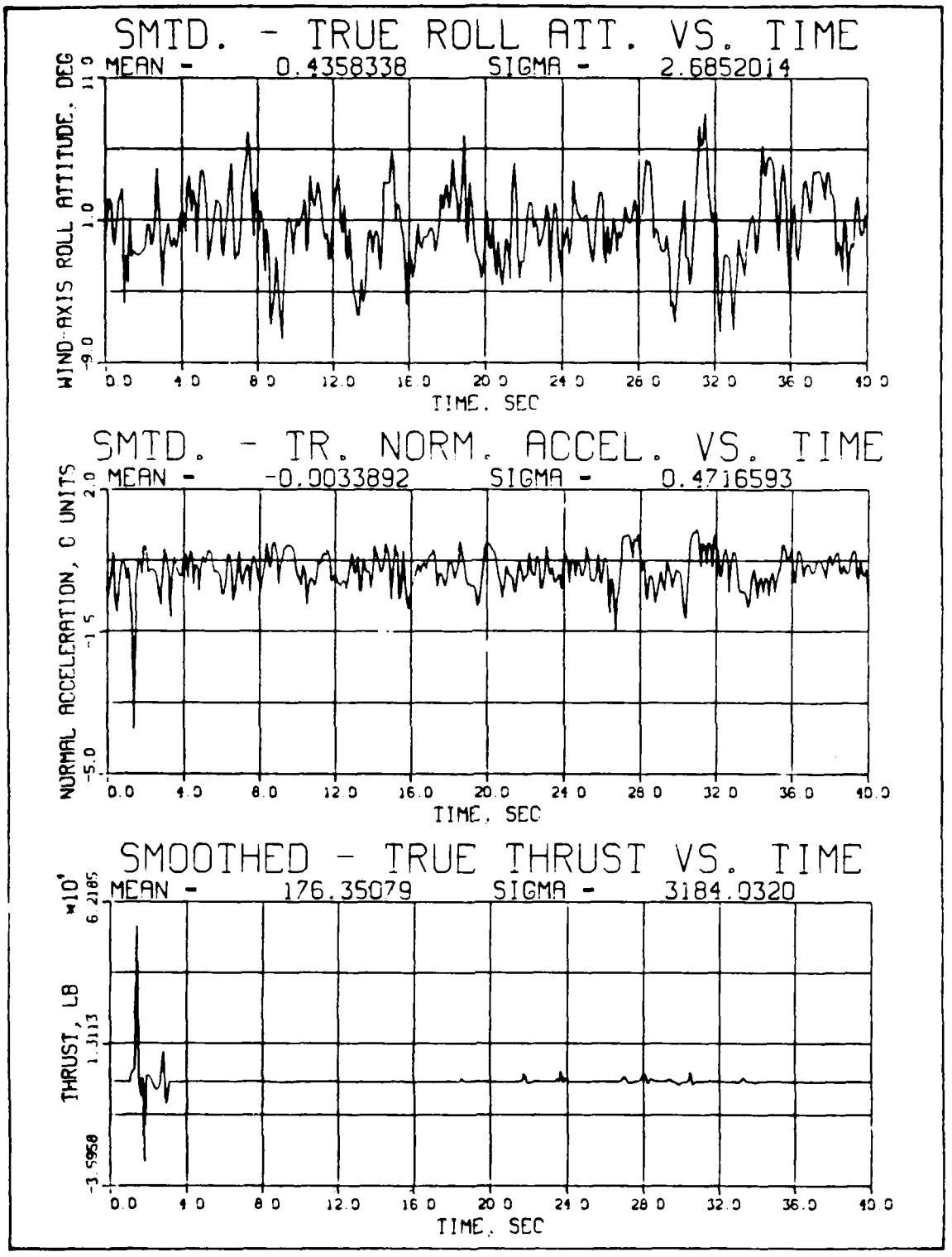

Figure 13 (continued)

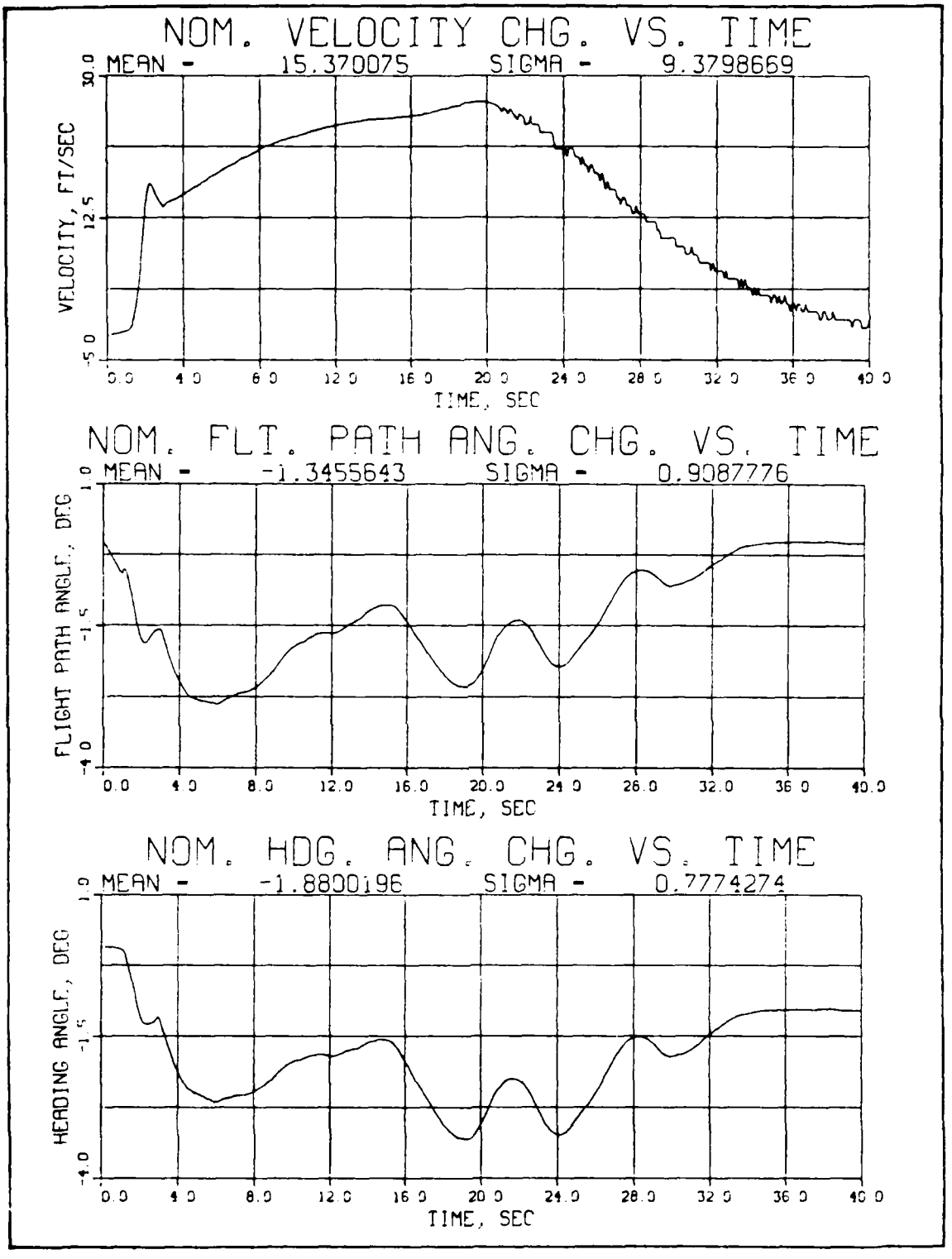

Figure 14. Change in Nominal Trajectory for Iteration 1 of Filter-Smoother -- Trajectory 1, Measurement Model FS-1

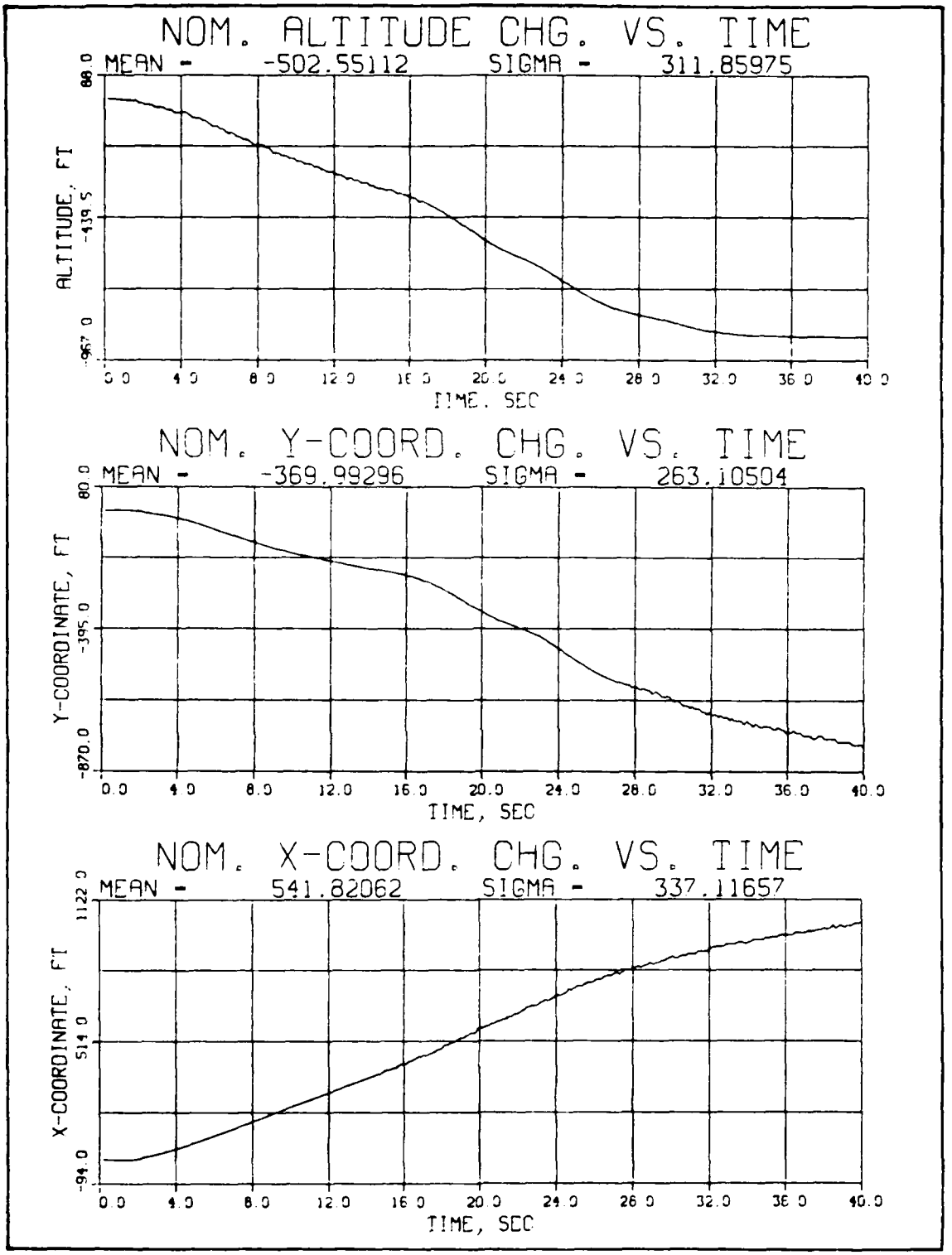

Figure 14 (continued)

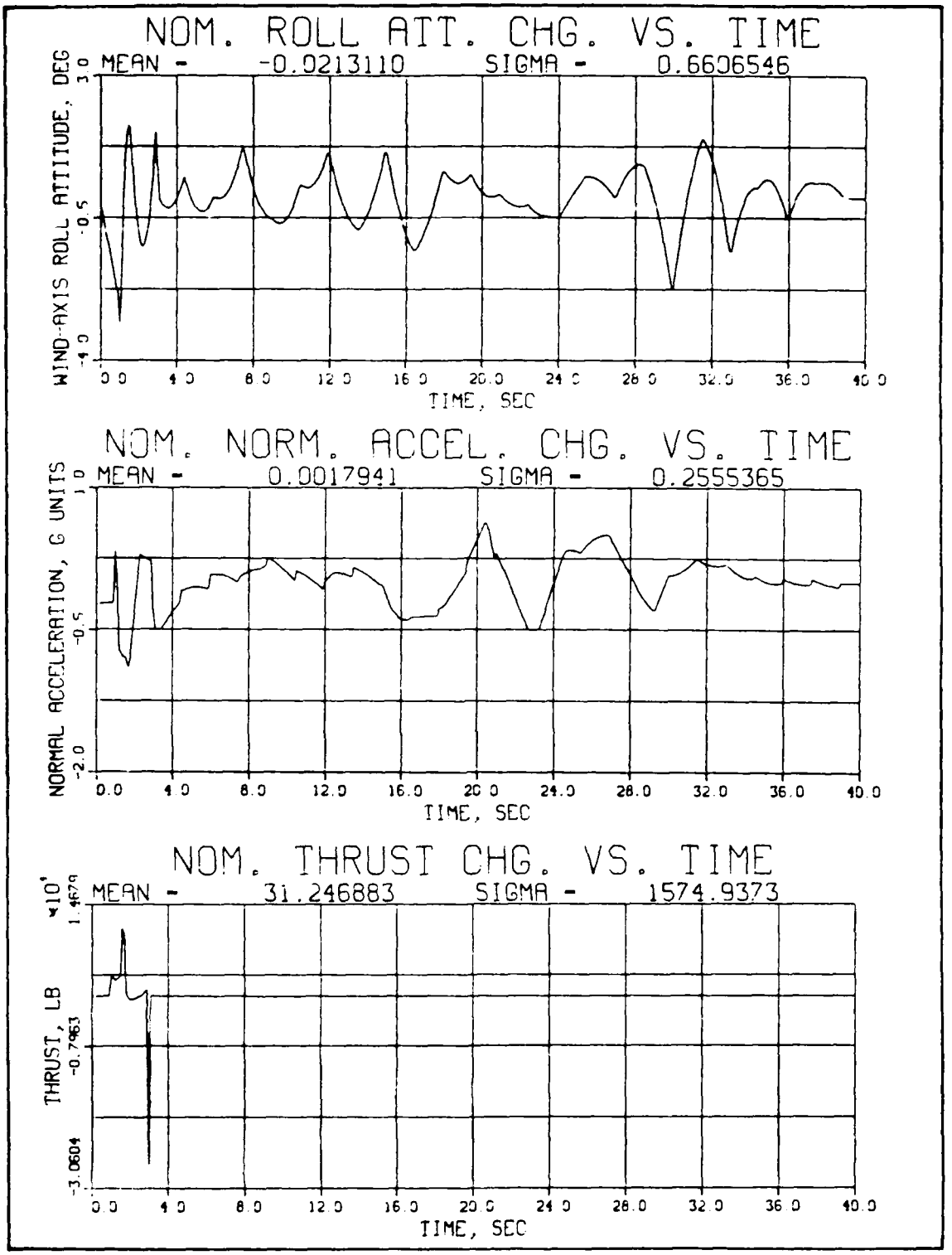

Figure 14 (continued)

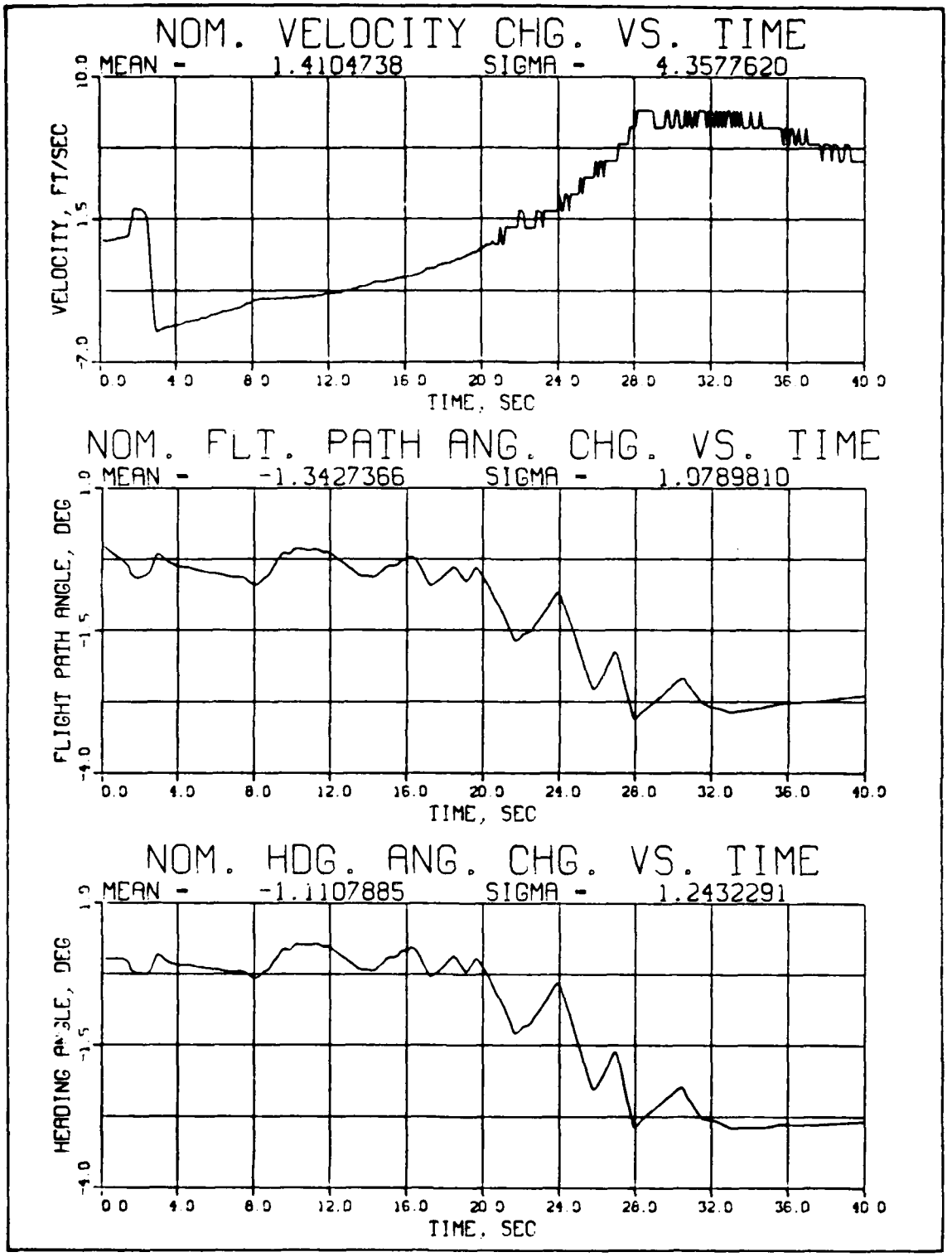

Figure 15. Change in Nominal Trajectory for Iteration 5 of Filter-Smoother -- Trajectory 1, Measurement Model FS-1

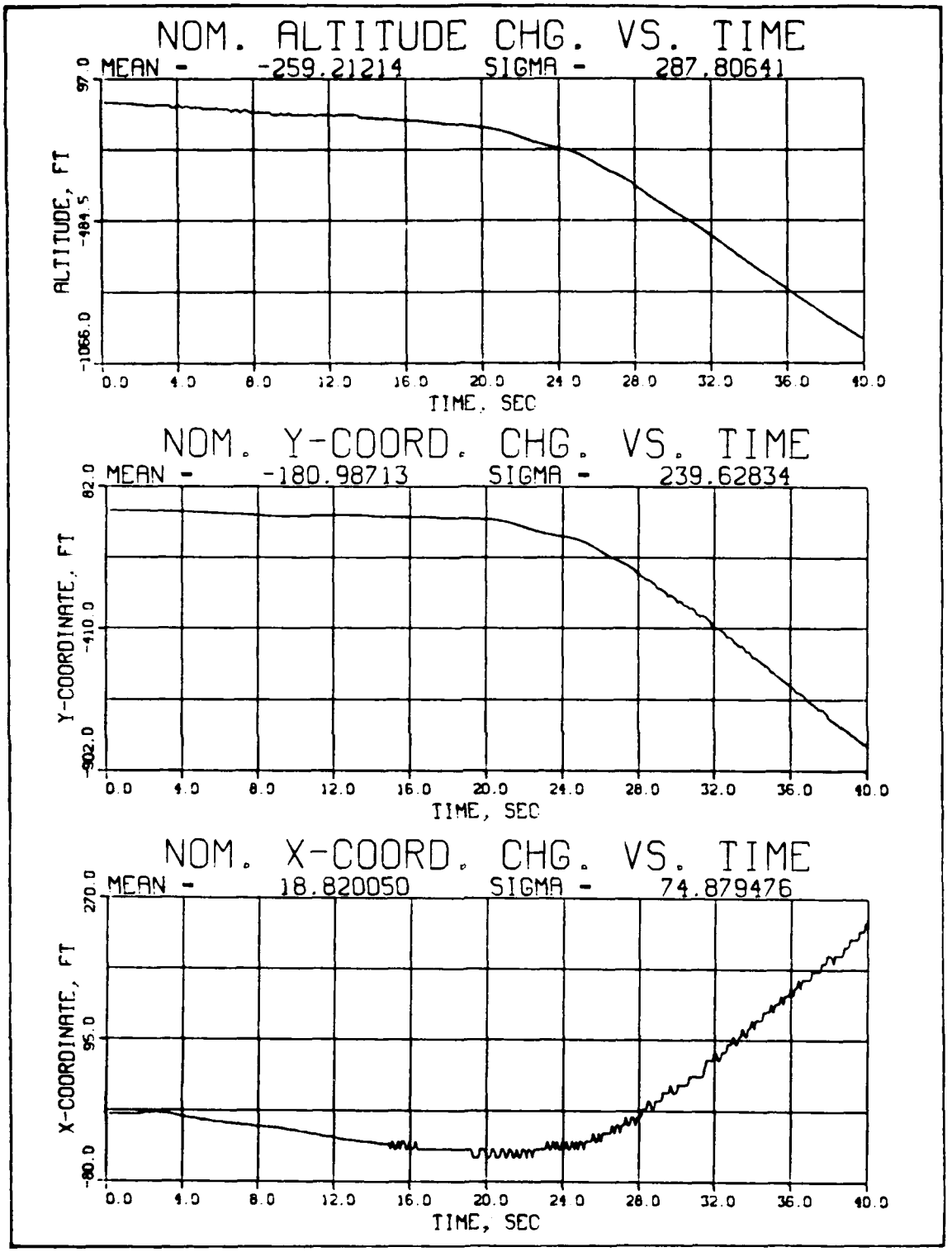

Figure 15 (continued)

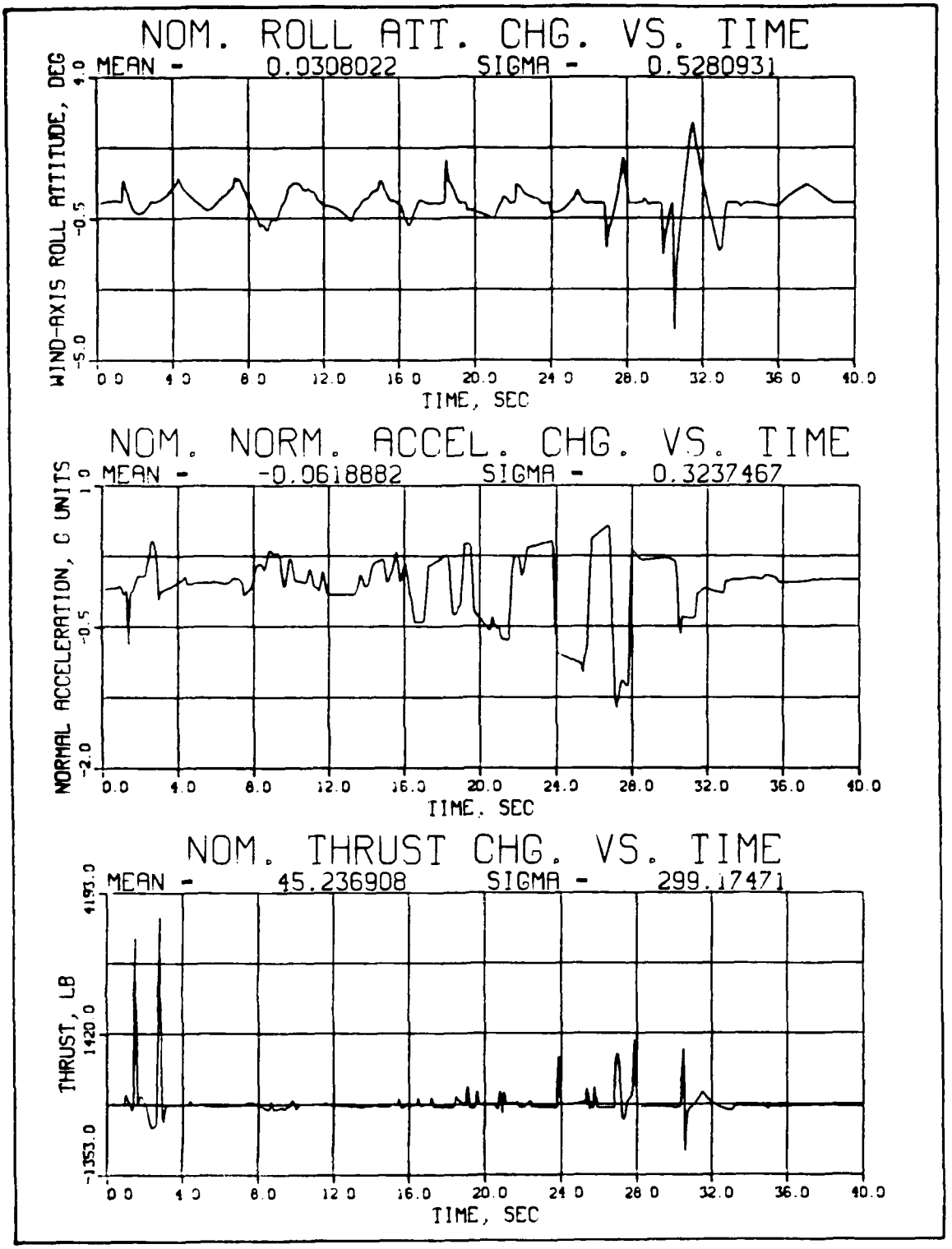

Figure 15 (continued)

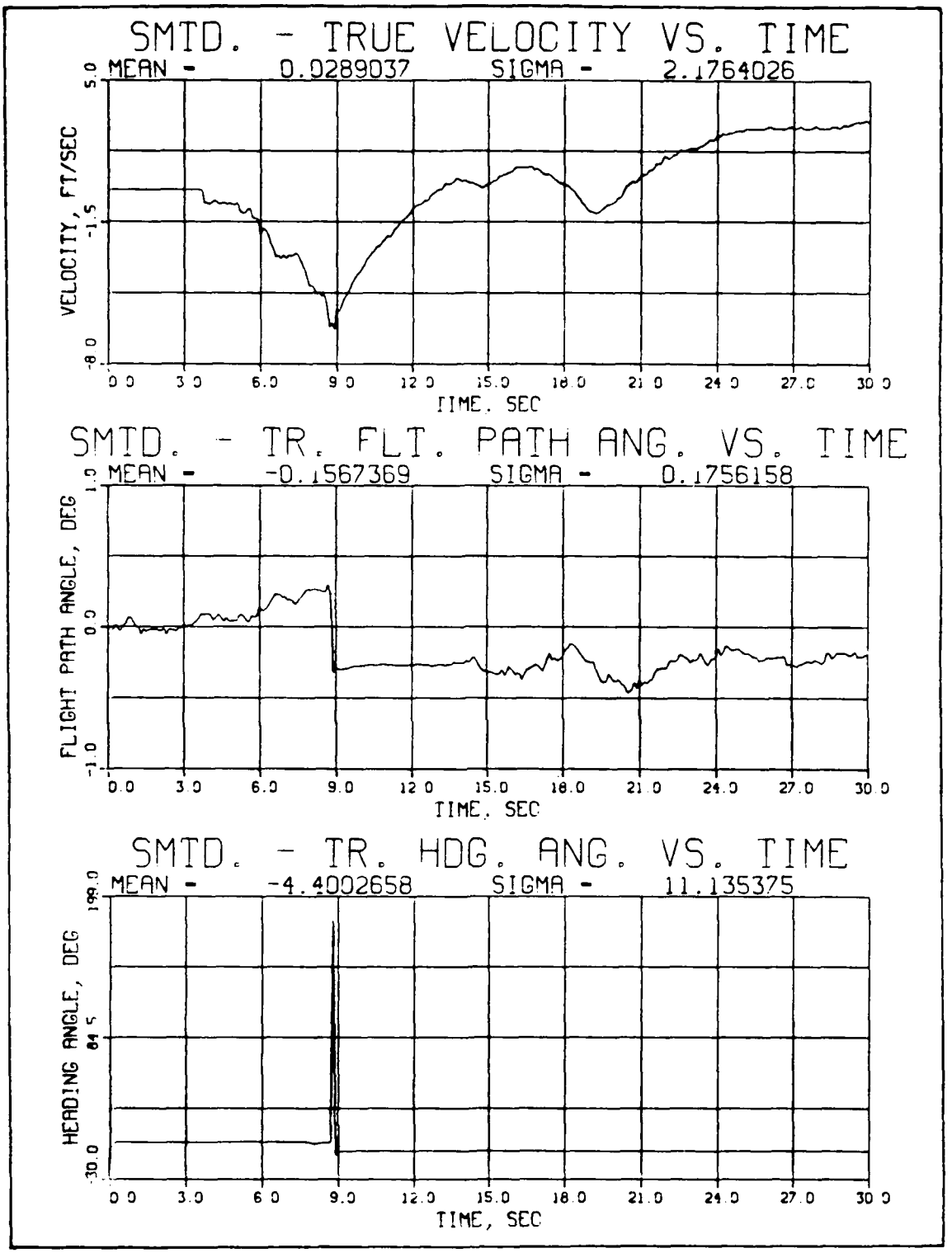

Figure 16. Errors Committed by Filter-Smoother Iteration 1, Trajectory 3, Measurement Model RR-2

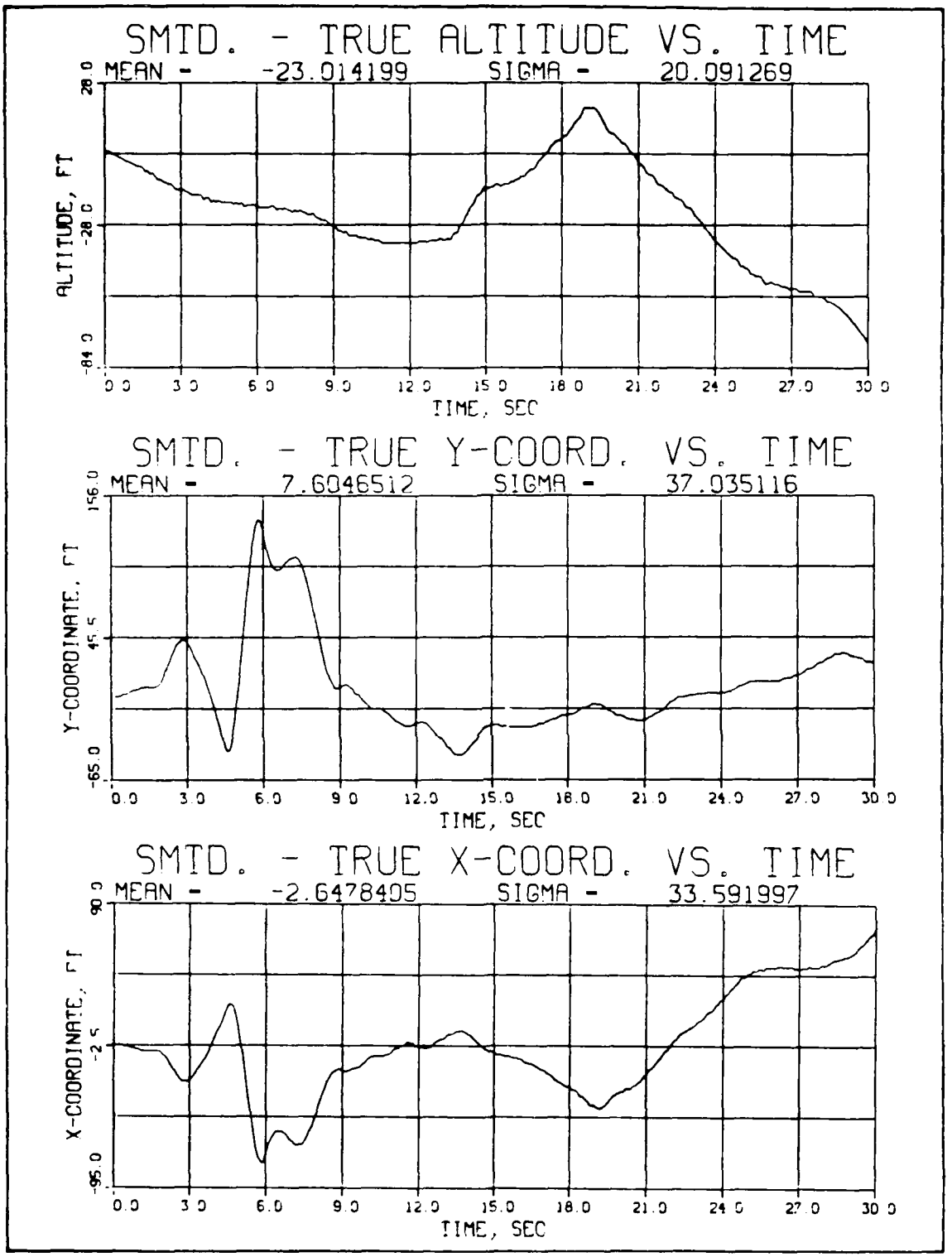

Figure 16 (continued)

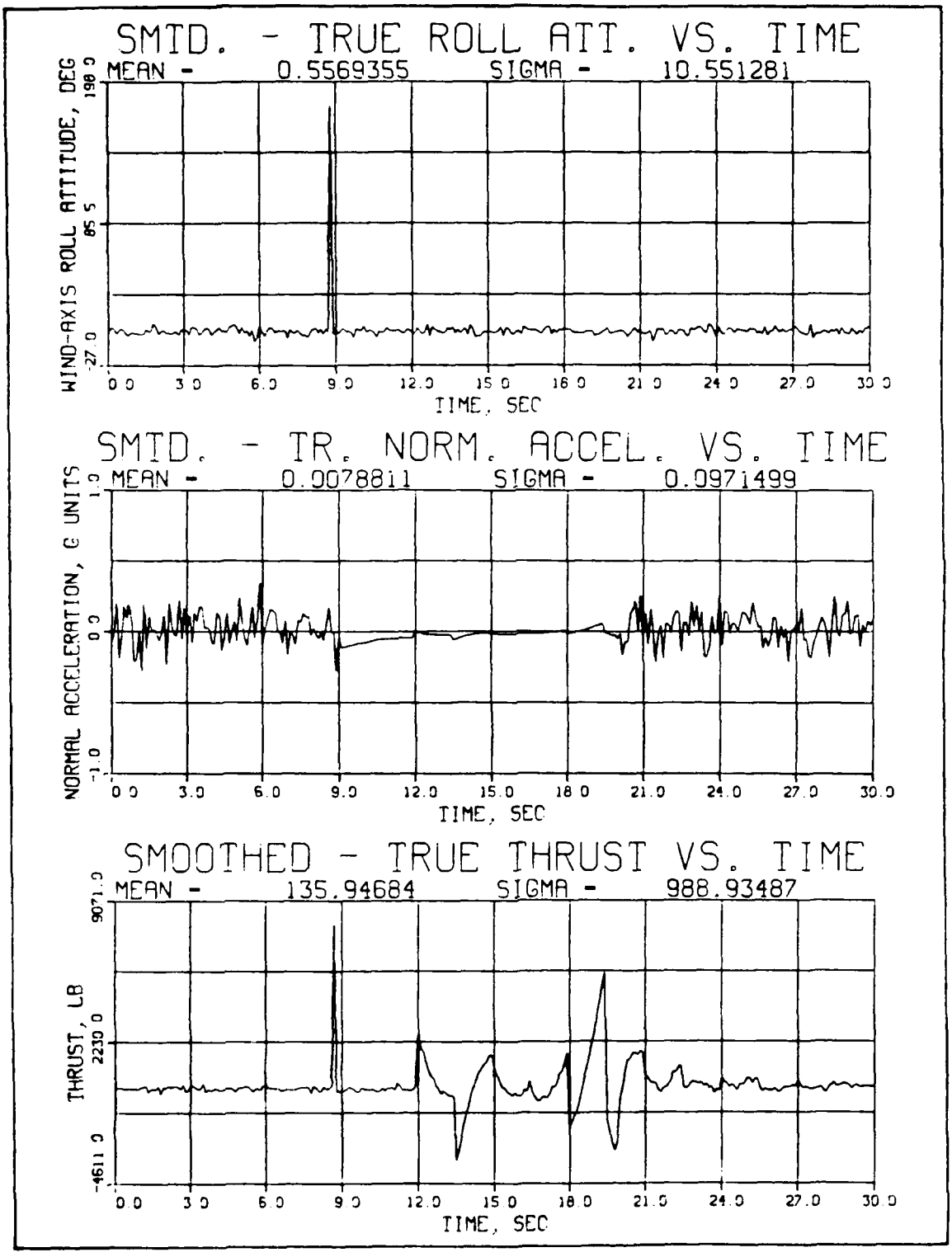

Figure 16 (continued)

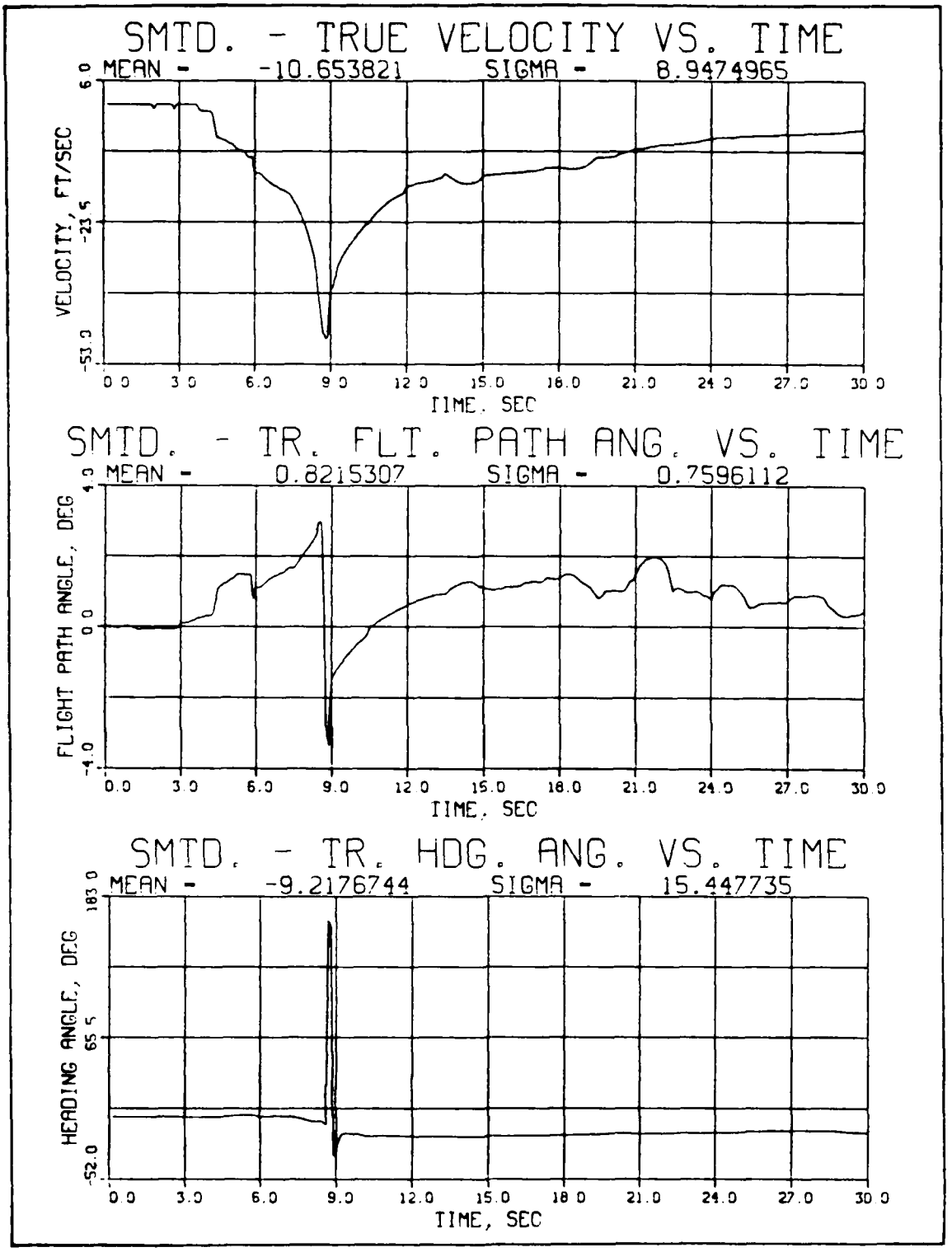

Figure 17. Errors Committed by Filter-Smoother Iteration 5, Trajectory 3, Measurement Model RR-2

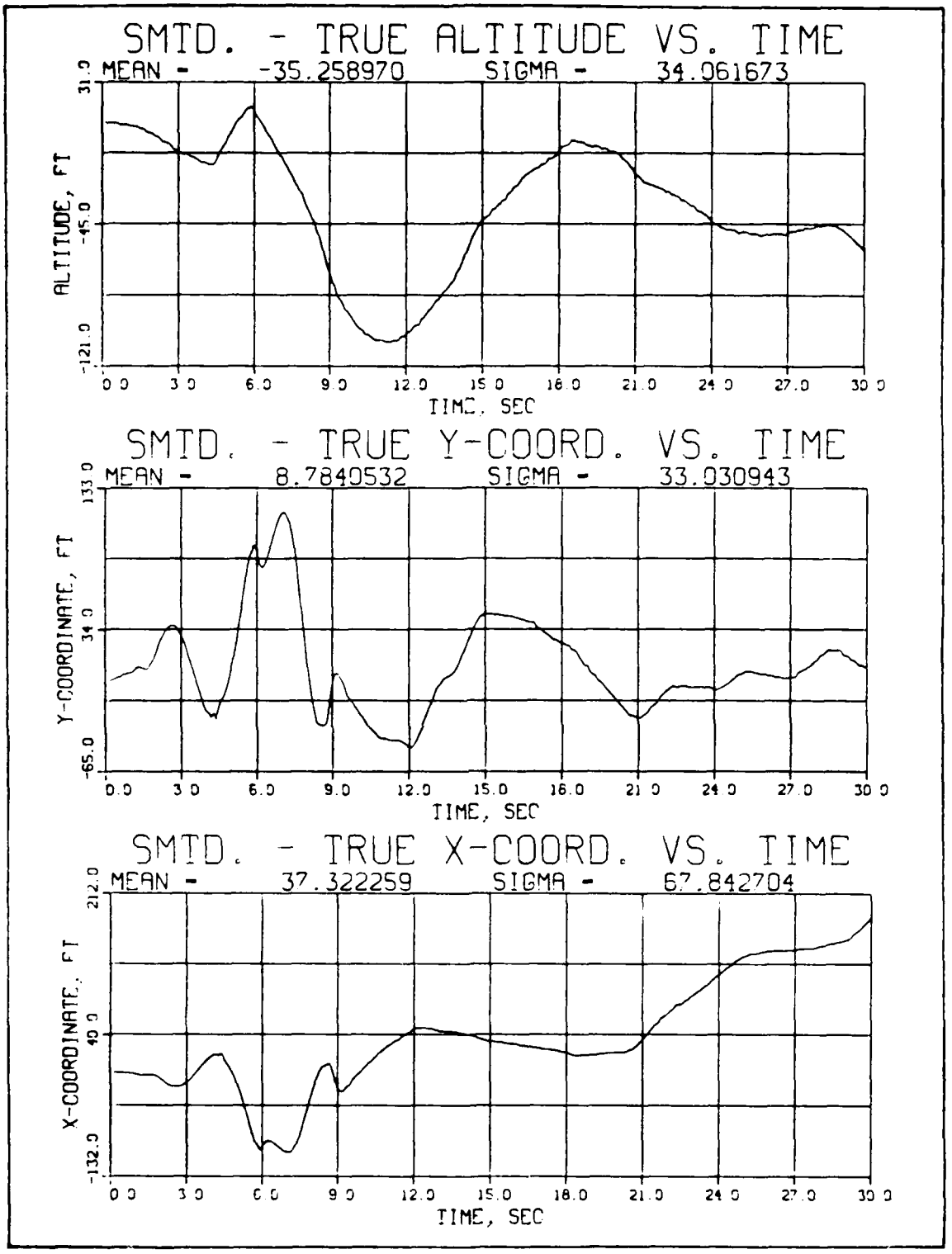

Figure 17 (continued)

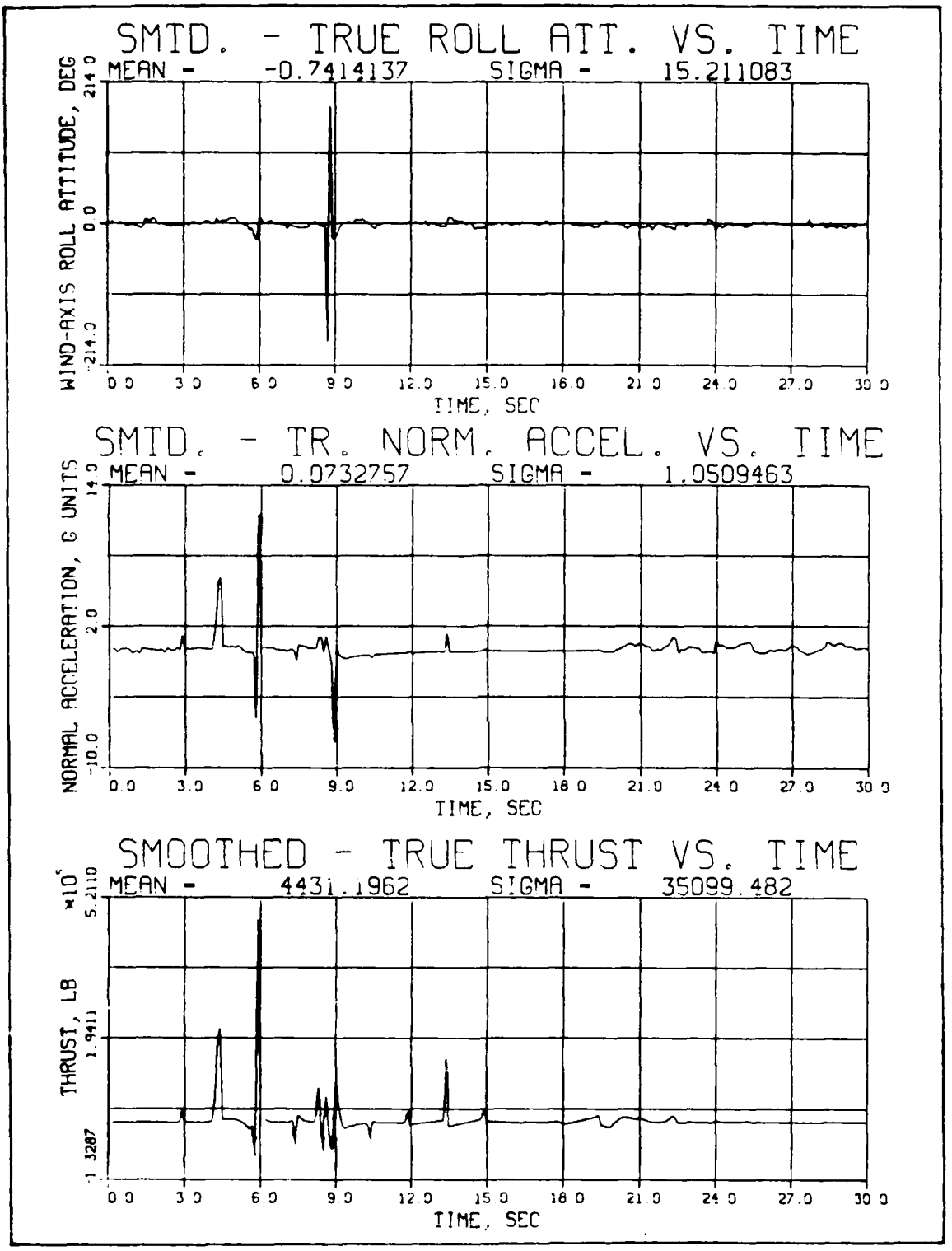

Figure 17 (continued)

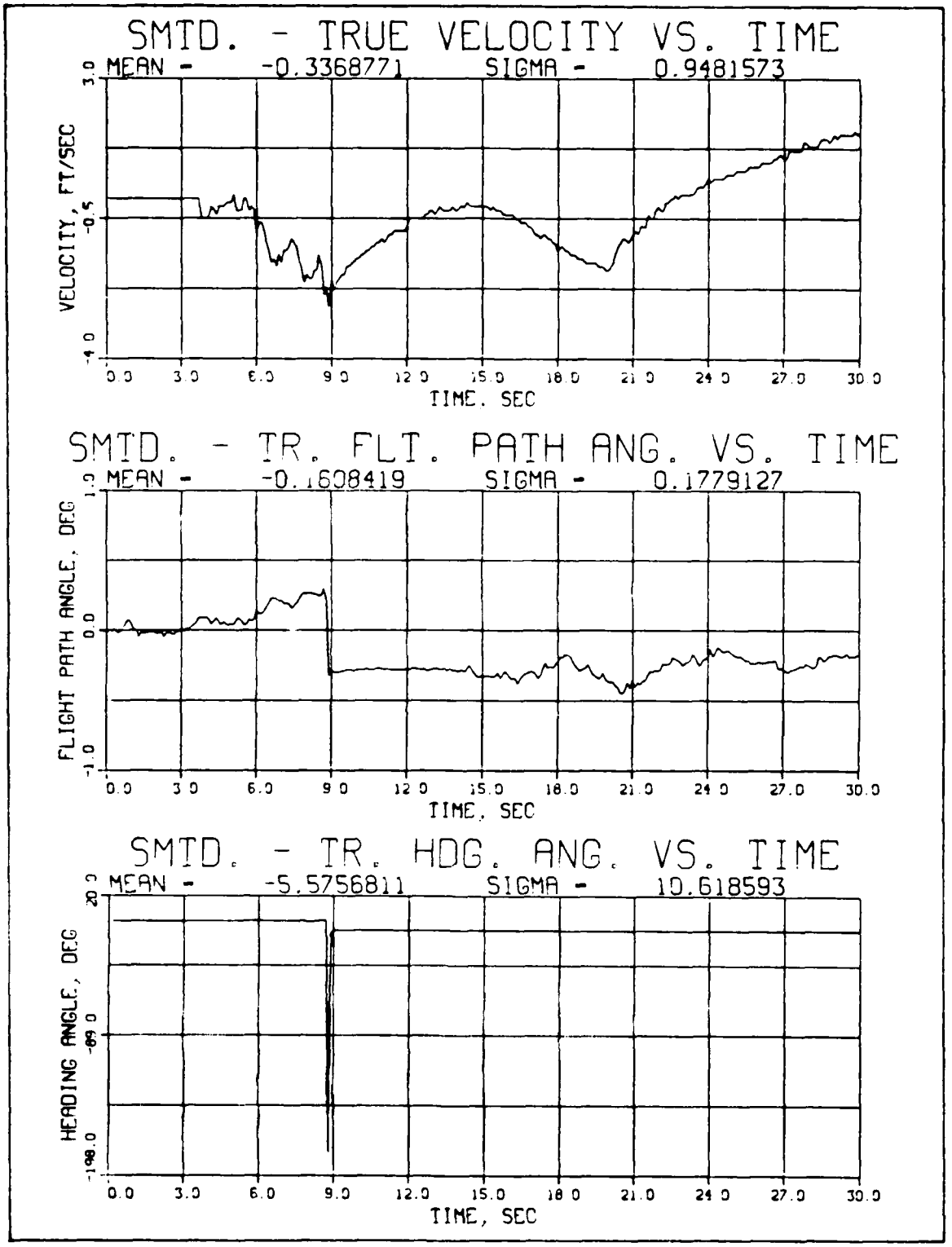

Figure 18. Errors Committed by Filter-Smoother with Increased Measurement Noise -- Trajectory 3

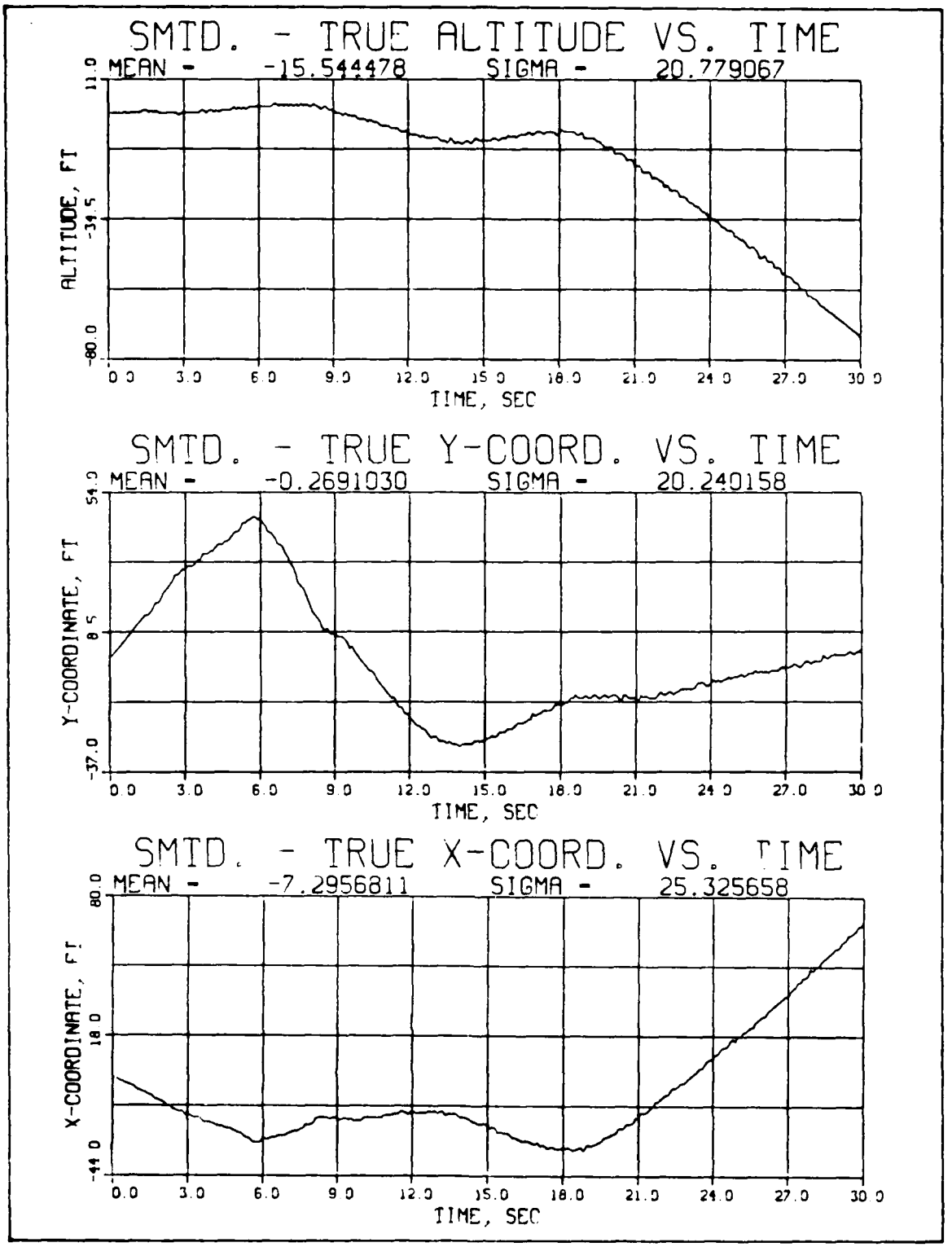

Figure 18 (continued)

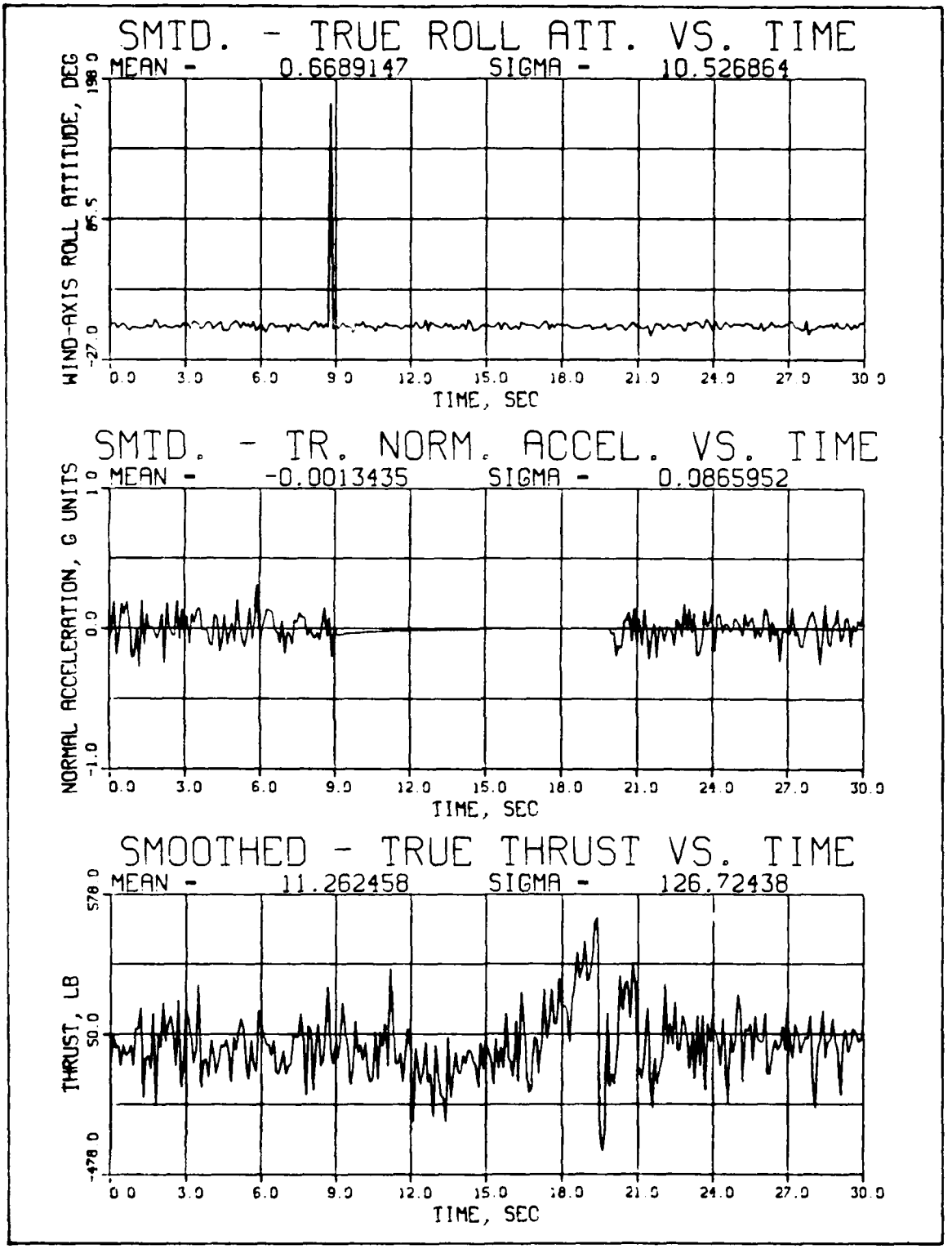

Figure 18 (continued)

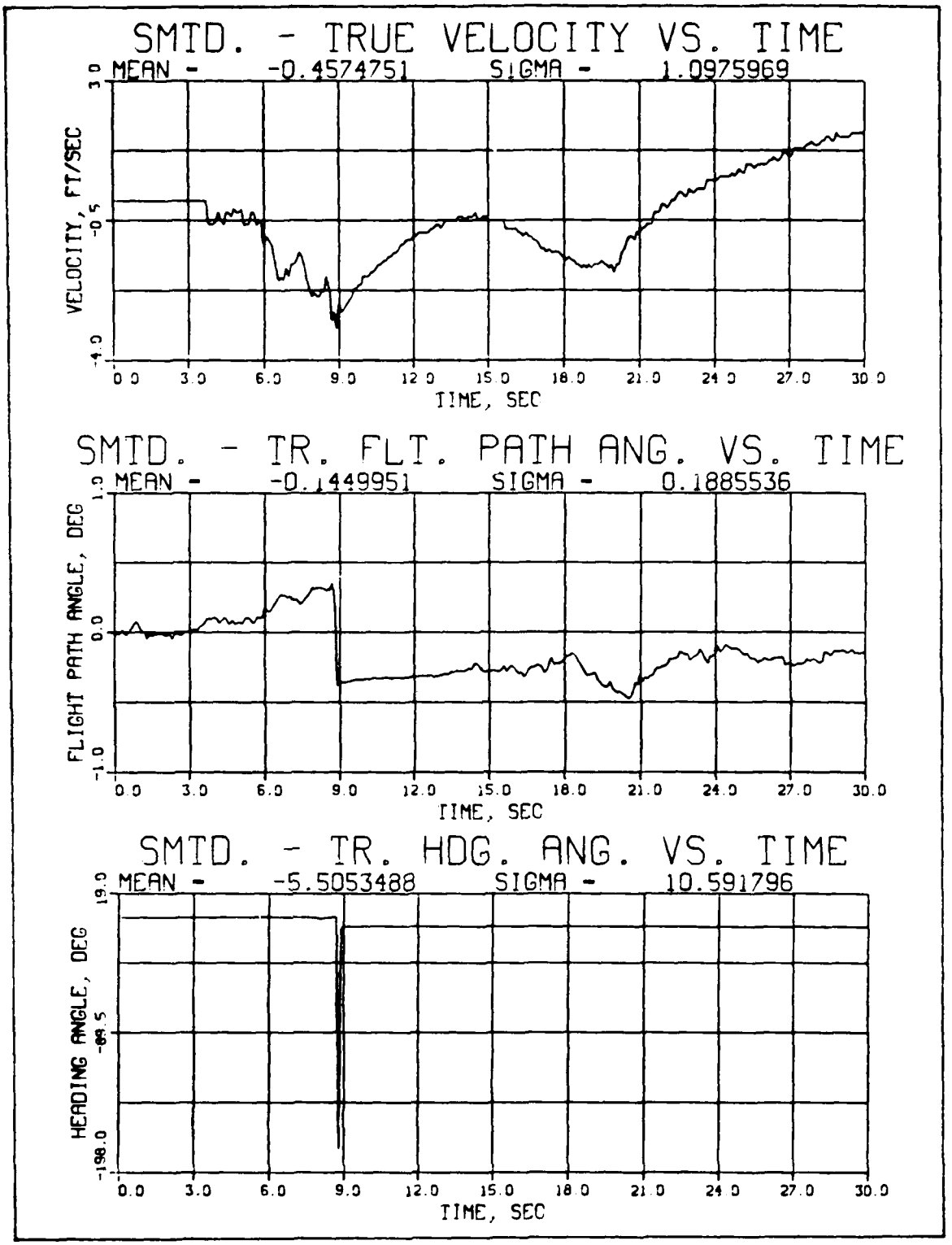

Figure 19. Errors Committed by Filter-Smoother with Increased Measurement Noise -- Trajectory 3

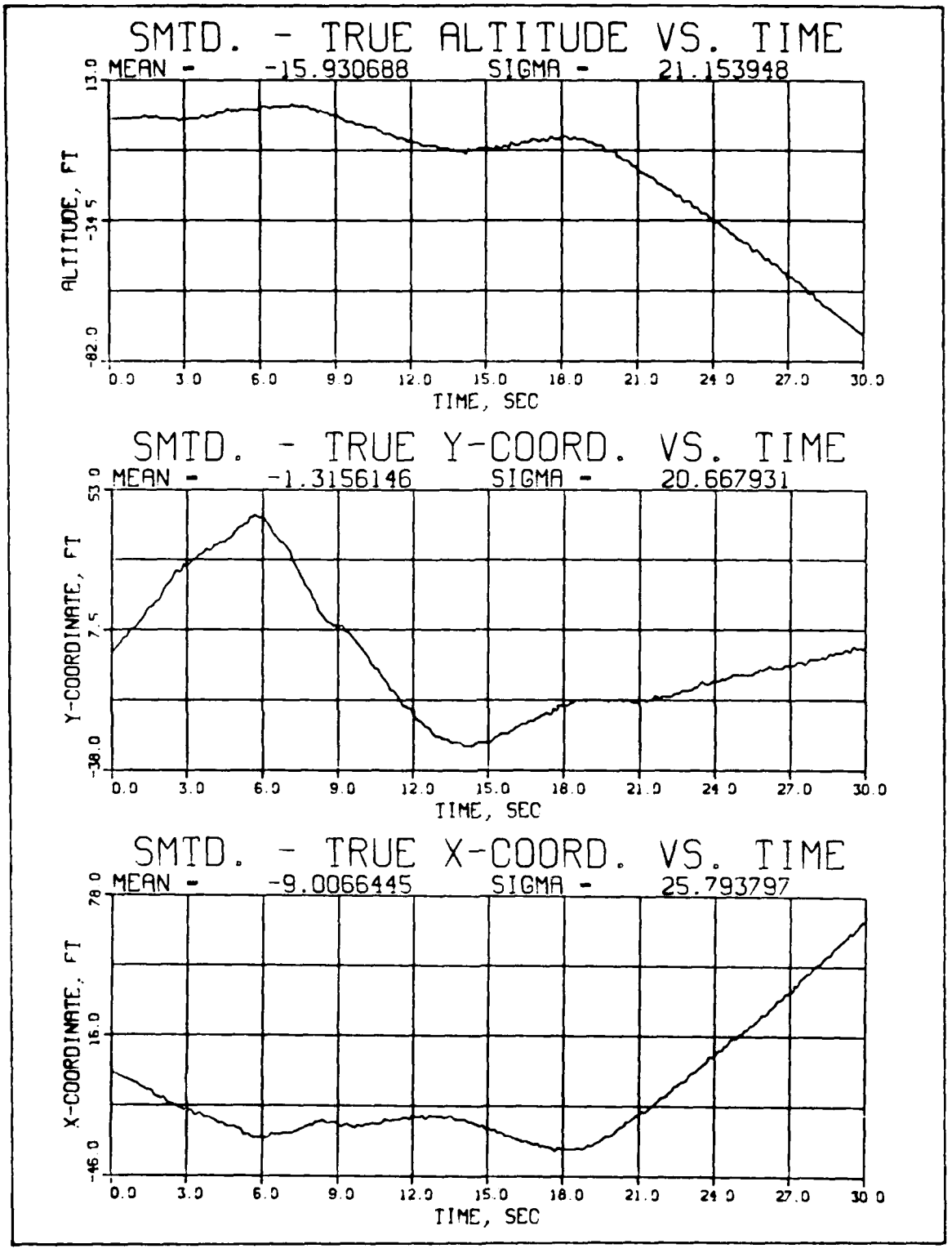

Figure 19 (continued)

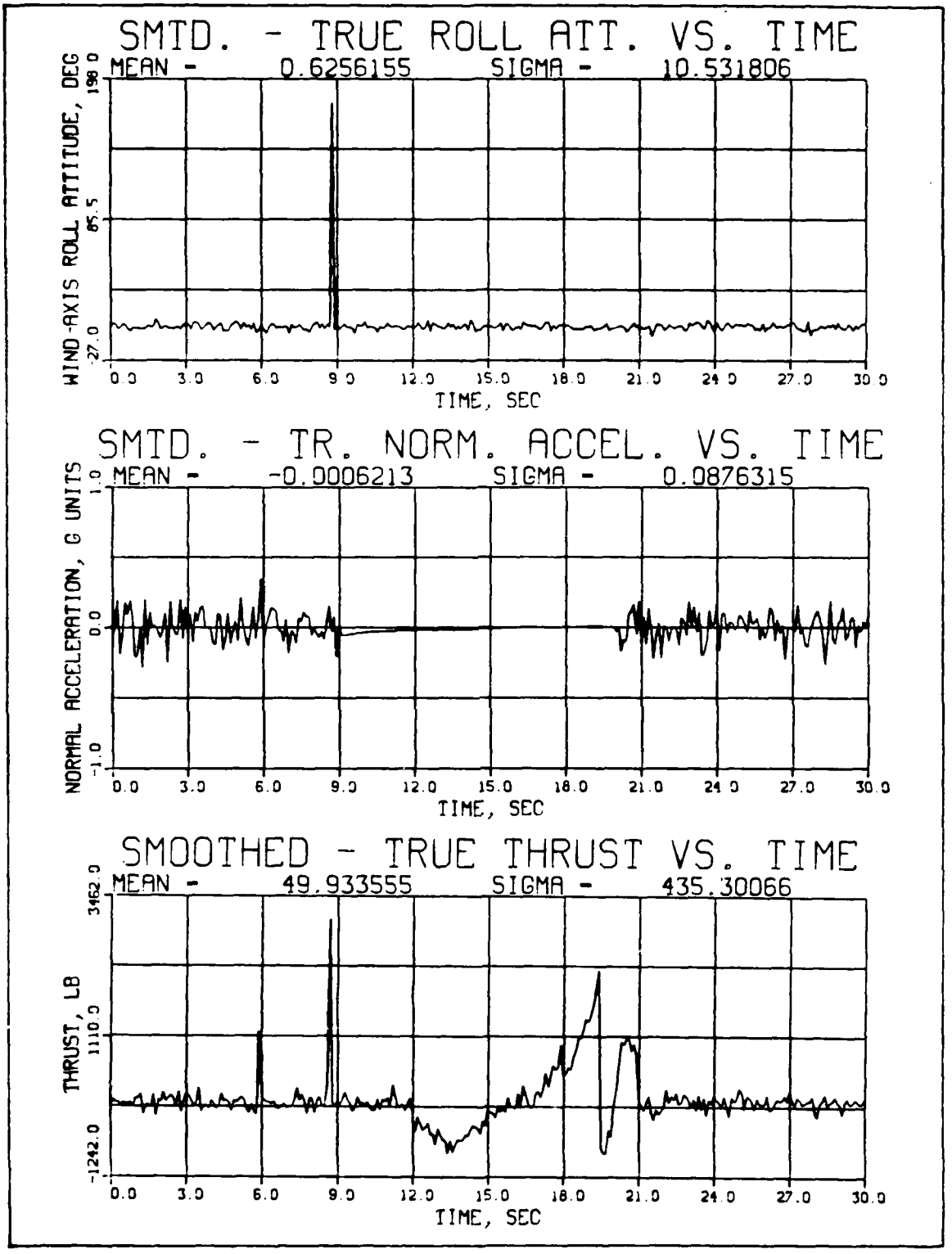

Figure 19 (continued)

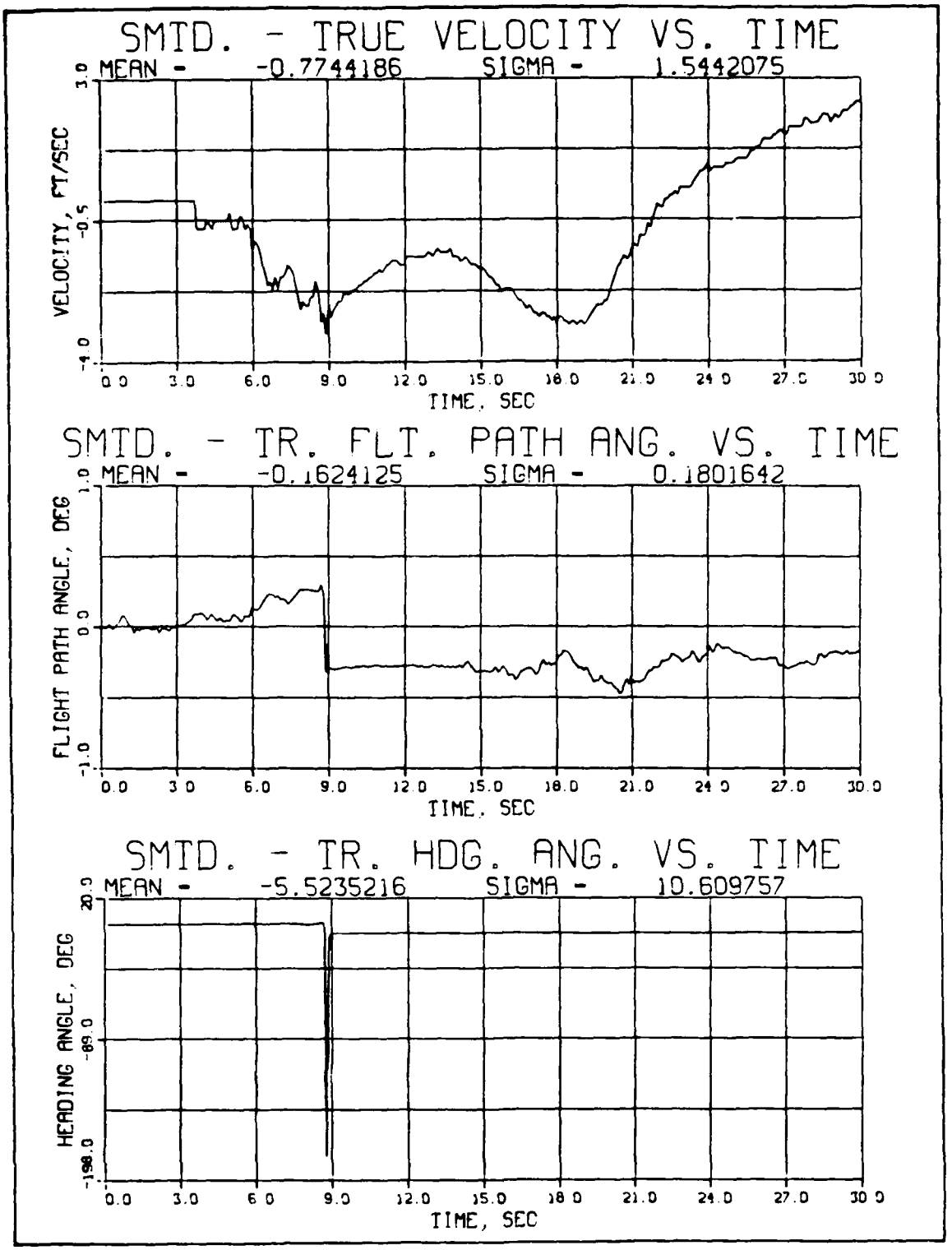

Figure 20. Errors Committed by Filter-Smoother with Smoothed Trajectory used as Nominal -- Traj. 3, Iteration 5

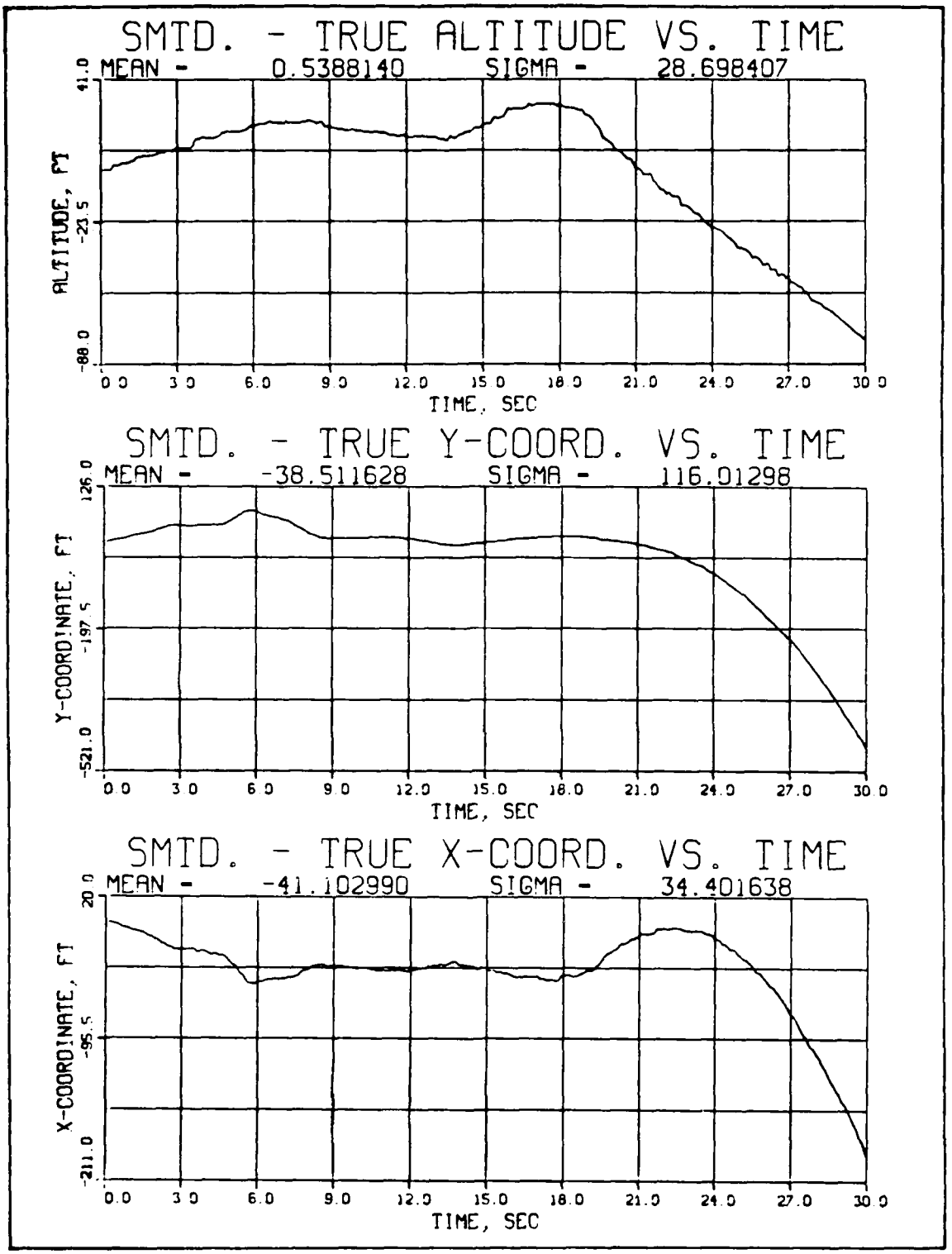

Figure 20 (continued)

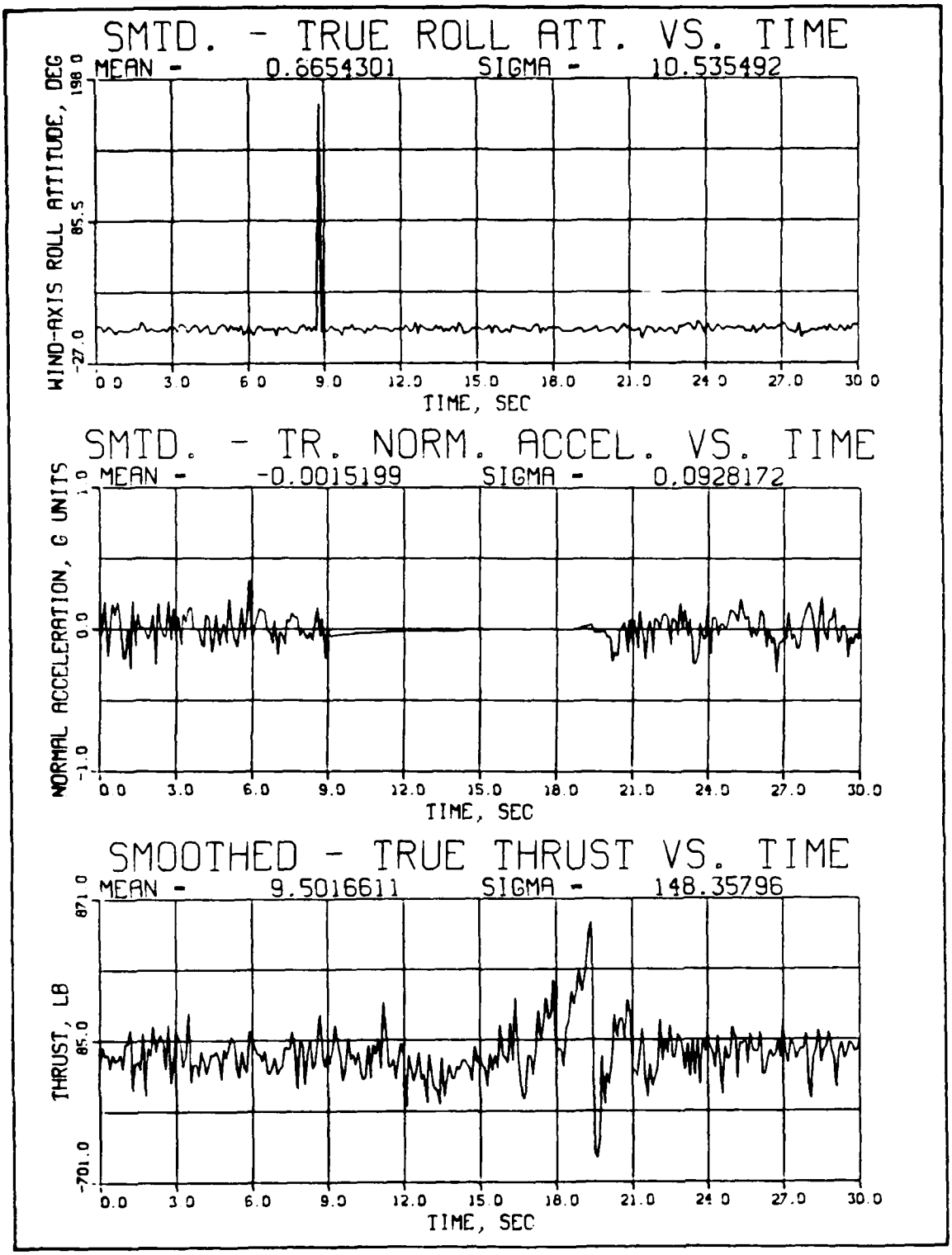

Figure 20 (continued)

Bibliography

Etkin, Bernard. Dynamics of Atmospheric Flight. New York: John Wiley and Sons, 1972.

Maybeck, Peter S. Stochastic Models, Estimation, and Control, Vol. 1. New York: Academic Press, 1979.

-----. Stochastic Models, Estimation, and Control, Vol. 2. New York: Academic Press, 1982.

McKern, R. A. A Study of Transformation Algorithms for Use in a Digital Computer, Report T-493. Massachusetts Institute of Technology Instrumentation Laboratory (now the C. S. Draper Laboratory), Cambridge, Massachusetts, January 1968.

Ruley, James M. OPSIM2 and OPSIM3 User's Guide. Unpublished report. ASD/ENFTC, Wright-Patterson AFB OH, 20 July 1987a.

-----. PMSIM User's Guide. Unpublished report. ASD/ENFTC, Wright-Patterson AFB OH, 20 July 1987b.

Whittaker, Edmund T. A Treatise on the Analytical Dynamics of Particles and Rigid Bodies. New York: Dover Publications, 1944.

VITA

James M. Ruley was born on 29 February 1960 in Honolulu, Hawaii. He graduated from Kenton Ridge High School, Springfield, Ohio in 1978 and thereafter entered Wright State University, Dayton, Ohio, from which he received the degree of Bachelor of Science in Engineering Physics, Summa cum Laude, in 1982. During his undergraduate years, he was employed part-time at Grimes Division, Midland-Ross Corporation, Urbana, Ohio. After receiving his degree, Mr. Ruley accepted a position as a Graduate Research Associate in the Aeronautical and Astronautical Engineering Department at Ohio State University, which he held until November 1983. At that time he entered the Federal service, first in the Foreign Technology Division, Air Force Systems Command, and (from March 1985) in the Flight Stability and Control Branch of the Aeronautical Systems Division, Air Force Systems Command. He entered the Air Force Institute of Technology as a part-time student in January 1984.

Permanent address: 4045 Tacoma Street
Springfield, Ohio 45503

SECURITY CLASSIFICATION OF THIS PAGE

REPORT DOCUMENTATION PAGE

Form Approved
OMB No. 0704-0188

1a. REPORT SECURITY CLASSIFICATION UNCLASSIFIED	1b. RESTRICTIVE MARKINGS
2a. SECURITY CLASSIFICATION AUTHORITY	3. DISTRIBUTION/AVAILABILITY OF REPORT
2b. DECLASSIFICATION/DOWNGRADING SCHEDULE	
4. PERFORMING ORGANIZATION REPORT NUMBER(S) AFIT/GAE/ENG/88J-1	5. MONITORING ORGANIZATION REPORT NUMBER(S)
6a. NAME OF PERFORMING ORGANIZATION School of Engineering 6b. OFFICE SYMBOL (*If applicable*) AFIT/ENA	7a. NAME OF MONITORING ORGANIZATION
6c. ADDRESS (*City, State, and ZIP Code*) Air Force Institute of Technology Wright-Patterson AFB, OH 45433-6583	7b. ADDRESS (*City, State, and ZIP Code*)
8a. NAME OF FUNDING/SPONSORING ORGANIZATION 8b. OFFICE SYMBOL (*If applicable*)	9. PROCUREMENT INSTRUMENT IDENTIFICATION NUMBER
8c. ADDRESS (*City, State, and ZIP Code*)	10. SOURCE OF FUNDING NUMBERS PROGRAM ELEMENT NO. / PROJECT NO. / TASK NO / WORK UNIT ACCESSION NO.

11. TITLE (*Include Security Classification*)
(UNCLASSIFIED)
APPLICATION OF LINEARIZED KALMAN FILTER-SMOOTHER TO AIRCRAFT TRAJECTORY ESTIMATION

12. PERSONAL AUTHOR(S)
James M. Ruley

13a. TYPE OF REPORT	13b. TIME COVERED	14. DATE OF REPORT (*Year, Month, Day*)	15. PAGE COUNT
MS Thesis	FROM _____ TO _____	1988 June	160

16. SUPPLEMENTARY NOTATION

17. COSATI CODES			18. SUBJECT TERMS (*Continue on reverse if necessary and identify by block number*)
FIELD	GROUP	SUB-GROUP	Kalman filtering, trajectories, aviation accidents, mathematical models, computerized simulation
01	02		

19. ABSTRACT (*Continue on reverse if necessary and identify by block number*)

Thesis Chairman: Dr. Peter S. Maybeck
Professor of Electrical Engineering

Approved for public release: IAW AFR 190-1.
LYNN E. WOLAVER 15 Jun 88
Dean for Research and Professional Development
Air Force Institute of Technology (AU)
Wright-Patterson AFB OH 45433-6583

20. DISTRIBUTION/AVAILABILITY OF ABSTRACT	21. ABSTRACT SECURITY CLASSIFICATION
☒ UNCLASSIFIED/UNLIMITED ☐ SAME AS RPT ☐ DTIC USERS	UNCLASSIFIED
22a. NAME OF RESPONSIBLE INDIVIDUAL Dr. Peter S. Maybeck	22b. TELEPHONE (*Include Area Code*) (513) 255-2024
	22c. OFFICE SYMBOL AFIT/ENG

DD Form 1473, JUN 86 *Previous editions are obsolete.* SECURITY CLASSIFICATION OF THIS PAGE

19. Abstract:

The purpose of this study was to investigate the potential utility of the linearized Kalman filter-smoother algorithm as a tool for aircraft mishap investigations. The immediate objective was to develop computer software to make an investigation of the algorithm's capabilities possible for generic aircraft trajectories. Other objectives included the determination of the sensitivity of the algorithm to noise strength variations, evaluation of its performance with different measurement devices of varying precision, and determination of the potential for iterative improvement of the results. All of these objectives were achieved.

The central finding of this study was that the linearized Kalman filter-smoother technique is a viable one for mishap trajectory analysis, and that the algorithm as implemented could be useful in actual mishap investigation work.

The study also found that although the effectiveness of the current algorithm is limited, some of the limitations could be removed through further work. Specifically, the problems of systematic nominal trajectory generation and control of unrealistic transients in the filter-smoother output warrant further attention. Suggestions for addressing these problems are included in the report.

END

DATE

FILMED

8-88

DTIC